

Drivers of plant nutrient acquisition and allocation strategies and their influence  
on plant responses to environmental change

by

Evan A. Perkowski, B.S.

A Dissertation

In

Biological Sciences

Submitted to the Graduate Faculty  
of Texas Tech University in  
Partial Fulfillment of  
the Requirements for  
the Degree of

Doctor of Philosophy

Approved

Dr. Nicholas G. Smith  
Chair of Committee

Dr. Aimée T. Classen

Dr. Natasja van Gestel

Dr. Lindsey C. Slaughter

Dr. Dylan W. Schwilk

Dr. Mark Sheridan  
Dean of the Graduate School

May 2023

Copyright 2023, Evan A. Perkowski

## Acknowledgements

Placeholder for text

## Table of Contents

<b>Acknowledgements . . . . .</b>	ii
<b>Abstract . . . . .</b>	vi
<b>List of Tables . . . . .</b>	vii
<b>List of Figures . . . . .</b>	viii
<b>1. Introduction . . . . .</b>	1
<b>2. Structural carbon costs to acquire nitrogen are determined by nitrogen and light availability in two species with different nitrogen acquisition strategies . . . . .</b>	3
2.1    Introduction . . . . .	3
2.2    Methods . . . . .	7
2.2.1 <i>Experiment setup</i> . . . . .	7
2.2.2 <i>Plant measurements and calculations</i> . . . . .	8
2.2.3 <i>Statistical analyses</i> . . . . .	9
2.3    Results . . . . .	11
2.3.1 <i>Carbon costs to acquire nitrogen</i> . . . . .	11
2.3.2 <i>Whole plant nitrogen biomass</i> . . . . .	14
2.3.3 <i>Root carbon biomass</i> . . . . .	16
2.3.4 <i>Root nodule biomass</i> . . . . .	18
2.4    Discussion . . . . .	22
<b>3. Soil nitrogen availability modifies leaf nitrogen economies in mature temperate deciduous forests: a direct test of photosynthetic least-cost theory . . . . .</b>	30
3.1    Introduction . . . . .	30
3.2    Methods . . . . .	34
3.2.1 <i>Study site description</i> . . . . .	34
3.2.2 <i>Experimental design</i> . . . . .	35
3.2.3 <i>Leaf gas exchange and trait measurements</i> . . . . .	35
3.2.4 <i><math>A_{net}/C_i</math> curve-fitting and parameter estimation</i> . . . . .	38

3.2.5 <i>Proportion of leaf nitrogen allocated to photosynthesis and structure</i> . . . . .	40
3.2.6 <i>Tradeoffs between nitrogen and water use</i> . . . . .	41
3.2.7 <i>Soil nitrogen availability and pH</i> . . . . .	42
3.2.8 <i>Statistical analyses</i> . . . . .	44
3.3 Results . . . . .	46
3.3.1 <i>Leaf N content</i> . . . . .	46
3.3.2 <i>Net photosynthesis and leaf biochemistry</i> . . . . .	49
3.3.3 <i>Leaf N allocation</i> . . . . .	52
3.3.4 <i>Tradeoffs between nitrogen and water use</i> . . . . .	55
3.4 Discussion . . . . .	58
3.4.1 <i>Soil nitrogen availability modifies tradeoffs between nitrogen and water use</i> . . . . .	59
3.4.2 <i>Soil pH did not modify tradeoffs between nitrogen and water usage</i> . . . . .	61
3.4.3 <i>Species identity explains a large amount of variation in leaf and whole plant traits</i> . . . . .	62
3.4.4 <i>Implications for photosynthetic least-cost theory model development</i> . . . . .	63
3.4.5 <i>Conclusions</i> . . . . .	65
4. The relative cost of resource use for photosynthesis drives variance in leaf nitrogen content across climate and soil resource availability gradients . . . . .	66
4.1 Introduction . . . . .	66
4.2 Methods . . . . .	68
4.2.1 <i>Site descriptions and sampling methodology</i> . . . . .	68
4.2.2 <i>Leaf trait measurements</i> . . . . .	68
4.2.3 <i>Site climate data</i> . . . . .	74
4.2.4 <i>Site edaphic characteristics</i> . . . . .	74
4.2.5 <i>Plant functional group assignments</i> . . . . .	76
4.2.6 <i>Data analysis</i> . . . . .	77

4.3 Results . . . . .	79
4.3.1 Cost to acquire nitrogen relative to water ( $\beta$ ) . . . . .	79
4.3.2 Leaf $C_i:C_a$ ( $\chi$ ) . . . . .	83
4.3.3 Leaf nitrogen content . . . . .	86
4.3.4 Structural equation model . . . . .	90
4.4 Discussion . . . . .	93
<b>5. Optimal resource investment to photosynthetic capacity maximizes nutrient allocation to whole plant growth under elevated CO<sub>2</sub> . . . . .</b>	<b>94</b>
5.1 Introduction . . . . .	94
5.2 Methods . . . . .	99
5.2.1 Seed treatments and experimental design . . . . .	99
5.2.2 Growth chamber conditions . . . . .	100
5.2.3 Leaf gas exchange measurements . . . . .	102
5.2.4 Leaf trait measurements . . . . .	103
5.2.5 $A/C_i$ curve fitting and parameter estimation . . . . .	105
5.2.6 Stomatal limitation . . . . .	105
5.2.7 Proportion of leaf nitrogen allocated to photosynthesis and structure . . . . .	106
5.2.8 Whole plant traits . . . . .	108
5.2.9 Statistical analyses . . . . .	109
5.3 Results . . . . .	111
5.4 Discussion . . . . .	111
<b>6. Conclusions . . . . .</b>	<b>112</b>
<b>References . . . . .</b>	<b>113</b>

**Abstract**

## List of Tables

2.1 Analysis of variance results exploring species-specific effects of light availability, nitrogen fertilization, and their interactions on carbon costs to acquire nitrogen, whole-plant nitrogen biomass, and root carbon biomass . . . . .	12
2.2 Analysis of variance results exploring effects of light availability, nitrogen fertilization, and their interactions on <i>G. max</i> root nodule biomass and the ratio of root nodule biomass to root biomass* . . . . .	19
2.3 Slopes of the regression line describing the relationship between each dependent variable and nitrogen fertilization at each light level* . . . . .	20
3.1 Effects of soil N availability, soil pH, and species on leaf N content per unit leaf area ( $N_{\text{area}}$ ), leaf N content per unit leaf mass ( $N_{\text{mass}}$ ), and leaf mass per unit leaf area ( $M_{\text{area}}$ ) . . . . .	47
3.2 Effects of soil N availability, soil pH, species, and $N_{\text{area}}$ on leaf biochemistry . . . . .	50
3.3 Effects of soil N availability, soil pH, and species on the proportion of leaf nitrogen content allocated to photosynthesis, Rubisco, bioenergetics, and structure . . . . .	53
3.4 Effects of soil N availability, soil pH, species, and $N_{\text{area}}$ on tradeoffs between nitrogen and water use . . . . .	56

## List of Figures

2.1 Relationships between soil nitrogen fertilization and light availability on carbon costs to acquire nitrogen in <i>G. hirsutum</i> and <i>G. max</i> . . . . .	13
2.2 Relationships between soil nitrogen fertilization and light availability on whole-plant nitrogen biomass in <i>G. hirsutum</i> and <i>G. max</i> . . . . .	15
2.3 Relationships between soil nitrogen fertilization and light availability on root carbon biomass in <i>G. hirsutum</i> and <i>G. max</i> . . . . .	17
2.4 Effects of shade cover and nitrogen fertilization on root nodule biomass and the ratio of root nodule biomass to root biomass in <i>G. max</i> . . . . .	21
3.1 Effects of soil N availability and species on leaf N content per unit leaf area, leaf nitrogen content per unit leaf biomass, and leaf mass per leaf area . . . . .	48
3.2 Effects of soil N availability, species, and leaf N content leaf biochemistry . . . . .	51
3.3 Effects of soil N availability, species, and leaf N content on the fraction of leaf nitrogen allocated to photosynthesis and structure	54
3.4 Effects of soil N availability, species, and leaf N content on tradeoffs between nitrogen and water use . . . . .	57

4.1	Maps that detail site locations along 2006-2020 mean annual precipitation (panel A) and mean annual temperature (panel B) gradients in Texas, USA. . . . .	73
4.2	Effects of soil nitrogen availability and soil moisture on the unit cost ratio $\beta$ . . . . .	82
4.3	Effects of 4-day mean vapor pressure deficit, 2-day soil moisture (per water holding capacity), and soil nitrogen availability on $\chi$ . . . . .	85
4.4	Effects of $\chi$ , soil nitrogen availability, and soil moisture on leaf nitrogen content per unit leaf area, leaf nitrogen content per unit leaf biomass, and leaf mass per area. . . . .	89
4.5	Structural equation model results exploring direct and indirect drivers of $N_{\text{area}}$ . . . . .	92

1                         **Chapter 1**  
2                         **Introduction**

3                     Terrestrial ecosystems are regulated by complex carbon and nutrient cy-  
4     cles. As a result, terrestrial biosphere models, which are beginning to include  
5     linked carbon and nutrient cycles (Shi et al. 2016; Davies-Barnard et al. 2020;  
6     Braghiere et al. 2022), must accurately represent these cycles under different en-  
7     vironmental scenarios to reliably simulate carbon and nitrogen fluxes between the  
8     atmosphere and terrestrial biosphere fluxes (Oreskes et al. 1994; Hungate et al.  
9     2003; Prentice et al. 2015). While the inclusion of coupled carbon and nitrogen  
10   cycles tends to reduce model uncertainty (Arora et al. 2020), carbon and nutrient  
11   flux simulations across terrestrial biosphere models tends to diverge under future  
12   environmental scenarios (Friedlingstein et al. 2014; Meyerholt et al. 2020). The  
13   widespread divergence of terrestrial biosphere model simulations may be driven by  
14   uncertainty in the response of photosynthetic processes across resource availability  
15   gradients and in response to environmental change. This is because photosynthesis  
16   is the largest carbon flux between the atmosphere and terrestrial biosphere, and is  
17   constrained by ecosystem carbon and nutrient cycles (Hungate et al. 2003; IPCC  
18   2021; LeBauer and Treseder 2008; Fay et al. 2015). Yet, open questions remain  
19   regarding the influence of soil resource availability and climate on plant nutrient  
20   acquisition, plant nutrient allocation, photosynthetic processes, and whole plant  
21   growth.

22                     Here, I conduct a nitrogen-by-light manipulative greenhouse experiment, a  
23     nitrogen-by-sulfur manipulative field experiment, a soil resource avaialbility and

24 climate environmental gradient field experiment, and a CO<sub>2</sub>-by-inoculation-by-  
25 nitrogen manipulative growth chamber experiment to test underlying assumptions  
26 of photosynthetic least-cost theory. Specifically, these experiments

27 test effects of soil resource availability and aboveground climate on plant  
28 nutrient acquisition, plant nutrient allocation, photosynthetic processes, and whole  
29 plant growth

30 In this dissertation, I test underlying assumptions of photosynthetic least-  
31 cost theory. Using a greenhouse nitrogen-by-light manipulation experiment, I  
32 show that

33 conducted a series of experiments to quantify effects of aboveground cli-  
34 mate and soil resource availability on nutrient acquisition and alloc

35 Here, I propose a series of experiments to quantify nutrient acquisition  
36 and allocaton responses to resource availability gradients dissertation designed to  
37 quantify nutrient acquisition and allocation responses to varying environmental  
38 conditions and resource availability gradients through the lens of the least-cost  
39 theory. Specifically, I will address five main questions:

40

## Chapter 2

41

Structural carbon costs to acquire nitrogen are determined by  
42 nitrogen and light availability in two species with different nitrogen  
43 acquisition strategies

44 2.1 Introduction

45 Carbon and nitrogen cycles are tightly coupled in terrestrial ecosystems.  
46 This tight coupling influences photosynthesis (Walker et al. 2014; Rogers et al.  
47 2017), net primary productivity (LeBauer and Treseder 2008; Thomas et al. 2013),  
48 decomposition (Cornwell et al. 2008; Bonan et al. 2013; Sulman et al. 2019), and  
49 plant resource competition (Gill and Finzi 2016; Xu-Ri and Prentice 2017). Ter-  
50 restrial biosphere models are beginning to include connected carbon and nitrogen  
51 cycles to improve the realism of their simulations (Fisher et al. 2010; Brzostek  
52 et al. 2014; Wieder et al. 2015; Shi et al. 2016; Zhu et al. 2019). Simula-  
53 tions from these models indicate that coupling carbon and nitrogen cycles can  
54 drastically influence future biosphere-atmosphere feedbacks under global change,  
55 such as elevated carbon dioxide or nitrogen deposition (Thornton et al. 2007;  
56 Goll et al. 2012; Wieder et al. 2015; Wieder et al. 2019). Nonetheless, there  
57 are still limitations in our quantitative understanding of connected carbon and  
58 nitrogen dynamics (Thomas et al. 2015; Meyerholt et al. 2016; Rogers et al.  
59 2017; Exbrayat et al. 2018; Shi et al. 2019), forcing models to make potentially  
60 unreliable assumptions.

61

Plant nitrogen acquisition is a process in terrestrial ecosystems by which  
62 carbon and nitrogen are tightly coupled (Vitousek and Howarth 1991; Delaire  
63 et al. 2005; Brzostek et al. 2014). Plants must allocate photosynthetically de-

64 rived carbon belowground to produce and maintain root systems or exchange with  
65 symbiotic soil microbes in order to acquire nitrogen (Högberg et al. 2008; Hög-  
66 berg et al. 2010). Thus, plants have an inherent carbon cost associated with  
67 acquiring nitrogen, which can include both direct energetic costs associated with  
68 nitrogen acquisition and indirect costs associated with building structures that  
69 support nitrogen acquisition (Gutschick 1981; Rastetter et al. 2001; Vitousek  
70 et al. 2002; Menge et al. 2008). Model simulations (Fisher et al. 2010; Brzostek  
71 et al. 2014; Shi et al. 2016; Allen et al. 2020) and meta-analyses (Terrer et al.  
72 2018) suggest that these carbon costs vary between species, particularly those  
73 with different nitrogen acquisition strategies. For example, simulations using iter-  
74 ations of the Fixation and Uptake of Nitrogen (FUN) model indicate that species  
75 that acquire nitrogen from non-symbiotic active uptake pathways (e.g. mass flow)  
76 generally have larger carbon costs to acquire nitrogen than species that acquire  
77 nitrogen through symbiotic associations with nitrogen-fixing bacteria (Brzostek  
78 et al. 2014; Allen et al. 2020).

79 Carbon costs to acquire nitrogen likely vary in response to changes in soil  
80 nitrogen availability. For example, if the primary mode of nitrogen acquisition  
81 is through non-symbiotic active uptake, then nitrogen availability could decrease  
82 carbon costs to acquire nitrogen as a result of increased per-root nitrogen up-  
83 take (Franklin et al. 2009; Wang et al. 2018). However, if the primary mode of  
84 nitrogen acquisition is through symbiotic active uptake, then nitrogen availabil-  
85 ity may incur additional carbon costs to acquire nitrogen if it causes microbial  
86 symbionts to shift toward parasitism along the parasitism–mutualism continuum  
87 (Johnson et al. 1997; Hoek et al. 2016; Friel and Friesen 2019) or if it reduces

88 the nitrogen acquisition capacity of a microbial symbiont (van Diepen et al. 2007;  
89 Soudzilovskaia et al. 2015; Muñoz et al. 2016). Species may respond to shifts in  
90 soil nitrogen availability by switching their primary mode of nitrogen acquisition  
91 to a strategy with lower carbon costs to acquire nitrogen in order to maximize  
92 the magnitude of nitrogen acquired from a belowground carbon investment and  
93 outcompete other individuals for soil resources (Rastetter et al. 2001; Menge et al.  
94 2008).

95 Environmental conditions that affect demand to acquire nitrogen to sup-  
96 port new and existing tissues could also be a source of variance in plant carbon  
97 costs to acquire nitrogen. For example, an increase in plant nitrogen demand could  
98 increase carbon costs to acquire nitrogen if this increases the carbon that must be  
99 allocated belowground to acquire a proportional amount of nitrogen (Kulmatiski  
100 et al. 2017; Noyce et al. 2019). This could be driven by a temporary state of  
101 diminishing return associated with investing carbon toward building and main-  
102 taining structures that are necessary to support enhanced nitrogen uptake, such  
103 as fine roots (Matamala and Schlesinger 2000; Norby et al. 2004; Arndal et al.  
104 2018), mycorrhizal hyphae (Saleh et al. 2020), or root nodules (Parvin et al. 2020).  
105 Alternatively, if the environmental factor that increases plant nitrogen demand  
106 causes nitrogen to become more limiting in the system (e.g. atmospheric CO<sub>2</sub>;  
107 Luo et al. (2004), LeBauer and Treseder (2008), Vitousek et al. (2010), Liang  
108 et al. (2016)), species might switch their primary mode of nitrogen acquisition to  
109 a strategy with lower relative carbon costs to acquire nitrogen in order to gain a  
110 competitive advantage over species with either different or more limited modes of  
111 nitrogen acquisition (Ainsworth and Long 2005; Taylor and Menge 2018).

112        Using a plant economics approach, we examined the influence of plant  
113    nitrogen demand and soil nitrogen availability on plant carbon costs to acquire  
114    nitrogen. This was done by growing a species capable of forming associations  
115    with nitrogen-fixing bacteria (*Glycine max* L. (Merr)) and a species not capable  
116    of forming these associations (*Gossypium hirsutum* L.) under four levels of light  
117    availability (plant nitrogen demand proxy) and four levels of soil nitrogen fertil-  
118    ization (soil nitrogen availability proxy) in a full-factorial, controlled greenhouse  
119    experiment. We used this experimental set-up to test the following hypotheses:

- 120        1. An increase in plant nitrogen demand due to increasing light availability will  
121        increase carbon costs to acquire nitrogen through a proportionally larger  
122        increase in belowground carbon than whole-plant nitrogen acquisition. This  
123        will be the result of an increased investment of carbon toward belowground  
124        structures that support enhanced nitrogen uptake, but at a lower nitrogen  
125        return.
- 126        2. An increase in soil nitrogen availability will decrease carbon costs to acquire  
127        nitrogen as a result of increased per root nitrogen uptake in *G. hirsutum*.  
128        However, soil nitrogen availability will not affect carbon costs to acquire  
129        nitrogen in *G. max* because of the already high return of nitrogen supplied  
130        through nitrogen fixation.

**131** 2.2 Methods

**132** 2.2.1 *Experiment setup*

**133** *Gossypium hirsutum* and *G. max* were planted in individual 3 liter pots  
**134** (NS-300; Nursery Supplies, Orange, CA, USA) containing a 3:1 mix of unfertil-  
**135** ized potting mix (Sungro Sunshine Mix #2, Agawam, MA, USA) to native soil  
**136** extracted from an agricultural field most recently planted with *G. max* at the  
**137** USDA-ARS Laboratory in Lubbock, TX, USA (33.59°N, -101.90°W). The field  
**138** soil was classified as Amarillo fine sandy loam (75% sand, 10% silt, 15% clay).  
**139** Upon planting, all *G. max* pots were inoculated with *Bradyrhizobium japonicum*  
**140** (Verdesian N-Dure™ Soybean, Cary, NC, USA) to stimulate root nodulation. In-  
**141** dividuals of both species were grown under similar, unshaded, ambient greenhouse  
**142** conditions for 2 weeks to germinate and begin vegetative growth. Three blocks  
**143** were set up in the greenhouse, each containing four light treatments created us-  
**144** ing shade cloth that reduced incoming radiation by either 0 (full sun), 30, 50,  
**145** or 80%. Two weeks post-germination, individuals were randomly placed in the  
**146** four light treatments in each block. Individuals received one of four nitrogen fer-  
**147** tilization doses as 100ml of a modified Hoagland solution (Hoagland and Arnon  
**148** 1950) equivalent to either 0, 70, 210, or 630 ppm N twice per week within each  
**149** light treatment. Nitrogen fertilization doses were received as topical agents to  
**150** the soil surface. Each Hoagland solution was modified to keep concentrations of  
**151** other macro- and micronutrients equivalent (Supplementary Table S1). Plants  
**152** were routinely well watered to eliminate water stress.

**153** 2.2.2 *Plant measurements and calculations*

**154** Each individual was harvested after 5 weeks of treatment, and biomass  
**155** was separated by organ type (leaves, stems, and roots). Nodules on *G. max*  
**156** roots were also harvested. With the exception of the 0% shade cover and 630  
**157** ppm N treatment combination, all treatment combinations in both species had  
**158** lower average dry biomass:pot volume ratios than the 1:1 ratio recommended by  
**159** Poorter et al. (2012) to minimize the likelihood of pot volume-induced growth  
**160** limitation (Supplementary Tables S2, S3; Supplementary Fig. S1). All harvested  
**161** material was dried, weighed, and ground by organ type. Carbon and nitrogen  
**162** content ( $\text{g g}^{-1}$ ) was determined by subsampling from ground and homogenized  
**163** biomass of each organ type using an elemental analyzer (Costech 4010; Costech,  
**164** Inc., Valencia, CA, USA). We scaled these values to total leaf, stem, and root  
**165** carbon and nitrogen biomass (g) by multiplying dry biomass of each organ type  
**166** by carbon or nitrogen content of each corresponding organ type. Whole-plant  
**167** nitrogen biomass (g) was calculated as the sum of total leaf (g), stem (g), and  
**168** root (g) nitrogen biomass. Root nodule carbon biomass was not included in the  
**169** calculation of root carbon biomass; however, relative plant investment toward root  
**170** or root nodule standing stock was estimated as the ratio of root biomass to root  
**171** nodule biomass ( $\text{g g}^{-1}$ ), following similar metrics to those adopted by Dovrat et al.  
**172** (2018) and Dovrat et al. (2020).

**173** Carbon costs to acquire nitrogen ( $\text{gC gN}^{-1}$ ) were estimated as the ratio of  
**174** total root carbon biomass (gC) to whole-plant nitrogen biomass (gN). This cal-  
**175** culation quantifies the relationship between carbon spent on nitrogen acquisition  
**176** and whole-plant nitrogen acquisition by using root carbon biomass as a proxy for

177 estimating the magnitude of carbon allocated toward nitrogen acquisition. This  
178 calculation therefore assumes that the magnitude of root carbon standing stock is  
179 proportional to carbon transferred to root nodules or mycorrhizae, or lost through  
180 root exudation or turnover. This assumption has been supported in species that  
181 associate with ectomycorrhizal fungi (Hobbie 2006; Hobbie and Hobbie 2008), but  
182 is less clear in species that acquire nitrogen through non-symbiotic active uptake  
183 or symbiotic nitrogen fixation. It is also unclear whether relationships between  
184 root carbon standing stock and carbon transfer to root nodules are similar in mag-  
185 nitude to carbon lost through exudation or when allocated toward other active  
186 uptake pathways. Thus, because of the way we performed our measurements, our  
187 proximal values of carbon costs to acquire nitrogen are underestimates.

188 2.2.3 *Statistical analyses*

189 We explored the effects of light and nitrogen availability on carbon costs to  
190 acquire nitrogen using separate linear mixed-effects models for each species. Mod-  
191 els included shade cover, nitrogen fertilization, and interactions between shade  
192 cover and nitrogen fertilization as continuous fixed effects, and also included block  
193 as a random intercept term. Three separate models for each species were built  
194 with this independent variable structure for three different dependent variables: (i)  
195 carbon costs to acquire nitrogen ( $\text{gC gN}^{-1}$ ); (ii) whole-plant nitrogen biomass (de-  
196 nominator of carbon cost to acquire nitrogen;  $\text{gN}$ ); and (iii) root carbon biomass  
197 (numerator of carbon cost to acquire nitrogen;  $\text{gC}$ ). We constructed two additional  
198 models for *G. max* with the same model structure described above to investigate  
199 the effects of light availability and nitrogen fertilization on root nodule biomass

200 (g) and the ratio of root nodule biomass to root biomass (unitless).

201 We used Shapiro–Wilk tests of normality to determine whether species-  
202 specifc linear mixed-effects model residuals followed a normal distribution. None  
203 of our models satisfied residual normality assumptions when models were fit using  
204 untransformed data (Shapiro–Wilk:  $P<0.05$  in all cases). We attempted to satisfy  
205 residual normality assumptions by first fitting models using dependent variables  
206 that were natural-log transformed. If residual normality assumptions were still  
207 not met (Shapiro–Wilk:  $P<0.05$ ), then models were fit using dependent variables  
208 that were square root transformed. All residual normality assumptions were satis-  
209 fied when models were fit with either a natural-log or square root transformation  
210 (Shapiro–Wilk:  $P>0.05$  in all cases). Specifically, we natural-log transformed *G.*  
211 *hirsutum* carbon costs to acquire nitrogen and *G. hirsutum* whole-plant nitrogen  
212 biomass. We also square root transformed *G. max* carbon costs to acquire nitro-  
213 gen, *G. max* whole-plant nitrogen biomass, root carbon biomass in both species,  
214 *G. max* root nodule biomass, and the *G. max* ratio of root nodule biomass to root  
215 biomass. We used the ‘lmer’ function in the ‘lme4’ R package (Bates et al. 2015)  
216 to fit each model and the ‘Anova’ function in the ‘car’ R package (Fox and Weis-  
217 berg 2019) to calculate Wald’s  $\chi^2$  to determine the significance ( $\alpha = 0.05$ ) of each  
218 fixed effect coefficient. Finally, we used the ‘emmeans’ R package (Lenth 2019)  
219 to conduct post-hoc comparisons of our treatment combinations using Tukey’s  
220 tests. Degrees of freedom for all Tukey’s tests were approximated using the Ken-  
221 ward–Roger approach (Kenward and Roger 1997). All analyses and plots were  
222 conducted in R version 4.0.1 (R Core Team 2021).

**223** 2.3 Results

**224** 2.3.1 *Carbon costs to acquire nitrogen*

**225** Carbon costs to acquire nitrogen in *G. hirsutum* increased with increasing  
**226** light availability ( $p < 0.001$ ; Table 2.1; Fig. 2.1) and decreased with increasing  
**227** nitrogen fertilization ( $p < 0.001$ ; Table 2.1; Fig. 2.1). There was no interaction  
**228** between light availability and nitrogen fertilization ( $p = 0.486$ , Table 2.1; Fig.  
**229** 2.1).

**230** Carbon costs to acquire nitrogen in *G. max* also increased with increasing  
**231** light availability ( $p < 0.001$ , Table 2.1; Fig. 2.1) and decreased with increasing  
**232** nitrogen fertilization ( $p < 0.001$ ; Table 2.1; Fig. 2.1). There was no interaction  
**233** between light availability and nitrogen fertilization ( $p = 0.261$ , Table 2.1; Fig.  
**234** 2.1).

**Table 2.1.** Analysis of variance results exploring species-specific effects of light availability, nitrogen fertilization, and their interactions on carbon costs to acquire nitrogen, whole-plant nitrogen biomass, and root carbon biomass

	Carbon costs to acquire nitrogen			Whole-plant nitrogen biomass			Root carbon biomass			
	df	Coefficient	$\chi^2$	p	Coefficient	$\chi^2$	p	Coefficient	$\chi^2$	p
<i>G. hirsutum</i>										
Intercept		1.594	-	-	-3.232	-	-	0.432	-	-
Light (L)	1	-1.09E-02	56.494	<0.001	-6.41E-03	91.275	<0.001	-2.62E-03	169.608	<0.001
Nitrogen (N)	1	-1.34E-03	54.925	<0.001	1.83E-03	118.784	<0.001	1.15E-04	2.901	0.089
L*N	1	3.88E-06	0.485	0.486	-1.34E-05	10.721	0.001	-1.67E-06	3.140	0.076
<i>G. max</i>										
Intercept		1.877	-	-	0.239	-	-	0.438	-	-
Light (L)	1	-7.67E-03	174.156	<0.001	-6.72E-04	39.799	<0.001	-2.55E-03	194.548	<0.001
Nitrogen (N)	1	-2.35E-04	21.948	<0.001	1.55E-04	70.771	<0.001	2.52E-04	19.458	<0.001
L*N	1	-2.89E-06	1.262	0.261	-6.32E-07	1.435	0.231	-3.16E-06	10.803	0.001

\*Significance determined using Wald's  $\chi^2$  tests ( $P=0.05$ ).  $P$ -values<0.05 are in bold and  $p$ -values between 0.05 and 0.1 are italicized. Negative coefficients for light treatments indicate a positive effect of increasing light availability on all response variables, as light availability is treated as percent shade cover in all linear mixed-effects models.

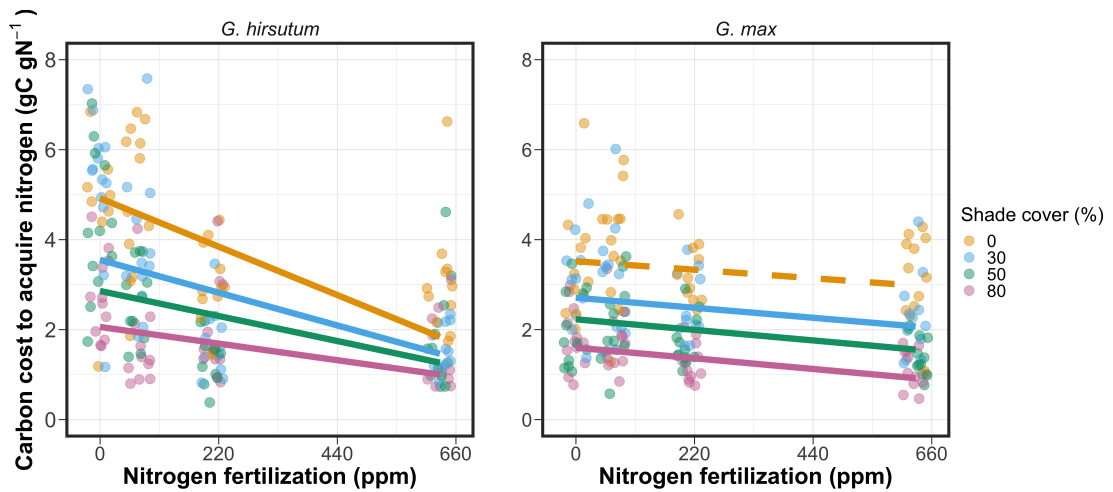


**Figure 2.1.** Relationships between soil nutrient fertilization and light availability on carbon costs to acquire nitrogen in *G. hirsutum* and *G. max*. Nitrogen fertilization treatments are represented on the x-axis. Shade cover treatments are represented through colored points and trendlines. Trendlines were created by back-transforming marginal mean slopes and intercepts from species-specific linear mixed-effects models. These values were calculated using the ‘emtrends’ and ‘emmmeans’ functions in the ‘emmeans’ R package (Lenth, 2019). Points are jittered for visibility. Yellow points and trendlines represent the 0% shade cover treatment, blue points and trendlines represent the 30% shade cover treatment, green points and trendlines represent the 50% shade cover treatment, and purple points and trendlines represent the 80% shade cover treatment. Solid trendlines indicate slopes that are significantly different from zero (Tukey:  $p < 0.05$ ), while dashed trendlines indicate slopes that are not statistically different from zero.

**235** 2.3.2 *Whole plant nitrogen biomass*

**236** Whole-plant nitrogen biomass in *G. hirsutum* was driven by an interaction  
**237** between light availability and nitrogen fertilization ( $p = 0.001$ ; Table 2.1; Fig.  
**238** 2.2). This interaction indicated a greater stimulation of whole-plant nitrogen  
**239** biomass by nitrogen fertilization as light levels increased (Table 2.1; Fig. 2.2).

**240** Whole-plant nitrogen biomass in *G. max* increased with increasing light  
**241** availability ( $p < 0.001$ ) and nitrogen fertilization ( $p < 0.001$ ), with no interaction  
**242** between light availability and nitrogen fertilization ( $p = 0.231$ ; Table 2.1; Fig.  
**243** 2.2).

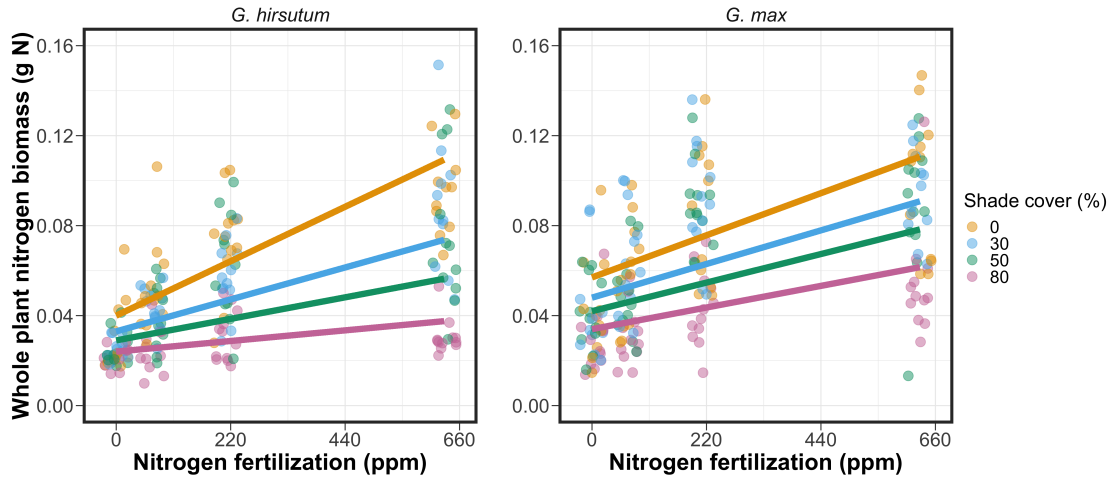


**Figure 2.2.** Relationships between soil nutrient fertilization and light availability on whole-plant nitrogen biomass in *G. hirsutum* and *G. max*. Whole-plant nitrogen biomass is the denominator of the carbon cost to acquire nitrogen calculation. Nitrogen fertilization treatments are represented on the x-axis. Shade cover treatments are represented through colored points and trendlines. Trendlines were created by back-transforming marginal mean slopes and intercepts from species-specific linear mixed-effects models. These values were calculated using the ‘emtrends’ and ‘emmmeans’ functions in the ‘emmeans’ R package (Lenth 2019). Points are jittered for visibility. Yellow points and trendlines represent the 0% shade cover treatment, blue points and trendlines represent the 30% shade cover treatment, green points and trendlines represent the 50% shade cover treatment, and purple points and trendlines represent the 80% shade cover treatment. Solid trendlines indicate slopes that are significantly different from zero (Tukey:  $P < 0.05$ ), while dashed trendlines indicate slopes that are not statistically different from zero.

**244** 2.3.3 *Root carbon biomass*

**245** Root carbon biomass in *G. hirsutum* significantly increased with increasing  
**246** light availability ( $p < 0.001$ ; Table 2.1; Fig. 2.3) and marginally increased with  
**247** nitrogen fertilization ( $p = 0.089$ ; Table 2.1; Fig. 2.3). There was also a marginal  
**248** interaction between light availability and nitrogen fertilization ( $p = 0.076$ ; Table  
**249** 2.1), driven by an increase in the positive response of root carbon biomass to  
**250** increasing nitrogen fertilization as light availability increased. This resulted in  
**251** significantly positive trends between root carbon biomass and nitrogen fertilization  
**252** in the two highest light treatments (Tukey:  $p < 0.05$  in both cases; Table 2.3;  
**253** Fig. 2.3) and no effect of nitrogen fertilization in the two lowest light treatments  
**254** (Tukey:  $p > 0.05$  in both cases; Table 2.3; Fig. 2.3).

**255** There was an interaction between light availability and nitrogen fertiliza-  
**256** tion on root carbon biomass in *G. max* ( $p = 0.001$ ; Table 2.1; Fig. 2.3). Post-hoc  
**257** analyses indicated that the positive effects of nitrogen fertilization on *G. max* root  
**258** carbon biomass increased with increasing light availability (Table 2.3; Fig. 2.3).  
**259** There were also positive individual effects of increasing nitrogen fertilization ( $p <$   
**260**  $0.001$ ) and light availability ( $p < 0.001$ ) on *G. max* root carbon biomass (Table  
**261** 2.1; Fig. 2.3).

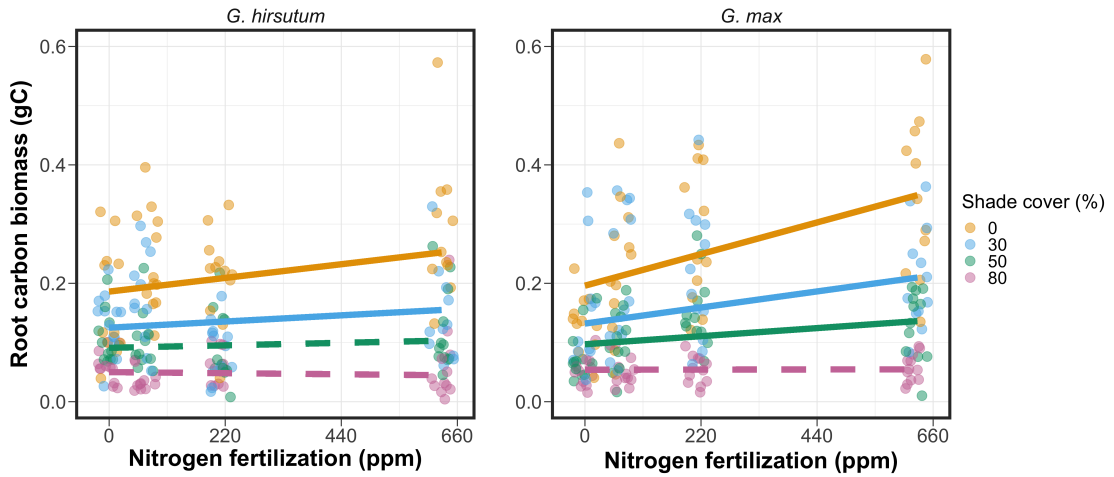


**Figure 2.3.** Relationships between soil nutrient fertilization and light availability on root carbon biomass in *G. hirsutum* and *G. max*. Root carbon biomass is the numerator of the carbon cost to acquire nitrogen calculation. Nitrogen fertilization treatments are represented on the x-axis. Shade cover treatments are represented through colored points and trendlines. Trendlines were created by back-transforming marginal mean slopes and intercepts from species-specific linear mixed-effects models. These values were calculated using the ‘emtrends’ and ‘emmmeans’ functions in the ‘emmeans’ R package (Lenth 2019). Points are jittered for visibility. Yellow points and trendlines represent the 0% shade cover treatment, blue points and trendlines represent the 30% shade cover treatment, green points and trendlines represent the 50% shade cover treatment, and purple points and trendlines represent the 80% shade cover treatment. Solid trendlines indicate slopes that are significantly different from zero (Tukey:  $p < 0.05$ ), while dashed trendlines indicate slopes that are not statistically different from zero.

**262** 2.3.4 *Root nodule biomass*

**263** Root nodule biomass in *G. max* increased with increasing light availability  
**264** ( $p < 0.001$ ; Table 2.2; Fig. 2.4A) and decreased with increasing nitrogen fertiliza-  
**265** tion ( $p < 0.001$ ; Table 2.2; Fig. 2.4A). There was no interaction between nitrogen  
**266** fertilization and light availability ( $p = 0.133$ ; Table 2.2; Fig. 2.4A). The ratio of  
**267** root nodule biomass to root biomass did not change in response to light avail-  
**268** ability ( $p = 0.481$ ; Table 2.2; Fig. 2.4B) but decreased with increasing nitrogen  
**269** fertilization ( $p < 0.001$ ; Table 2.2; Fig. 2.4B). There was no interaction between  
**270** nitrogen fertilization and light availability on the ratio of root nodule biomass to  
**271** root biomass ( $p = 0.621$ ; Table 2.2; Fig. 2.4B).

**Table 2.2.** Analysis of variance results exploring effects of light availability, nitrogen fertilization, and their interactions on *G. max* root nodule biomass and the ratio of root nodule biomass to root biomass\*

	Nodule biomass			Nodule biomass: root biomass			
	df	Coefficient	$\chi^2$	p	coefficient	$\chi^2$	p
(Intercept)		0.302	-	-	0.448	-	-
Light (L)	1	-1.81E-03	72.964	<b>&lt;0.001</b>	-8.76E-05	0.496	0.481
Nitrogen (N)	1	-2.83E-04	115.377	<b>&lt;0.001</b>	-5.09E-04	156.476	<b>&lt;0.001</b>
L*N	1	1.14E-06	2.226	0.133	-7.30E-07	0.244	0.621

\*Significance determined using Wald's  $\chi^2$  tests ( $\alpha = 0.05$ ). *p*-values less than 0.05 are in bold. Negative coefficients for light treatments indicate a positive effect of increasing light availability on all response variables, as light availability is treated as percent shade cover in all linear mixed-effects models. Root nodule biomass and nodule biomass: root biomass models were only constructed for *G. max* because *G. hirsutum* was not inoculated with *B. japonicum* and is not capable of forming root nodules.

**Table 2.3.** Slopes of the regression line describing the relationship between each dependent variable and nitrogen fertilization at each light level\*

Shade cover	Carbon cost to acquire nitrogen	Whole-plant nitrogen biomass	Root carbon biomass	Root nodule biomass	Nodule biomass root biomass
<i>G. hirsutum</i>					
0%	<b>-1.34E-03<sup>a</sup></b>	<b>1.83E-03<sup>a</sup></b>	<b>1.15E-04<sup>b</sup></b>	-	-
30%	<b>-1.22E-03<sup>a</sup></b>	<b>1.43E-03<sup>a</sup></b>	<b>1.17E-04<sup>b</sup></b>	-	-
50%	<b>-1.14E-03<sup>a</sup></b>	<b>1.17E-03<sup>a</sup></b>	3.12E-05 <sup>b</sup>	-	-
80%	<b>-1.02E-03<sup>a</sup></b>	<b>7.66E-04<sup>a</sup></b>	-1.89E-06 <sup>b</sup>	-	-
<i>G. max</i>					
0%	-2.35E-04 <sup>b</sup>	<b>1.55E-05<sup>b</sup></b>	<b>2.51E-04<sup>b</sup></b>	<b>-2.83E-04<sup>b</sup></b>	<b>-5.09E-04<sup>b</sup></b>
30%	<b>-3.22E-04<sup>b</sup></b>	<b>1.35E-05<sup>b</sup></b>	<b>1.57E-04<sup>b</sup></b>	<b>-2.49E-04<sup>b</sup></b>	<b>-5.31E-04<sup>b</sup></b>
50%	<b>-3.80E-04<sup>b</sup></b>	<b>1.23E-05<sup>b</sup></b>	<b>9.37E-05<sup>b</sup></b>	<b>-2.26E-04<sup>b</sup></b>	<b>-5.45E-04<sup>b</sup></b>
80%	<b>-4.66E-04<sup>b</sup></b>	<b>1.04E-05<sup>b</sup></b>	-9.95E-07 <sup>b</sup>	<b>-1.92E-04<sup>b</sup></b>	<b>-5.67E-04<sup>b</sup></b>

\*Slopes represent estimated marginal mean slopes from linear mixed-effects models described in the Methods. Slopes were calculated using the ‘emmeans’ R package (Lenth 2019). Superscripts indicate slopes fit to natural-log (<sup>a</sup>) or square root (<sup>b</sup>) transformed data. Slopes statistically different from zero (Tukey:  $p < 0.05$ ) are indicated in bold. Marginally significant slopes (Tukey:  $0.05 < p < 0.1$ ) are italicized.

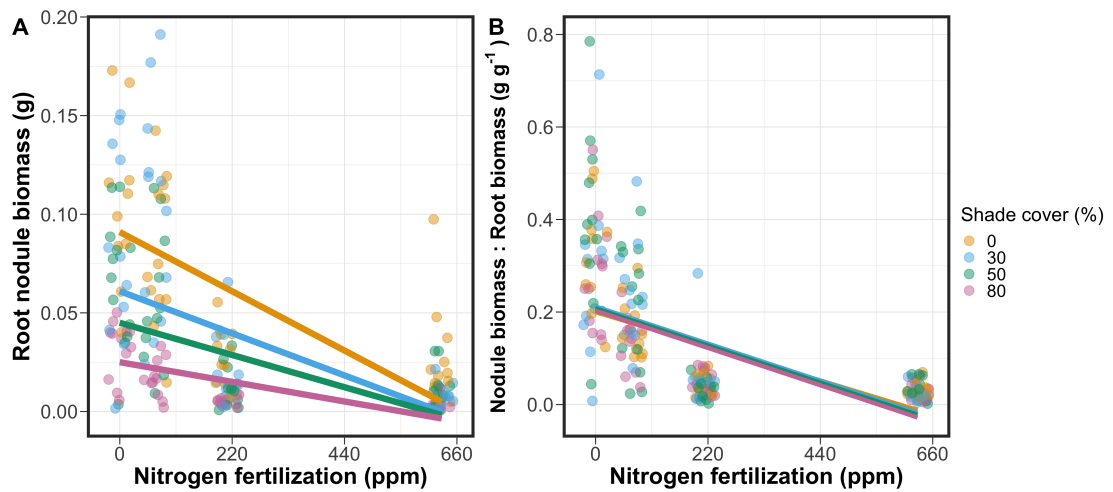


**Figure 2.4.** Effects of shade cover and nitrogen fertilization on root nodule biomass (A) and the ratio of root nodule biomass to root biomass (B) in *G. max*. Nitrogen fertilization treatments are represented on the x-axis. Shade cover treatments are represented through colored points and trendlines. Trendlines were created by back-transforming marginal mean slopes and intercepts from species-specific linear mixed-effects models. These values were calculated using the ‘emtrends’ and ‘emmeans’ functions in the ‘emmeans’ R package (Lenth 2019). Points are jittered for visibility. Yellow points and trendlines represent the 0% shade cover treatment, blue points and trendlines represent the 30% shade cover treatment, green points and trendlines represent the 50% shade cover treatment, and purple points and trendlines represent the 80% shade cover treatment. Solid trendlines indicate slopes that are significantly different from zero (Tukey:  $p < 0.05$ ), while dashed trendlines indicate slopes that are not statistically different from zero.

**272** 2.4 Discussion

**273** In this chapter, we determined the effects of light availability and soil ni-  
**274** trogen fertilization on root mass carbon costs to acquire nitrogen in *G. hirsutum*  
**275** and *G. max*. In support of our hypotheses, we found that carbon costs to acquire  
**276** nitrogen generally increased with increasing light availability and decreased with  
**277** increasing soil nitrogen fertilization in both species. These findings suggest that  
**278** carbon costs to acquire nitrogen are determined by factors that influence plant  
**279** nitrogen demand and soil nitrogen availability. In contrast to our second hypothe-  
**280** sis, root nodulation data suggested that *G. max* and *G. hirsutum* achieved similar  
**281** directional carbon cost responses to nitrogen fertilization despite a likely shift in  
**282** G.!max allocation from nodulation to root biomass along the nitrogen fertilization  
**283** gradient (Fig. 2.4B).

**284** Both *G. max* and *G. hirsutum* experienced an increase in carbon costs to  
**285** acquire nitrogen due to increasing light availability. These patterns were driven by  
**286** a larger increase in root carbon biomass than whole-plant nitrogen biomass. In-  
**287** creases in root carbon biomass due to factors that increase plant nitrogen demand  
**288** are a commonly observed pattern, as carbon allocated belowground provides sub-  
**289** strate needed to produce and maintain structures that satisfy aboveground plant  
**290** nitrogen demand (Nadelhoffer and Raich 1992; Giardina et al. 2005; Raich et al.  
**291** 2014). Our findings suggest that plants allocate relatively more carbon for acquir-  
**292** ing nitrogen when demand increases over short temporal scales, which may cause  
**293** a temporary state of diminishing return due to asynchrony between belowground  
**294** carbon and whole-plant nitrogen responses to plant nitrogen demand (Kulmatiski  
**295** et al. 2017; Noyce et al. 2019). These responses might be attributed to a temporal

296 lag associated with producing structures that enhance nitrogen acquisition. For  
297 example, fine roots (Matamala and Schlesinger 2000; Norby et al. 2004; Arndal  
298 et al. 2018) and root nodules (Parvin et al. 2020) take time to build and first  
299 require the construction of coarse roots. Thus, full nitrogen returns from these  
300 investments may not occur immediately (Kayler et al. 2010; Kayler et al. 2017),  
301 and may vary by species acquisition strategy. We speculate that increases in ni-  
302 trogen acquisition from a given carbon investment may occur beyond the 5 week  
303 scope of this experiment. A similar study conducted over a longer temporal scale  
304 would address this.

305 Increasing soil nitrogen fertilization generally decreased carbon costs to  
306 acquire nitrogen in both species. These patterns were driven by a larger increase  
307 in whole-plant nitrogen biomass than root carbon biomass. In *G. hirsutum*, re-  
308 ductions in carbon costs to acquire nitrogen may have been due to an increase in  
309 per-root nitrogen uptake, allowing individuals to maximize the amount of nitro-  
310 gen acquired from a belowground carbon investment. Interestingly, increased soil  
311 nitrogen fertilization increased whole-plant nitrogen biomass in *G. max* despite  
312 reductions in root nodule biomass that likely reduced the nitrogen-fixing capac-  
313 ity of *G. max* (Andersen et al. 2005; Muñoz et al. 2016). While reductions in  
314 root nodulation due to increased soil nitrogen availability are commonly observed  
315 (Gibson and Harper 1985; Fujikake et al. 2003), our responses were observed in  
316 tandem with increased root carbon biomass, implying that *G. max* shifted relative  
317 carbon allocation from nitrogen fixation to soil nitrogen acquisition (Markham and  
318 Zekveld 2007; Dovrat et al. 2020). This was likely because there was a reduction in  
319 the carbon cost advantage of acquiring fixed nitrogen relative to soil nitrogen, and

320 suggests that species capable of associating with symbiotic nitrogen-fixing bacte-  
321 ria shift their relative nitrogen acquisition pathway to optimize nitrogen uptake  
322 (Rastetter et al. 2001). Future studies should further investigate these patterns  
323 with a larger quantity of phylogenetically related species, or different varieties  
324 of a single species that differ in their ability to form associations with symbiotic  
325 nitrogen-fixing bacteria to more directly test the impact of nitrogen fixation on  
326 the patterns observed in this study.

327 Carbon costs to acquire nitrogen are subsumed in the general discussion of  
328 economic analogies to plant resource uptake (Bloom et al. 1985; Rastetter et al.  
329 2001; Vitousek et al. 2002; Phillips et al. 2013; Terrer et al. 2018; Henneron et al.  
330 2020). Despite this, terrestrial biosphere models rarely include these carbon costs  
331 within their framework for predicting plant nitrogen uptake. There is currently  
332 one plant resource uptake model, FUN, that quantitatively predicts carbon costs  
333 to acquire nitrogen within a framework for predicting plant nitrogen uptake for  
334 different nitrogen acquisition strategies (Fisher et al. 2010; Brzostek et al. 2014)  
335 (Fisher et al. 2010; Brzostek et al. 2014). Iterations of FUN are currently  
336 coupled to two terrestrial biosphere models: the Community Land Model 5.0 and  
337 the Joint UK Land Environment Simulator (Shi et al. 2016; Lawrence et al.  
338 2019; Clark et al. 2011). Recent work suggests that coupling FUN to CLM 5.0  
339 caused a large overprediction of plant nitrogen uptake associated with nitrogen  
340 fixation (Davies-Barnard et al. 2020). Thus, empirical data from manipulative  
341 experiments that explicitly quantify carbon costs to acquire nitrogen in species  
342 capable of associating with nitrogen-fixing bacteria across different environmental  
343 contexts is an important step toward identifying potential biases in models such

**344** as FUN.

**345** Our findings broadly support the FUN formulation of carbon costs to ac-  
**346** quire nitrogen in response to soil nitrogen availability. FUN calculates carbon  
**347** costs to acquire nitrogen based on the sum of carbon costs to acquire nitrogen  
**348** via nitrogen fixation, mycorrhizal active uptake, non-mycorrhizal active uptake,  
**349** and retranslocation (Fisher et al. 2010; Brzostek et al. 2014). Carbon costs to  
**350** acquire nitrogen via mycorrhizal or non-mycorrhizal active uptake pathways are  
**351** derived as a function of nitrogen availability, root biomass, and two parameterized  
**352** values based on nitrogen acquisition strategy (Brzostek et al. 2014). Due to this,  
**353** FUN simulates a net decrease in carbon costs to acquire nitrogen with increasing  
**354** nitrogen availability for mycorrhizal and non-mycorrhizal active uptake pathways,  
**355** assuming constant root biomass. This was a pattern we observed in *G. hirsutum*  
**356** regardless of light availability. In contrast, FUN would not simulate a net change  
**357** in carbon costs to acquire nitrogen via nitrogen fixation due to nitrogen avail-  
**358** ability. This is because carbon costs to acquire nitrogen via nitrogen fixation are  
**359** derived from a well-established function of soil temperature, which is independent  
**360** of soil nitrogen availability (Houlton et al. 2008; Fisher et al. 2010). We observed  
**361** a net reduction in carbon costs to acquire nitrogen in *G. max*, except when in-  
**362** dividuals were grown under 0% shade cover (Fig. 2.1). While a net reduction of  
**363** carbon costs in response to nitrogen fertilization runs counter to nitrogen fixa-  
**364** tion carbon costs simulated by FUN, these patterns were likely because *G. max*  
**365** individuals switched their primary mode of nitrogen acquisition from symbiotic  
**366** nitrogen fixation to a non-symbiotic active uptake pathway (Fig. 2.4B).

**367** It should be noted that the metric used in this study to determine carbon

368 costs to acquire nitrogen has several limitations. Most notably, this metric uses  
369 root carbon biomass as a proxy for estimating the amount of carbon spent on  
370 nitrogen acquisition. While it is true that most carbon allocated belowground  
371 has at least an indirect structural role in acquiring soil resources, it remains un-  
372 clear whether this assumption holds true for species that acquire nitrogen via  
373 symbiotic nitrogen fixation. We also cannot quantify carbon lost through root  
374 exudates or root turnover, which may increase due to factors that increase plant  
375 nitrogen demand (Tingey et al. 2000; Phillips et al. 2011), and can increase the  
376 magnitude of available nitrogen from soil organic matter through priming effects  
377 on soil microbial communities (Uselman et al. 2000; Bengtson et al. 2012). It is  
378 also not clear whether these assumptions hold under all environmental conditions,  
379 such as those that shift belowground carbon allocation toward a different mode of  
380 nitrogen acquisition (Taylor and Menge 2018; Friel and Friesen 2019) or between  
381 species with different acquisition strategies. In this study, increasing soil nitrogen  
382 fertilization increased carbon investment to roots relative to carbon transferred  
383 to root nodules (Fig. 2.4B). By assuming that carbon allocated to root carbon  
384 was proportional to carbon allocated to root nodules across all treatment com-  
385 binations, these observed responses to soil nitrogen fertilization were likely to be  
386 overestimated in *G. max*. We encourage future research to quantify these carbon  
387 fates independently.

388 Researchers conducting pot experiments must carefully choose pot volume  
389 to minimize the likelihood of pot volume-induced growth limitation (Poorter et al.  
390 2012). Poorter et al. (2012) indicate that researchers are likely to avoid growth  
391 limitations associated with pot volume if measurements are collected when the

392 plant biomass:pot volume ratio is less than  $1 \text{ g L}^{-1}$ . In this experiment, all treat-  
393 ment combinations in both species had biomass:pot volume ratios less than  $1 \text{ g}$   
394  $\text{L}^{-1}$  except for *G. max* and *G. hirsutum* that were grown under 0% shade cover  
395 and had received 630 ppm N. Specifically, *G. max* and *G. hirsutum* had average  
396 respective biomass:pot volume ratios of  $1.24 \pm 0.07 \text{ g L}^{-1}$  and  $1.34 \pm 0.13 \text{ g L}^{-1}$ , when  
397 grown under 0% shade cover and received 630 ppm N (Supplementary Tables S2,  
398 S3; Supplementary Fig. S1). If growth in this treatment combination was limited  
399 by pot volume, then individuals may have had larger carbon costs to acquire ni-  
400 trogen than would be expected if they were grown in larger pots. This pot volume  
401 induced growth limitation could cause a reduction in per-root nitrogen uptake as-  
402 sociated with more densely packed roots, which could reduce the positive effect  
403 of nitrogen fertilization on whole-plant nitrogen biomass relative to root carbon  
404 biomass (Poorter et al. 2012).

405 Growth limitation associated with pot volume provides a possible explana-  
406 tion for the marginally insignificant effect of increasing nitrogen fertilization on *G.*  
407 *max* carbon costs to acquire nitrogen when grown under 0% shade cover (Table  
408 2.3; Fig. 2.1). This is because the regression line describing the relationship be-  
409 tween carbon costs to acquire nitrogen and nitrogen fertilization in *G. max* grown  
410 under 0% shade cover would have flattened if growth limitation had caused larger  
411 than expected carbon costs to acquire nitrogen in the 0% shade cover, 630 ppm  
412 N treatment combination. This may have been exacerbated by the fact that *G.*  
413 *max* likely shifted relative carbon allocation from nitrogen fixation to soil nitrogen  
414 acquisition, which could have increased the negative effect of more densely packed  
415 roots on nitrogen uptake. These patterns could have also occurred in *G. hirsutum*

416 grown under 0% shade cover; however, there was no change in the effect of nitro-  
417 gen fertilization on *G. hirsutum* carbon costs to acquire nitrogen grown under 0%  
418 shade cover relative to other shade cover treatments. Regardless, the possibility  
419 of growth limitation due to pot volume suggests that effects of increasing nitro-  
420 gen fertilization on carbon costs to acquire nitrogen in both species grown under  
421 0% shade cover could have been underestimated. Follow-up studies using a simi-  
422 lar experimental design with a larger pot volume would be necessary in order to  
423 determine whether these patterns were impacted by pot volume-induced growth  
424 limitation.

425 In conclusion, this study provides empirical evidence that carbon costs to  
426 acquire nitrogen are influenced by light availability and soil nitrogen fertilization  
427 in a species capable of acquiring nitrogen via symbiotic nitrogen fixation and a  
428 species not capable of forming such associations. We show that carbon costs to  
429 acquire nitrogen generally increase with increasing light availability and decrease  
430 with increasing nitrogen fertilization. This study provides important empirical  
431 data needed to evaluate the formulation of carbon costs to acquire nitrogen in  
432 terrestrial biosphere models, particularly carbon costs to acquire nitrogen that  
433 are associated with symbiotic nitrogen fixation. Our findings broadly support  
434 the general formulation of these carbon costs in the FUN biogeochemical model  
435 in response to shifts in nitrogen availability. However, there is a need for future  
436 studies to explicitly quantify carbon costs to acquire nitrogen under different en-  
437 vironmental contexts, over longer temporal scales, and using larger selections of  
438 phylogenetically related species. In addition, we suggest that future studies mini-  
439 mize the limitations associated with the metric used here by explicitly measuring

**440** belowground carbon fates independently.

441

## Chapter 3

442 Soil nitrogen availability modifies leaf nitrogen economies in mature  
443 temperate deciduous forests: a direct test of photosynthetic least-cost  
444 theory

445 3.1 Introduction

446 Photosynthesis represents the largest carbon flux between the atmosphere  
447 and land surface (IPCC 2021), and plays a central role in biogeochemical cycling  
448 at multiple spatial and temporal scales (Vitousek and Howarth 1991; LeBauer and  
449 Treseder 2008; Kaiser et al. 2015; Wieder et al. 2015). Therefore, carbon and  
450 energy fluxes simulated by terrestrial biosphere models are sensitive to the formu-  
451 lation of photosynthetic processes (Ziehn et al. 2011; Bonan et al. 2011; Booth  
452 et al. 2012; Smith et al. 2016; Smith et al. 2017) and must be represented using  
453 robust, empirically tested processes (Prentice et al. 2015; Wieder et al. 2019).  
454 Current formulations of photosynthesis vary across terrestrial biosphere models  
455 (Smith and Dukes 2013; Rogers et al. 2017), which causes variation in modeled  
456 ecosystem processes (Knorr 2000; Knorr and Heimann 2001; Bonan et al. 2011;  
457 Friedlingstein et al. 2014) and casts uncertainty on the ability of these models to  
458 accurately predict terrestrial ecosystem responses and feedbacks to global change  
459 (Zaehle et al. 2005; Schaefer et al. 2012; Davies-Barnard et al. 2020).

460 Terrestrial biosphere models commonly represent C<sub>3</sub> photosynthesis through  
461 variants of the Farquhar et al. (1980) biochemical model (Smith and Dukes 2013;  
462 Rogers 2014; Rogers et al. 2017). This well-tested photosynthesis model es-  
463 timates leaf-level carbon assimilation, or photosynthetic capacity, as a function  
464 of the maximum rate of Ribulose-1,5-bisphosphate carboxylase-oxygenase (Ru-

465 bisco) carboxylation ( $V_{cmax}$ ) and the maximum rate of Ribulose-1,5-bisphosphate  
466 (RuBP) regeneration ( $J_{max}$ ) (Farquhar et al. 1980). Many terrestrial biosphere  
467 models predict these model inputs based on plant functional group specific linear  
468 relationships between leaf nutrient content and  $V_{cmax}$  (Smith and Dukes 2013;  
469 Rogers 2014; Rogers et al. 2017) under the tenet that a large fraction of leaf  
470 nutrients, and nitrogen (N) in particular, are partitioned toward building and  
471 maintaining enzymes that support photosynthetic capacity, such as Rubisco (Brix  
472 1971; Gulmon and Chu 1981; Evans 1989; Kattge et al. 2009; Walker et al. 2014).  
473 Terrestrial biosphere models also predict leaf nutrient content from soil nutrient  
474 availability based on the assumption that increasing soil nutrients generally in-  
475 creases leaf nutrients (Firn et al. 2019; Li et al. 2020; Liang et al. 2020) which, in  
476 the case of N, generally corresponds with an increase in photosynthetic processes  
477 (Li et al. 2020; Liang et al. 2020).

478 Recent work calls the generality of relationships between soil nutrient avail-  
479 ability, leaf nutrient content, and photosynthetic capacity into question, suggest-  
480 ing instead that leaf nutrients and photosynthetic capacity are better predicted as  
481 an integrated product of aboveground climate, leaf traits, and soil nutrient avail-  
482 ability, rather than soil nutrient availability alone (Dong et al. 2017; Dong et al.  
483 2020; Dong et al. 2022; Firn et al. 2019; Smith et al. 2019; Peng et al. 2021).  
484 It has been reasoned that this result is because plants allocate added nutrients to  
485 growth and storage rather than alterations in leaf chemistry (Smith et al. 2019),  
486 perhaps as a result of nutrient limitation of primary productivity (LeBauer and  
487 Treseder 2008; Fay et al. 2015). Additionally, recent work suggests that relation-  
488 ships between leaf nutrient content and photosynthesis vary across environments,

489 and that the proportion of leaf nutrient content allocated to photosynthetic tis-  
490 sue varies over space and time with plant acclimation and adaptation responses  
491 to light availability, vapor pressure deficit, soil pH, soil nutrient availability, and  
492 environmental factors that influence leaf mass per area (Pons and Pearcy 1994;  
493 Niinemets and Tenhunen 1997; Evans and Poorter 2001; Hikosaka and Shigeno  
494 2009; Ghimire et al. 2017; Onoda et al. 2017; Luo et al. 2021). The use of linear  
495 relationships between leaf nutrient content and Vcmax to predict photosynthetic  
496 capacity, as commonly used in terrestrial biosphere models (Rogers 2014), is not  
497 capable of detecting such responses.

498 Photosynthetic least-cost theory provides an alternative framework for un-  
499 derstanding relationships between soil nutrient availability, leaf nutrient content,  
500 and photosynthetic capacity (Harrison et al. 2021). Leveraging a two-input mi-  
501 croeconomics approach (Wright et al. 2003), the theory posits that plants accli-  
502 mate to a given environment by optimizing leaf photosynthesis rates at the lowest  
503 summed cost of using nutrients and water (Prentice et al. 2014; Wang et al. 2017;  
504 Smith et al. 2019; Paillassa et al. 2020). Across resource availability gradients,  
505 the theory predicts that optimal photosynthetic rates can be achieved by trading  
506 less efficient use of a resource that is less costly to acquire (or more abundant)  
507 for more efficient use of a resource more costly to acquire (or less abundant). For  
508 example, an increase in soil nutrient availability should reduce the cost of acquir-  
509 ing and using nutrients (Bae et al. 2015; Eastman et al. 2021; Perkowski et al.  
510 2021), which could increase leaf nutrient investments in photosynthetic proteins to  
511 allow similar photosynthetic rates to be achieved with higher nutrient use (lower  
512 nutrient use efficiency) but lower water use (greater water use efficiency). The

513 theory suggests similar tradeoffs in response to increasing soil pH (Paillassa et al.  
514 2020), specifically, that increasing soil pH should reduce the cost of acquiring soil  
515 nutrients due to an increase in plant-available nutrient concentration (Paillassa  
516 et al. 2020; Dong et al. 2022). The theory is also capable of reconciling dynamic  
517 leaf nutrient-photosynthesis relationships at global scales (Luo et al. 2021).

518 Patterns expected from photosynthetic least-cost theory have recently re-  
519 ceived empirical support both in global environmental gradient (Smith et al.  
520 2019; Paillassa et al. 2020; Luo et al. 2021; Querejeta et al. 2022; Wester-  
521 band et al. 2023) and local manipulative invasion (Bialic-Murphy et al. 2021)  
522 studies. However, nutrient addition experiments that directly examine nutrient-  
523 water use tradeoffs expected from the theory are rare (Guerrieri et al. 2011), and  
524 only global gradient studies testing the theory have considered soil pH in their  
525 analyses. As a result, there is a need to use nutrient addition and soil pH manu-  
526 lation experiments to test mechanisms driving responses predicted by the theory.  
527 Such experiments would also be useful to detect whether patterns expected from  
528 theory translate to finer spatial scales.

529 In this study, we measured leaf responses to soil N availability in five decid-  
530 uous tree species growing in the upper canopy of mature closed canopy temperate  
531 forests in the northeastern United States. Soil N availability and pH were manip-  
532 ulated through a N-by-pH field manipulation experiment with treatments applied  
533 since 2011, eight years prior to measurement. Two different soil N treatments were  
534 applied to increase N availability with opposing effects on soil pH. An additional  
535 N-free acidifying treatment was expected to decrease soil pH. We hypothesized  
536 that increased soil N availability would enable plants to increase nutrient uptake

537 and create more photosynthetic enzymes per leaf, allowing similar photosynthetic  
538 rates achieved with lower leaf C<sub>i</sub>:C<sub>a</sub> and increased leaf N content allocated to  
539 photosynthetic leaf tissue. We expected that this response would be driven by a  
540 reduction in the cost of acquiring N, which would cause trees to sacrifice efficient  
541 N use to enable more efficient use of other limiting resources (i.e., water). We  
542 hypothesized similar leaf responses to increasing soil pH.

543 3.2 Methods

544 3.2.1 *Study site description*

545 We conducted this study in summer 2019 at three stands located within  
546 a 20-km radius of Ithaca, NY, USA (42.444 °N, 76.502 °W). All stands contain  
547 mature, closed-canopy forests dominated by deciduous tree species. Stands con-  
548 tained abundant sugar maple (*Acer saccharum* Marshall), American beech (*Fagus*  
549 *grandifolia* Ehrh.), and white ash (*Fraxinus americana* L.), accounting for 43%,  
550 15%, and 17% of the total aboveground biomass across the three stands, respec-  
551 tively, with less frequent red maple (*Acer rubrum* L.; 9% of total aboveground  
552 biomass) and red oak occurrences (*Quercus rubra* L.; 10% of total aboveground  
553 biomass). Soils at each site were broadly classified as a channery silt loam Incep-  
554 tisols using the USDA NRCS Web Soil Survey data product (Soil Survey Staff  
555 2022). Between 2006 and 2020, study sites averaged 972 mm of precipitation per  
556 year and had an average temperature of 7.9 °C per a weather station located near  
557 the Cornell University campus (42.449 °N, 76.449 °W) part of the NOAA NCEI  
558 Global Historical Climatology Network (Menne et al. 2012).

**559** 3.2.2 *Experimental design*

**560** Four 40 m x 40 m plots were set up at each site in 2009, each with an  
**561** additional 10 m buffer along plot perimeters (60 m x 60 m total). The plots  
**562** were set up as a nitrogen-by-pH field manipulation experiment, with one each of  
**563** four treatments at each site. Two nitrogen treatments were applied, both at 50  
**564** kg N ha<sup>-1</sup> yr<sup>-1</sup>, as either sodium nitrate (NaNO<sub>3</sub>) to raise soil pH, or ammonium  
**565** sulfate ((NH<sub>4</sub>)<sub>2</sub>SO<sub>4</sub>) to acidify; an elemental sulfur treatment was selected to acid-  
**566** ify without N, applied at the same rate of S addition (57 kg S ha<sup>-1</sup> yr<sup>-1</sup>); and  
**567** control plots received no additions. All amendments were added in pelletized form  
**568** using hand-held fertilizer spreaders to both the main plots and buffers. Amend-  
**569** ments were divided into three equal doses distributed across the growing season  
**570** from 2011-2017 and added as a single dose from 2018 onward. During 2019, plots  
**571** were fertilized during the week of May 20.

**572** 3.2.3 *Leaf gas exchange and trait measurements*

**573** We sampled one leaf each from 6 to 10 individuals per plot between June  
**574** 25 and July 12, 2019 for gas exchange measurements (Table S1). Leaves were  
**575** collected from deciduous broadleaf trees represented across all sites and plots and  
**576** were replicated in efforts to mimic the species abundance of each plot at each  
**577** site. We also attempted to collect leaves from the upper canopy to reduce differ-  
**578** ential shading effects on leaf physiology. Leaves were accessed by pulling down  
**579** small branches using an arborist's slingshot and weighted beanbag attached to a  
**580** throwline. Branches were immediately recut under deionized water and remained  
**581** submerged to reduce stomatal closure and avoid xylem embolism (as in Smith &

582 Dukes, 2018) until gas exchange data were collected.

583 Randomly selected leaves with little to no visible external damage were  
584 attached to a Li-COR LI-6800 (Li-COR Bioscience, Lincoln, Nebraska, USA)  
585 portable photosynthesis machine to measure net photosynthesis ( $A_{\text{net}}$ ;  $\mu\text{mol m}^{-2} \text{s}^{-1}$ ),  
586 stomatal conductance ( $g_{\text{sw}}$ ;  $\text{mol m}^{-2} \text{s}^{-1}$ ), and intercellular  $\text{CO}_2$  concentration  
587 ( $C_i$ ;  $\mu\text{mol mol}^{-1}$ ) at different reference  $\text{CO}_2$  concentrations ( $C_a$ ;  $\mu\text{mol mol}^{-1}$ )  
588 concentrations (i.e., an  $A_{\text{net}}/C_i$  curve) under saturating light conditions (2,000  
589  $\mu\text{mol m}^{-2} \text{s}^{-1}$ ). Reference  $\text{CO}_2$  concentrations followed the sequence: 400, 300,  
590 200, 100, 50, 400, 400, 600, 800, 1000, 1200, 1500, and 2000  $\mu\text{mol mol}^{-1} \text{CO}_2$ . Leaf  
591 temperatures were not controlled in the cuvette and ranged from 21.8 °C to 31.7  
592 °C (mean±SD:  $27.2 \pm 2.2$  °C). A linear and second order log-polynomial nonlinear  
593 regression suggested no effect of temperature on stomatal conductance measured  
594 at 400  $\mu\text{mol mol}^{-1} \text{CO}_2$  or net photosynthesis measured at  $\mu\text{mol mol}^{-1} \text{CO}_2$  (Ta-  
595 ble S2-3; Fig. S1). All  $A_{\text{net}}/C_i$  curves were generated within one hour of branch  
596 severance.

597 Leaf morphological and chemical traits were collected on the same leaf used  
598 to generate each  $A_{\text{net}}/C_i$  curve. Images of each leaf were taken using a flat-bed  
599 scanner to determine fresh leaf area using the ‘LeafArea’ R package (Katabuchi  
600 2015), which automates leaf area calculations using ImageJ software (Schneider  
601 et al. 2012). Each leaf was dried at 65°C for at least 48 hours, weighed, and  
602 ground using a Retsch MM200 ball mill grinder (Verder Scientific, Inc., Newtown,  
603 PA, USA) until homogenized. Leaf mass per area ( $M_{\text{area}}$ ,  $\text{g m}^{-2}$ ) was calculated  
604 as the ratio of dry leaf biomass to fresh leaf area. Using a subsample of ground and  
605 homogenized leaf biomass, leaf N content ( $N_{\text{mass}}$ ;  $\text{gN g}^{-1}$ ) and leaf  $\delta^{13}\text{C}$  (‰, rela-

**606** tive to VPDB) were measured at the Cornell Stable Isotope Lab with an elemental  
**607** analyzer (NC 2500, CE Instruments, Wigan, UK) interfaced to an isotope ratio  
**608** mass spectrometer (Delta V Isotope Ratio Mass Spectrometer, ThermoFisher Sci-  
**609** entific, Waltham, MA, USA). Leaf N content per unit leaf area ( $N_{\text{area}}$ ; gN m<sup>-2</sup>)  
**610** was calculated by multiplying  $N_{\text{mass}}$  by  $M_{\text{area}}$ .

**611** We used leaf  $\delta^{13}\text{C}$  values to estimate  $\chi$  (unitless), which is an isotope-  
**612** derived estimate of the leaf  $C_i:C_a$  ratio. While intercellular and atmospheric CO<sub>2</sub>  
**613** concentrations were directly measured during each  $A_{\text{net}}/C_i$  curve, deriving  $\chi$  from  
**614**  $\delta^{13}\text{C}$  provides a more integrative estimate of the  $C_i:C_a$  over an individual leaf's  
**615** lifespan. We derived  $\chi$  following the approach of Farquhar et al. (1989) described  
**616** in Cernusak et al. (2013):

$$\chi = \frac{\Delta^{13}\text{C} - a}{b - a} \quad (3.1)$$

**617** where  $\Delta^{13}\text{C}$  represents the relative difference between leaf  $\delta^{13}\text{C}$  (‰) and air  $\delta^{13}\text{C}$   
**618** (‰), and is calculated from the following equation:

$$\Delta^{13}\text{C} = \frac{\delta^{13}\text{C}_{\text{air}} - \delta^{13}\text{C}_{\text{leaf}}}{1 + \delta^{13}\text{C}_{\text{leaf}}} \quad (3.2)$$

**619** where  $\delta^{13}\text{C}_{\text{air}}$  is assumed to be -8‰ (Keeling et al. 1979; Farquhar et al. 1989), a  
**620** represents the fractionation between <sup>12</sup>C and <sup>13</sup>C due to diffusion in air, assumed  
**621** to be 4.4‰, and b represents the fractionation caused by Rubisco carboxylation,  
**622** assumed to be 27‰ (Farquhar et al. 1989).

**623** 3.2.4  $A_{net}/C_i$  curve-fitting and parameter estimation

**624** We fit  $A_{net}/C_i$  curves of each individual using the ‘fitaci’ function in the  
**625** ‘plantecophys’ R package (Duursma 2015). This function estimates the maximum  
**626** rate of Rubisco carboxylation  $V_{cmax}$ ;  $\mu\text{mol m}^{-2} \text{s}^{-1}$ ) and maximum rate of electron  
**627** transport for RuBP regeneration ( $J_{max}$ ;  $\mu\text{mol m}^{-2} \text{s}^{-1}$ ) based on the Farquhar,  
**628** von Caemmerer, and Berry biochemical model of C<sub>3</sub> photosynthesis (Farquhar  
**629** et al. 1980). For each curve fit, we included triose phosphate utilization (TPU)  
**630** limitation to avoid underestimating  $J_{max}$  (Gregory et al. 2021). Curves were  
**631** visually examined to confirm the likely presence of TPU limitation.

**632** We determined Michaelis-Menten coefficients for Rubisco affinity to CO<sub>2</sub>  
**633** ( $K_c$ ;  $\mu\text{mol mol}^{-1}$ ) and O<sub>2</sub> ( $K_o$ ;  $\mu\text{mol mol}^{-1}$ ), and the CO<sub>2</sub> compensation point  
**634** ( $\Gamma^*$ ;  $\mu\text{mol mol}^{-1}$ ) using leaf temperature and equations described in Medlyn et al.  
**635** (2002) and derived in Bernacchi et al. (2001). Specifically,  $K_c$  and  $K_o$  were  
**636** calculated as:

$$K_c = 404.9 * \exp^{\frac{79430(T_k - 298)}{298RT_k}} \quad (3.3)$$

**637** and

$$K_o = 278.4 * \exp^{\frac{36380(T_k - 298)}{298RT_k}} \quad (3.4)$$

**638** while  $\Gamma^*$  was calculated as:

$$\Gamma^* = 42.75 * \exp^{\frac{37830(T_k - 298)}{298RT_k}} \quad (3.5)$$

**639** In all three equations,  $T_k$  is the leaf temperature (in Kelvin) during each  $A_{\text{net}}/C_i$

**640** curve and R is the universal gas constant ( $8.314 \text{ J mol}^{-1} \text{ K}^{-1}$ ).

**641** We standardized  $V_{\text{cmax}}$  and  $J_{\text{max}}$  estimates to  $25^\circ\text{C}$  using a modified Ar-

**642** rhenius equation (Kattge and Knorr 2007):

$$k_{25} = \frac{k_{\text{obs}}}{e^{\frac{H_a(T_{\text{obs}} - T_{\text{ref}})}{T_{\text{ref}}RT_{\text{obs}}}} * \frac{1+e^{\frac{T_{\text{ref}}\Delta S - H_d}{T_{\text{obs}}}}}{1+e^{\frac{T_{\text{obs}}\Delta S - H_d}{T_{\text{obs}}}}}} \quad (3.6)$$

**643**  $k_{25}$  represents the standardized  $V_{\text{cmax}}$  or  $J_{\text{max}}$  rate at  $25^\circ\text{C}$ ,  $k_{\text{obs}}$  represents

**644** the  $V_{\text{cmax}}$  or  $J_{\text{max}}$  estimate at the average leaf temperature measured inside the

**645** cuvette during the  $A_{\text{net}}/C_i$  curve.  $H_a$  is the activation energy of  $V_{\text{cmax}}$  ( $71,513$

**646**  $\text{J mol}^{-1}$ ) Kattge and Knorr (2007) or  $J_{\text{max}}$  ( $49,884 \text{ J mol}^{-1}$ ) (Kattge and Knorr

**647** 2007).  $H_d$  represents the deactivation energy of both  $V_{\text{cmax}}$  and  $J_{\text{max}}$  ( $200,000 \text{ J}$

**648**  $\text{mol}^{-1}$ ) (Medlyn et al. 2002), and R represents the universal gas constant ( $8.314$

**649**  $\text{J mol}^{-1} \text{ K}^{-1}$ ).  $T_{\text{ref}}$  represents the standardized temperature of  $298.15 \text{ K}$  ( $25^\circ\text{C}$ )

**650** and  $T_{\text{obs}}$  represents the mean leaf temperature (in K) during each  $A_{\text{net}}/C_i$  curve.

**651**  $\Delta S$  is an entropy term that (Kattge and Knorr 2007) derived as a linear relation-

**652** ship with average growing season temperature ( $T_g$ ;  $^\circ\text{C}$ ), where:

$$\Delta S_{vcmax} = -1.07 T_g + 668.39 \quad (3.7)$$

**653** and

$$\Delta S_{jmax} = -0.75 T_g + 659.70 \quad (3.8)$$

**654** We estimated  $T_g$  in Equations 3.7 and 3.8 based on mean daily (24-hour) air  
**655** temperature of the 30 days leading up to the day of each sample collection using  
**656** the same weather station reported in the site description. We then used  $V_{cmax25}$   
**657** and  $J_{max25}$  estimates to calculate the ratio of  $J_{max25}$  to  $V_{cmax25}$  ( $J_{max25}:V_{cmax25}$ ;  
**658** unitless).

**659** 3.2.5 *Proportion of leaf nitrogen allocated to photosynthesis and structure*

**660** We used equations from Niinemets and Tenhunen (1997) to estimate the  
**661** proportion of leaf N content allocated to Rubisco and bioenergetics. The propor-  
**662** tion of leaf N allocated to Rubisco ( $\rho_{rub}$ ; gN gN $^{-1}$ ) was calculated as a function  
**663** of  $V_{cmax25}$  and  $N_{area}$ :

$$\rho_{rubisco} = \frac{V_{cmax25} N_r}{V_{cr} N_{area}} \quad (3.9)$$

**664** where  $N_r$  is the amount of nitrogen in Rubisco, set to 0.16 gN (gN in Rubisco) $^{-1}$   
**665** and  $V_{cr}$  is the maximum rate of RuBP carboxylation per unit Rubisco protein,  
**666** set to 20.5  $\mu$ mol CO $_2$  (g Rubisco) $^{-1}$ . The proportion of leaf nitrogen allocated to  
**667** bioenergetics ( $\rho_{bioe}$ ; gN gN $^{-1}$ ) was similarly calculated as a function of  $J_{max25}$  and  
**668**  $N_{area}$ :

$$\rho_{bioe} = \frac{J_{max25} N_b}{J_{mc} N_{area}} \quad (3.10)$$

**669** where  $N_b$  is the amount of nitrogen in cytochrome f, set to 0.12407 gN ( $\mu$ mol  
**670** cytochrome f) $^{-1}$  assuming a constant 1: 1: 1.2 cytochrome f: ferredoxin NADP  
**671** reductase: coupling factor molar ratio (Evans and Seemann 1989; Niinemets and

**672** Tenhunen 1997), and  $J_{mc}$  is the capacity of electron transport per cytochrome f,  
**673** set to  $156 \mu\text{mol electron} (\mu\text{mol cytochrome f})^{-1}\text{s}^{-1}$ .

**674** We estimated the proportion of leaf N content allocated to photosynthetic  
**675** tissue ( $\rho_{photo}$ ; gN gN<sup>-1</sup>) as the sum of  $\rho_{rub}$  and  $\rho_{bioe}$ . This calculation is an un-  
**676** derestimate of the proportion of leaf N allocated to photosynthetic tissue because  
**677** it does not include N allocated to light harvesting proteins. This leaf N pool was  
**678** not included because we did not perform chlorophyll extractions on focal leaves.  
**679** However, the proportion of leaf N content allocated to light harvesting proteins  
**680** tends to be small relative to  $\rho_{rub}$  and  $\rho_{bioe}$ , and may scale with changes in  $\rho_{rub}$   
**681** and  $\rho_{bioe}$  (Niinemets and Tenhunen 1997).

**682** Finally, we estimated the proportion of leaf N content allocated to struc-  
**683** tural tissue ( $\rho_{str}$ ; gN gN<sup>-1</sup>) using an empirical equation from Onoda et al. (2017):

$$N_{cw} = 0.000355 * M_{area}^{1.39} \quad (3.11)$$

**684** where  $N_{cw}$  is the leaf N content allocated to cell walls (gN m<sup>-2</sup>).  $\rho_{str}$  was estimated  
**685** by dividing  $N_{cw}$  by  $N_{area}$ .

**686** 3.2.6 *Tradeoffs between nitrogen and water use*

**687** Photosynthetic nitrogen use efficiency (PNUE;  $\mu\text{mol CO}_2 \text{ mol}^{-1} \text{ N s}^{-1}$ )  
**688** was calculated by dividing  $A_{net}$  by  $N_{area}$ , first converting  $N_{area}$  to mol N m<sup>-2</sup>  
**689** using the molar mass of N (14 g mol<sup>-1</sup>). We used  $\chi$  as an indicator of water  
**690** use efficiency, which exploratory analyses suggest had similar responses to soil N  
**691** availability and pH as intrinsic water use efficiency measured from gas exchange

692 ( $A_{\text{net}}/g_s$ ). Tradeoffs between nitrogen and water use were determined by cal-  
693 culating the ratio of  $N_{\text{area}}$  to  $\chi$  ( $N_{\text{area}}:\chi$ ; g N m<sup>-2</sup>) and  $V_{\text{cmax25}}$  to  $\chi$  ( $V_{\text{cmax25}}:\chi$ ;  
694  $\mu\text{mol m}^{-2} \text{s}^{-1}$ ). This approach is similar to tradeoff calculations in which nitrogen-  
695 water use tradeoffs are measured as the ratio of  $N_{\text{area}}$  or  $V_{\text{cmax25}}$  to  $g_s$  (Paillassa  
696 et al. 2020; Bialic-Murphy et al. 2021). In this study, we quantify these re-  
697 lationships using  $\chi$  in lieu of  $g_s$  because  $g_s$  rapidly changes with environmental  
698 conditions and therefore may have been altered by recent tree branch severance  
699 and/or placement in the cuvette.

700 3.2.7 *Soil nitrogen availability and pH*

701 To characterize soil N availability at the time of our leaf gas exchange  
702 measurements, we used mixed bed resin bags to quantify mobile ammonium-N  
703 and nitrate-N concentrations in each plot. Lycra mesh bags were filled with 5 g  
704 of Dowex® Marathon MR-3 hydrogen and hydroxide form resin (MilliporeSigma,  
705 Burlington, MA USA) and sealed with a zip tie. Each bag was activated by  
706 soaking in 0.5 M HCl for 20 minutes, then in 2 M NaCl until pH of the saline  
707 solution stabilized, as described in Allison et al. (2008). Five resin bags were  
708 inserted about 10 cm below the soil surface at each plot on June 25, 2019: one  
709 near each of the four plot corners and one near the plot center. All resin bags  
710 were collected 24 days later on July 19, 2019 and were frozen until extracted.

711 Prior to anion and cation extraction, each resin bag was rinsed with ul-  
712 trapure water (MilliQ IQ 7000; Millipore Sigma, Burlington, MA) to remove any  
713 surface soil residues. Anions and cations were extracted from surface-cleaned resin  
714 bags by individually soaking and shaking each bag in 100 mL of a 0.1 M HCl/2.0

715 M NaCl matrix for one hour. Using a microplate reader (Biotek Synergy H1;  
716 Biotek Instruments, Winooski, VT USA), nitrate-N concentrations were quanti-  
717 fied spectrophotometrically at 540 nm with the end product of a single reagent  
718 vanadium (III) chloride reaction (Doane and Horwáth 2003), and ammonium-N  
719 concentrations quantified at 650 nm with the end product of a modified phenol-  
720 hypochlorite reaction (Weatherburn 1967; Rhine et al. 1998). Both the single  
721 reagent vanadium (III) chloride and modified phenol-hypochlorite methodologies  
722 have been well established for determining nitrate-N and ammonium-N concen-  
723 trations in resin bag extracts (Arnone 1997; Allison et al. 2008). We used a  
724 series of negative and positive controls throughout each well plate to verify the  
725 accuracy and precision of our measurements, assaying each resin bag extract and  
726 control in triplicate. Soil N availability was estimated as the sum of the nitrate-N  
727 and ammonium-N concentration in each resin bag, normalized per g of resin and  
728 duration in the field ( $\mu\text{g N g}^{-1} \text{ resin d}^{-1}$ ), then subsequently averaged across all  
729 resin bags in a plot for a plot-level mean.

730 Soil pH was measured on 0-10 cm mineral soil samples collected prior to  
731 fertilization in 2019. Near each of the four plot corners, three 5.5 cm diameter soil  
732 cores were collected after first removing the forest floor where present. Each set  
733 of three cores was placed in a plastic bag, and later composited by hand mixing  
734 and sieved to 4mm. Soil pH was determined for a 1:2 soil:water slurry (10 g field-  
735 moist soil to 20 mL DI water) of each sample using an Accumet AB15 pH meter  
736 with flushable junction probe (Fisher Scientific; Hampton, NH, USA), and was  
737 estimated at the plot level as the mean soil pH within each plot.

**738** 3.2.8 *Statistical analyses*

**739** We built two separate series of linear mixed-effects models to explore effects  
**740** of soil N availability, soil pH, species, and leaf N content on leaf physiological  
**741** traits. In the first series of linear mixed-effects models, we explored the effect  
**742** of soil N availability, soil pH, and species on leaf N content, leaf photosynthesis,  
**743** stomatal conductance, and nitrogen-water use tradeoffs. Models included plot-  
**744** level soil N availability and plot-level soil pH as continuous fixed effects, species  
**745** as a categorical fixed effect, and site as a categorical random intercept term.  
**746** Interaction terms between fixed effects were not included due to the small number  
**747** of experimental plots. We built a series of separate models with this independent  
**748** variable structure to quantify individual effects of soil N availability, soil pH,  
**749** and species on  $N_{\text{area}}$ ,  $M_{\text{area}}$ ,  $N_{\text{mass}}$ ,  $A_{\text{net}}$ ,  $V_{\text{cmax25}}$ ,  $J_{\text{max25}}$ ,  $J_{\text{max25}}:V_{\text{cmax25}}$ ,  $\rho_{\text{rubisco}}$ ,  
**750**  $\rho_{\text{bioenergetics}}$ ,  $\rho_{\text{photo}}$ ,  $\rho_{\text{structure}}$ ,  $\chi$ , PNUE,  $N_{\text{area}}:\chi$ , and  $V_{\text{cmax25}}:\chi$ .

**751** A second series of linear mixed-effects models were built to investigate  
**752** relationships between leaf N content and photosynthetic parameters. Statistical  
**753** models included  $N_{\text{area}}$  as a single continuous fixed effect with species and site des-  
**754** ignated as individual random intercept terms. We used this independent variable  
**755** structure to quantify individual effects of leaf N content on  $A_{\text{net}}$ ,  $V_{\text{cmax25}}$ ,  $J_{\text{max25}}$ ,  
**756**  $J_{\text{max25}}:V_{\text{cmax25}}$ , and  $\chi$ .

**757** For all linear mixed-effects models, we used Shapiro-Wilk tests of normal-  
**758** ity to determine whether linear mixed-effects models satisfied residual normality  
**759** assumptions. If residual normality assumptions were not met, then models were  
**760** fit using dependent variables that were natural log transformed. If residual nor-  
**761** mality assumptions were still not met (Shapiro-Wilk:  $p < 0.05$ ), then models were

762 fit using dependent variables that were square root transformed. All residual nor-  
763 mality assumptions for both sets of models that did not originally satisfy residual  
764 normality assumptions were met with either a natural log or square root data  
765 transformation (Shapiro-Wilk:  $p > 0.05$  in all cases).

766 In the first series of models, models for  $N_{\text{area}}$ ,  $M_{\text{area}}$ ,  $N_{\text{mass}}$ ,  $V_{\text{cmax25}}$ ,  $J_{\text{max25}}$ ,  
767  $\chi$ ,  $N_{\text{area}}:\chi$ , and  $V_{\text{cmax25}}:\chi$ ,  $\rho_{\text{rubisco}}$ ,  $\rho_{\text{bioenergetics}}$ ,  $\rho_{\text{photo}}$ ,  $\rho_{\text{structure}}$  satisfied residual  
768 normality assumptions without data transformations (Shapiro-Wilk:  $p > 0.05$  in  
769 all cases). The model for  $J_{\text{max25}}:V_{\text{cmax25}}$  satisfied residual normality assumptions  
770 with a natural log data transformation, while models for  $A_{\text{net}}$  and PNUE each  
771 satisfied residual normality assumptions with square root data transformations.  
772 In the second series of models, models for  $V_{\text{cmax25}}$ ,  $J_{\text{max25}}$ ,  $\chi$ , and  $V_{\text{cmax25}}:\chi$  satisfied  
773 residual normality assumptions without data transformations (Shapiro-Wilk:  $p$   
774  $> 0.05$  in all cases). The model for  $J_{\text{max25}}:V_{\text{cmax25}}$  required a natural log data  
775 transformation and the model for  $A_{\text{net}}$  required a square root data transformation  
776 (Shapiro-Wilk:  $p > 0.05$  in both cases).

777 In all models, we used the ‘lmer’ function in the ‘lme4’ R package (Bates  
778 et al. 2015) to fit each model and the ‘Anova’ function in the ‘car’ R package (Fox  
779 and Weisberg 2019) to calculate Type II Wald’s  $\chi^2$  and determine the significance  
780 level ( $\alpha = 0.05$ ) of each fixed effect coefficient. Finally, we used the ‘emmeans’  
781 R package (Lenth, 2019) to conduct post-hoc comparisons using Tukey’s tests,  
782 where degrees of freedom were approximated using the Kenward-Roger approach  
783 (Kenward and Roger 1997). All analyses and plots were conducted in R version  
784 4.1.1 (R Core Team 2021)). All figure regression lines and associated 95% confi-  
785 dence interval error bars were plotted using predictions generated across the soil

**786** nitrogen availability gradient using the ‘emmeans’ R package (Lenth 2019).

**787** 3.3 Results

**788** 3.3.1 *Leaf N content*

**789** Increasing soil N availability generally increased  $N_{\text{area}}$  (Table 3.1; Fig.  
**790** 3.1a). This pattern was driven by an increase in  $N_{\text{mass}}$  (Table 3.1; Fig. 3.1c)  
**791** and a marginal increase in  $M_{\text{area}}$  (Table 3.1; Fig. 3.1e) with increasing soil N  
**792** availability. There was no effect of soil pH on  $N_{\text{area}}$ ,  $N_{\text{mass}}$ , or  $M_{\text{area}}$  (Table 3.1);  
**793** however, we did observe strong differences in  $N_{\text{area}}$  (Fig. 3.1b),  $N_{\text{mass}}$  (Fig. 3.1d),  
**794** and  $M_{\text{area}}$  (Fig. 3.1e) between species (Table 3.1).

**Table 3.1.** Effects of soil N availability, soil pH, and species on leaf N content per unit leaf area ( $N_{\text{area}}$ ), leaf N content per unit leaf mass ( $N_{\text{mass}}$ ), and leaf mass per unit leaf area ( $M_{\text{area}}$ )

	df	$N_{\text{area}}$			$N_{\text{mass}}$			$M_{\text{area}}$		
		Coefficient	$\chi^2$	p	Coefficient	$\chi^2$	p	Coefficient	$\chi^2$	p
Intercept	-	9.03E-01	-	-	1.68E+00	-	-	4.60E+01	-	-
Soil N	1	1.68E-02	11.990	<b>0.001</b>	1.25E-02	6.902	<b>0.009</b>	4.87E-01	4.143	<b>0.042</b>
Soil pH	1	9.28E-02	0.836	0.361	8.08E-02	0.663	0.415	4.05E+00	0.653	0.419
Species	4	-	72.128	<b>&lt;0.001</b>	-	35.074	<b>&lt;0.001</b>	-	29.869	<b>&lt;0.001</b>

\*Significance determined using Type II Wald  $\chi^2$  tests ( $\alpha = 0.05$ ). P-values  $< 0.05$  are in bold.

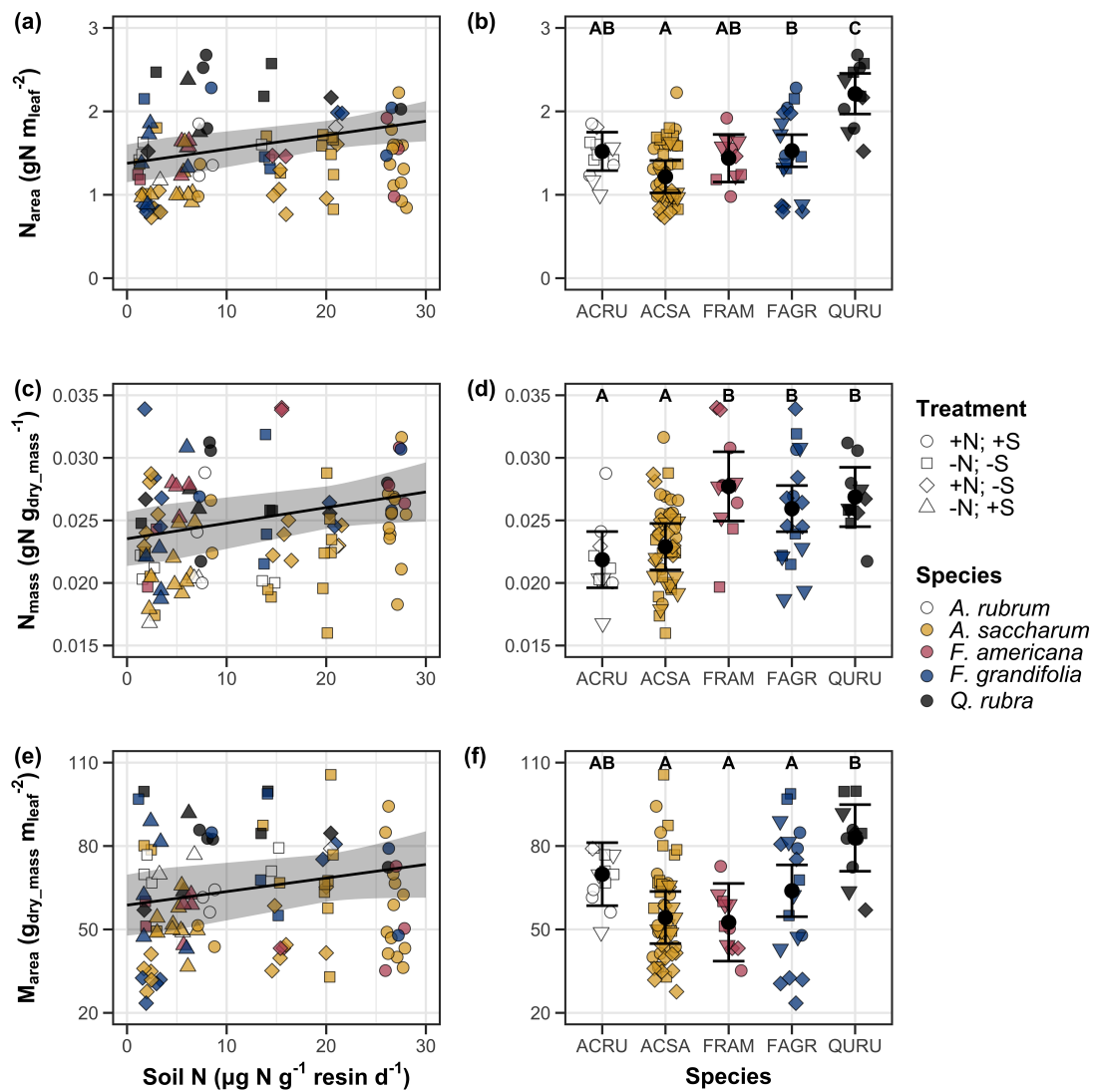


**Figure 3.1.** Effects of soil N availability and species on leaf N content per unit leaf area (a-b), leaf nitrogen content per unit leaf biomass (c-d), and leaf mass per unit leaf area (e-f). Soil N availability is represented on the x-axis in the left column of panels, while species is represented on the x-axis in the right column of panels. Tree species are represented as colored points and treatment plots are represented as shaped points, jittered for visibility. Species are abbreviated in the right column of panels through their assigned NRCS PLANTS Database symbol (USDA NRCS 2022), grouped along the x-axis per common mycorrhizal association, where the first three species commonly associate with arbuscular mycorrhizae (ACRU, ASCA, FAGR) and the second two species with ectomycorrhizae (FAGR, QURU). Trendlines are only included when the regression slope is statistically different from zero ( $p < 0.05$ ).

**795** 3.3.2 *Net photosynthesis and leaf biochemistry*

**796** Increasing soil N availability generally had no effect on  $A_{\text{net}}$ ,  $V_{\text{cmax25}}$ ,  $J_{\text{max25}}$ ,  
**797** or  $J_{\text{max25}}:V_{\text{cmax25}}$  (Table 3.2, Figs. 3.2a, 3.2d, 3.2g). We also observed strong  
**798** species effects on all measured leaf photosynthetic traits (Table 3.2; Figs. 3.2b,  
**799** 3.2e, 3.2h). Increasing soil pH had a marginal negative effect on  $A_{\text{net}}$ , but had no  
**800** effect on  $V_{\text{cmax25}}$ ,  $J_{\text{max25}}$ , or  $J_{\text{max25}}:V_{\text{cmax25}}$  (Table 3.2). There was a weak positive  
**801** effect of increasing  $N_{\text{area}}$  on  $A_{\text{net}}$  (Fig. 3.2c), but quite strong positive effects of  
**802** increasing  $N_{\text{area}}$  on  $V_{\text{cmax25}}$  and  $J_{\text{max25}}$  (Table 3.2; Fig. 3.2f and 3.2i).

**Table 3.2.** Effects of soil N availability, soil pH, species, and  $N_{\text{area}}$  on leaf biochemistry

	$A_{\text{net}}$			$V_{\text{cmax25}}$			$J_{\text{max25}}$			
	df	Coefficient	$\chi^2$	p	Coefficient	$\chi^2$	p	Coefficient	$\chi^2$	p
(Intercept)	-	3.29E+00 <sup>b</sup>	-	-	6.38E+01	-	-	1.12E+02	-	-
Soil N	1	-1.23E-03 <sup>b</sup>	1.798	0.180	-3.84E-01	1.745	0.187	-6.70E-01	2.172	0.141
Soil pH	1	-3.09E-01 <sup>b</sup>	3.312	0.069	-4.91E+00	0.655	0.418	-8.18E+00	0.742	0.389
Species	4	-	11.838	<b>0.019</b>	-	31.748	<0.001	-	27.291	<0.001
( $N_{\text{area}}$ int.)	-	6.59E-01 <sup>b</sup>	-	-	1.45E-01	-	-	2.86E+01	-	-
$N_{\text{area}}$	4	3.13E-01 <sup>b</sup>	4.790	<b>0.029</b>	2.43E+01	22.616	<0.001	4.04E+01	28.259	<0.001

	$J_{\text{max25}}:V_{\text{cmax25}}$			
	df	Coefficient	$\chi^2$	p
(Intercept)	-	6.59E-01 <sup>a</sup>	-	-
Soil N	1	7.04E-04 <sup>a</sup>	0.088	0.767
Soil pH	1	-7.84E-03 <sup>a</sup>	0.025	0.874
Species	4	-	12.745	<b>0.013</b>
( $N_{\text{area}}$ int.)	-	6.69E-01 <sup>a</sup>	-	-
$N_{\text{area}}$	4	-4.69E-02 <sup>a</sup>	1.142	0.285

\*Significance determined using Type II Wald  $\chi^2$  tests ( $\alpha = 0.05$ ).  $P$ -values  $< 0.05$  are in bold, while  $p$ -values between 0.05 and 0.1 are italicized. Superscript letters indicate model coefficients fit to natural-log (<sup>a</sup>) or square-root (<sup>b</sup>) transformed data. Relationships between  $N_{\text{area}}$  and each response variable were fit using the second series of bivariate mixed-effects models, so model coefficients and results are independent from model coefficients and results reported for relationships between soil N, soil pH, and species for each response variable. Key:  $A_{\text{net}}$  – light saturated net photosynthesis rate;  $V_{\text{cmax25}}$  – maximum rate of Rubisco carboxylation at 25°C;  $J_{\text{max25}}$  – maximum rate of electron transport for RuBP regeneration at 25°C,  $J_{\text{max25}}:V_{\text{cmax25}}$  – the ratio of  $J_{\text{max25}}$  to  $V_{\text{cmax25}}$ .

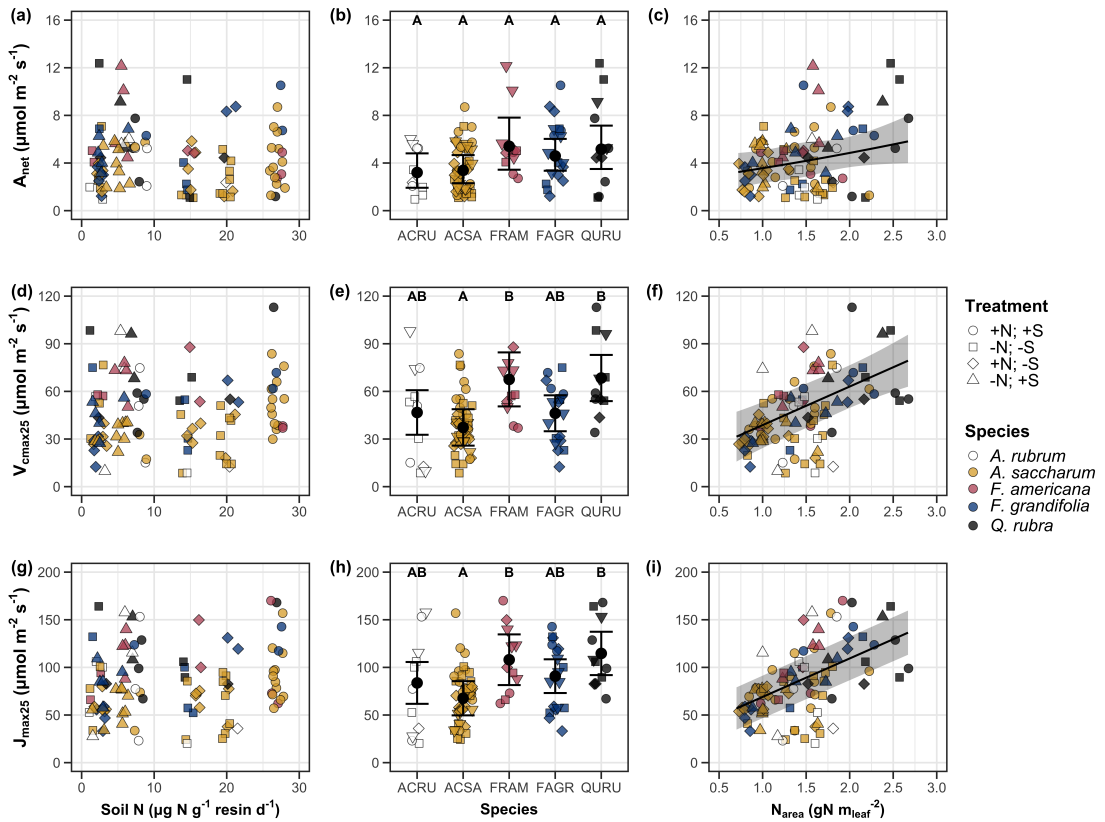


**Figure 3.2.** Effects of soil N availability (left column of panels), species (middle column of panels), and leaf N content per unit leaf area (right column of panels) on net photosynthesis (a-c), maximum Rubisco carboxylation rate (d-f), and maximum RuBP regeneration rate (g-i). Soil N availability is represented on the x-axis in the left column of panels, species is represented on the x-axis in the middle column of panels, and leaf N content per unit leaf area is represented continuously on the x-axis in the right column of panels. Species abbreviations and position along the x-axis in the middle column of panels, colored points, shapes, and trendlines are as explained in Figure 3.1.

**803** 3.3.3 *Leaf N allocation*

**804** Neither soil N availability nor soil pH affected the proportion of leaf N  
**805** allocated to Rubisco or bioenergetics (Table 3.3; Fig. 3.3a, Fig. 3.3c), nor was  
**806** there any subsequent effect on the proportion of leaf N allocated to photosynthesis  
**807** (Table 3.3; Fig. 3.3f). We also found no effect of soil N availability or soil pH on  
**808** the proportion of leaf N allocated to structure (Table 3.3; Fig 3.3g). Species varied  
**809** in the proportion of leaf N allocated to Rubisco, photosynthesis, and structure (Fig  
**810** 3.3b, Fig. 3.3d, Fig 3.3h), with no detectable species effect on the proportion of  
**811** leaf N allocated to bioenergetics (Table 3.3).

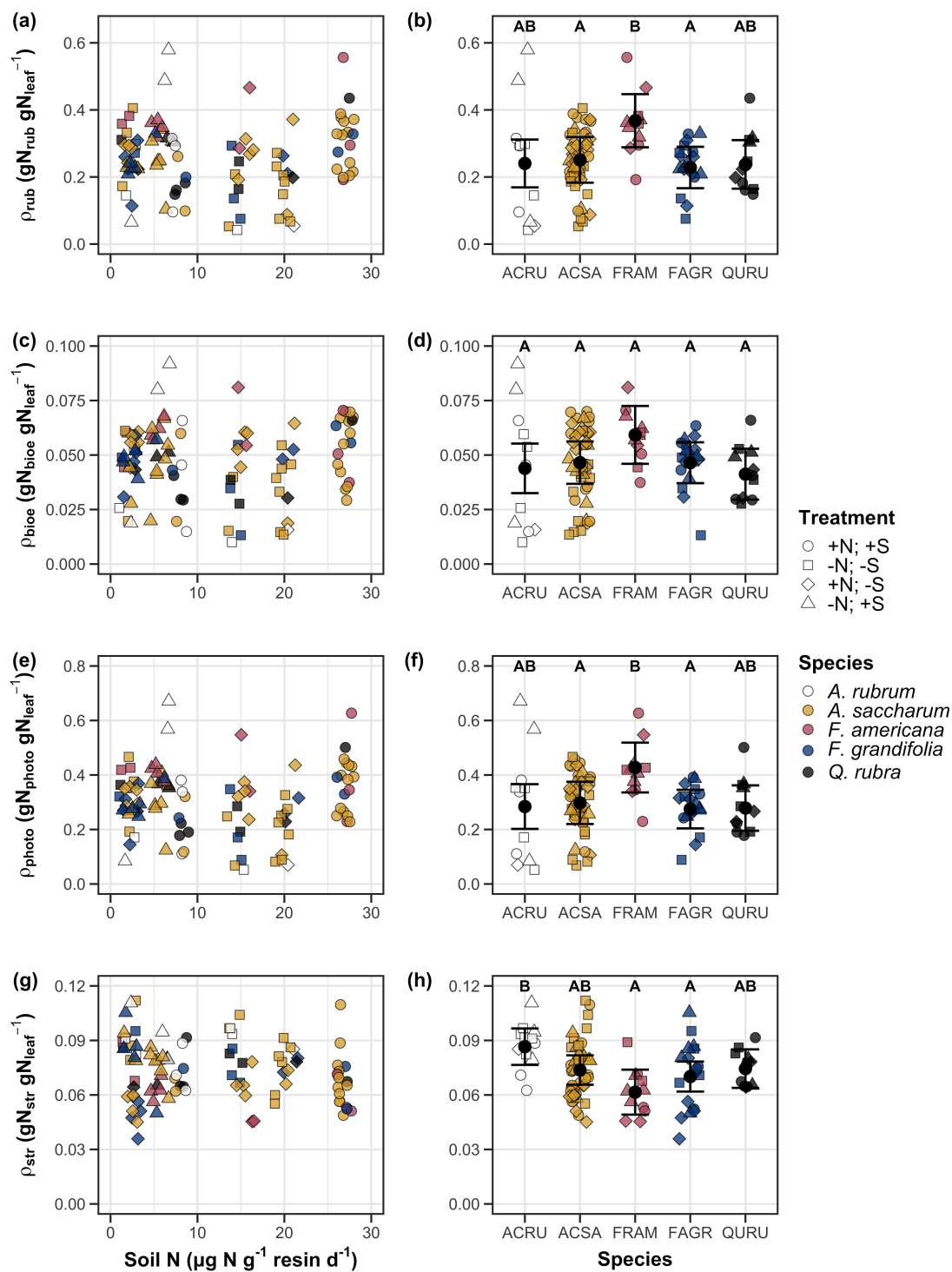
**Table 3.3.** Effects of soil N availability, soil pH, and species on the proportion of leaf nitrogen content allocated to photosynthesis, Rubisco, bioenergetics, and structure

	$\rho_{\text{photo}}$			$\rho_{\text{rub}}$			$\rho_{\text{bioe}}$			
	df	Coefficient	$\chi^2$	p	Coefficient	$\chi^2$	p	Coefficient	$\chi^2$	p
Intercept	-	4.93E-01	-	-	4.17E-01	-	-	7.64E-02	-	-
Soil N	1	-1.23E-03	0.521	0.470	-1.04E-03	0.501	0.479	-1.77E-04	0.557	0.455
Soil pH	1	-4.37E-02	1.581	0.209	-3.70E-02	1.511	0.219	-6.84E-03	1.941	0.164
Species	4	-	13.106	<b>0.011</b>	-	14.152	<b>0.007</b>	-	7.300	0.121

	$\rho_{\text{str}}$			
	df	Coefficient	$\chi^2$	p
Intercept	-	9.77E-02	-	-
Soil N	1	-2.29E-04	1.165	0.280
Soil pH	1	-1.87E-03	0.179	0.672
Species	4	-	16.428	<b>0.002</b>

\*Significance determined using Type II Wald  $\chi^2$  tests ( $\alpha = 0.05$ ). P-values  $< 0.05$  are in bold. Key:  $\rho_{\text{photo}}$  - proportion of leaf nitrogen content allocated to photosynthesis;  $\rho_{\text{rub}}$  - proportion of leaf nitrogen content allocated to Rubisco;  $\rho_{\text{bioe}}$  - proportion of leaf nitrogen content allocated to bioenergetics;  $\rho_{\text{str}}$  - proportion of leaf nitrogen content allocated to structure.



**Figure 3.3.** Effects of soil nitrogen availability and species on the proportion of leaf nitrogen content allocated to Rubisco (a-b), bioenergetics (c-d), photosynthesis (e-f), and structure (g-h)

**812** 3.3.4 *Tradeoffs between nitrogen and water use*

**813** Although soil N availability did not affect  $\chi$  (Table 3.4; Fig. 3.4a), increasing  
**814** soil N availability decreased PNUE (Table 3.4; Fig. 3.4d) and increased the  
**815** ratio of  $N_{\text{area}}:\chi$  (Table 3.4; Fig. 3.4f). Specifically, this response yielded a 26%  
**816** reduction in PNUE and 37% stimulation in  $N_{\text{area}}:\chi$  across the soil nitrogen avail-  
**817** ability gradient. There was no apparent effect of soil N availability on  $V_{\text{cmax25}}:\chi$   
**818** (Table 3.4; Fig. 3.4h). Increasing soil pH had a weak marginal negative effect  
**819** on PNUE, but did not influence  $\chi$ ,  $N_{\text{area}}:\chi$ , or  $V_{\text{cmax25}}:\chi$  (Table 3.4). We also  
**820** observed differences in  $\chi$  (Fig. 3.4b), PNUE (Fig. 3.4e),  $N_{\text{area}}:\chi$  (Fig. 3.4g), and  
**821**  $V_{\text{cmax25}}:\chi$  (Fig. 3.4i) between species (Table 3.4). Finally, increasing  $N_{\text{area}}$  had a  
**822** strong negative effect on  $\chi$  (Table 3.4; Fig. 3.4c) and a strong positive effect on  
**823**  $V_{\text{cmax25}}:\chi$  (Table 3.4; Fig. 3.4j).

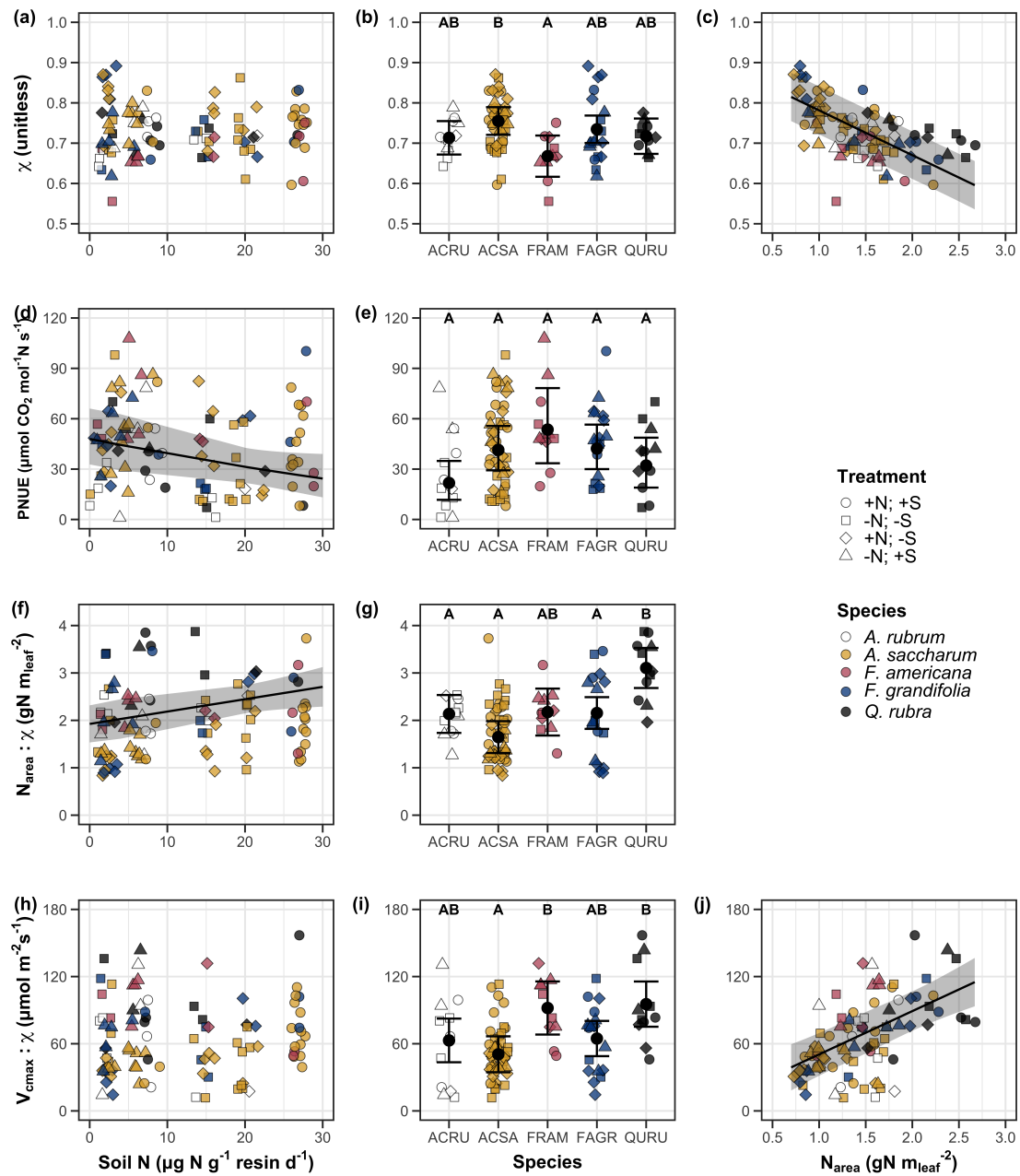
**Table 3.4.** Effects of soil N availability, soil pH, species, and  $N_{\text{area}}$  on tradeoffs between nitrogen and water use

	$\chi$			PNUE			$N_{\text{area}}:\chi$			
	df	Coefficient	$\chi^2$	p	Coefficient	$\chi^2$	p	Coefficient	$\chi^2$	p
(Intercept)	-	8.12E-01	-	-	9.57E+00	-	-	9.19E-01	-	-
Soil N	1	-1.14E-03	1.698	0.193	-6.63E-02	6.396	<b>0.011</b>	2.60E-02	9.533	<b>0.002</b>
Soil pH	1	-1.91E-02	1.087	0.297	-9.25E-01	2.843	<i>0.092</i>	2.03E-01	1.321	0.250
Species	4	-	18.843	<b>0.001</b>	-	13.454	<b>0.009</b>	-	52.983	<b>&lt;0.001</b>
( $N_{\text{area}}$ int.)	-	8.93E-01	-	-	-	-	-	-	-	-
$N_{\text{area}}$	1	-1.11E-01	80.606	<b>&lt;0.001</b>	-	-	-	-	-	-

	$V_{\text{cmax25}}:\chi$			
	df	Coefficient	$\chi^2$	p
(Intercept)	-	7.20E+01	-	-
Soil N	1	3.99E-01	0.963	0.326
Soil pH	1	-3.12E+00	0.138	0.711
Species	4	-	31.450	<b>&lt;0.001</b>
( $N_{\text{area}}$ int.)	-	1.18E+01	-	-
$N_{\text{area}}$	4	3.87E+01	32.797	<b>&lt;0.001</b>

\*Significance determined using Type II Wald  $\chi^2$  tests ( $\alpha = 0.05$ ).  $P$ -values  $< 0.05$  are in bold, while  $p$ -values between 0.05 and 0.1 are italicized. Superscript letters indicate model coefficients fit to natural-log <sup>(a)</sup> or square-root <sup>(b)</sup> transformed data. Relationships between  $N_{\text{area}}$  and each response variable were fit using the second series of bivariate mixed-effects models, so model coefficients and results are independent from model coefficients and results reported for relationships between soil N, soil pH, and species for each response variable. Key:  $\chi$  - isotope-derived estimate of the  $C_i:C_a$ ; PNUE - photosynthetic N use efficiency, ratio of net photosynthesis to leaf N content per unit leaf area;  $N_{\text{area}}:\chi$  - ratio of  $N_{\text{area}}$  to  $\chi$ ;  $V_{\text{cmax25}}:\chi$  - ratio of  $V_{\text{cmax25}}$  to  $\chi$ .



**Figure 3.4.** Effects of soil nitrogen availability and species on the proportion of leaf nitrogen content allocated to Rubisco (a-b), bioenergetics (c-d), photosynthesis (Rubisco + bioenergetics; e-f), and structure (g-h). Soil nitrogen availability is represented on the x-axis in the left column of panels and species are represented on the x-axis in the right column of panels. Species abbreviations and position along the x-axis in the middle column of panels, colored points, shapes, trendlines, error bars, and compact lettering are as explained in Figure 3.1.

**824** 3.4 Discussion

**825** Photosynthetic least-cost theory provides an explanation for understand-  
**826** ing relationships between soil nutrient availability, leaf nutrient allocation, and  
**827** photosynthetic capacity. The theory suggests that plants acclimate to a given  
**828** environment by optimizing leaf photosynthesis rates at the lowest summed cost  
**829** of using nutrients and water Prentice et al. (2014), Wang et al. (2017), Smith  
**830** et al. (2019), Paillassa et al. (2020). The theory predicts that an increase in  
**831** soil nutrient availability should allow similar photosynthesis rates to be achieved  
**832** with increased leaf nutrient content and photosynthetic capacity (i.e.,  $V_{cmax25}$  and  
**833**  $J_{max25}$ ) at lower leaf  $C_i:C_a$  ( $\chi$ ), resulting in an increase in water use efficiency,  
**834** decrease in nutrient use efficiency, and increase in both leaf nutrient content and  
**835** photosynthetic capacity per unit  $\chi$ . The theory predicts similar leaf responses to  
**836** increasing soil pH under acidic conditions, presumably due to generally faster nu-  
**837** trient cycle dynamics and consequent reductions in the cost of acquiring nutrients  
**838** relative to water with increasing soil pH (Wang et al. 2017; Paillassa et al. 2020;  
**839** Dong et al. 2020).

**840** Supporting the theory, we showed that increasing soil N availability was  
**841** associated with increased leaf N content (Fig 3.1a, 3.1c), a pattern that reduced  
**842** photosynthetic N use efficiency (Fig 3.4d) and increased leaf N content per unit  
**843**  $\chi$  (Fig 3.4f). Increasing soil N coincided with slight, but non-significant decreases  
**844** in  $\chi$  and increases in  $V_{cmax25}$  and  $J_{max25}$  ( $p < 0.2$ , Table 3.2). The positive trend  
**845** between soil N availability and photosynthetic capacity was supported by the con-  
**846** current strong increase in leaf N content with increasing soil N availability, which  
**847** resulted in no change in the proportion of leaf N content allocated to photosynthe-

848 sis across the soil N availability gradient. Additionally, leaf N content exhibited a  
849 strong negative correlation with  $\chi$ , indicative of strong nitrogen-water use trade-  
850 offs at the leaf level. Responses tended to vary more due to soil N availability  
851 than soil pH. Overall, these findings are consistent with the nutrient-water use  
852 tradeoffs predicted from theory.

853 3.4.1 *Soil nitrogen availability modifies tradeoffs between nitrogen and water use*

854 In support of expected least-cost outcomes and past environmental gradient  
855 studies (Dong et al. 2017; Paillassa et al. 2020), we found that increasing soil N  
856 availability was associated with increased leaf N content. Soil N availability had  
857 smaller impacts on measures of net photosynthesis and  $\chi$ , which led to reductions  
858 in PNUE and increases in leaf N content per unit  $\chi$ , as expected from theory.  
859 Photosynthetic least-cost theory suggests that reductions in PNUE should be  
860 driven by an increase in the proportion of leaf N allocated to photosynthetic tissue,  
861 a pattern that should allow plants to achieve optimal photosynthetic rates with  
862 greater photosynthetic capacity to make better use of available light. Contrasting  
863 theory predictions, we found no effect of soil N availability on photosynthetic  
864 capacity. However, photosynthetic capacity did tend to increase with increasing  
865 soil N availability ( $p < 0.20$ ; Table 3.2) resulting in no effect of soil N availability on  
866 the relative fraction of leaf N allocated to photosynthesis, Rubisco, or bioenergetics  
867 (Fig. 3.3). These lines of evidence support the idea that trees use additional N  
868 to support increased leaf N allocation toward photosynthetic tissue and enhance  
869 photosynthetic capacity (Wright et al. 2003).

870 Soil N availability had a stronger effect on leaf N than photosynthetic ca-

871 pacity. This pattern suggests that additional plant N uptake due to increased  
872 soil N availability was also being used to support non-photosynthetic N pools,  
873 possibly to structural tissue or stress-induced amino acid and polyamine synthe-  
874 sis (Minocha et al. 2000; Onoda et al. 2004; Bubier et al. 2011). While we  
875 found no change in the proportion of leaf N allocated to leaf structural tissue, the  
876 overall stimulation in leaf N content with increasing soil N availability suggests an  
877 increase in the net amount of N invested in leaf structural tissue along the N avail-  
878 ability gradient. Importantly, leaf N allocated to structure was calculated using  
879 an empirical relationship between  $M_{\text{area}}$  and the amount of leaf N allocated to cell  
880 walls (Onoda et al. 2017). As the generality of relationships between  $M_{\text{area}}$  and  
881 the amount of leaf N allocated to cell walls has been called into question (Harrison  
882 et al. 2009), future work should consider explicitly measuring N allocation to cell  
883 wall tissue and stress-induced amino acid synthesis to confirm these patterns.

884 In opposition to patterns expected from least cost theory, increasing soil  
885 N availability had no apparent effect on  $\chi$  (Fig. 3.4a). Interestingly, despite  
886 the null effect of soil N availability on  $\chi$ , we observed a strong negative effect of  
887 increasing  $N_{\text{area}}$  on  $\chi$  (Fig. 3.4c), consistent with the nitrogen-water use tradeoffs  
888 expected from theory. The null response of  $\chi$  to increasing soil N availability may  
889 have been due to a lack of water limitation in the system, given that the area  
890 received approximately 20% more precipitation (1167 mm) during the 12-month  
891 period leading up to our measurement period than normally expected (972 mm).  
892 However, droughts can and do occur in temperate forests of the northeastern  
893 United States (Sweet et al. 2017), so the observed increase in leaf N content  
894 with increasing soil N availability could be a strategy that allows trees to hedge

895 bets against drier than normal growing seasons (Onoda et al. 2004; Onoda et al.  
896 2017; Hallik et al. 2009). As was suggested in Paillassa et al. (2020), and more  
897 recently by Querejeta et al. (2022), negative effects of soil N availability on  $\chi$  may  
898 increase with increasing aridity. This strategy would be especially advantageous if  
899 it allows individuals growing in arid regions to maintain carbon assimilation rates  
900 with reduced water loss. Future work should attempt to quantify interactive roles  
901 of climate and soil nitrogen availability on nitrogen-water use tradeoffs, which  
902 could be done by leveraging coordinated and multi-factor nutrient (Borer et al.  
903 2014) and water (Knapp et al. 2017) manipulation experiments across broad  
904 climatic gradients.

905 3.4.2 *Soil pH did not modify tradeoffs between nitrogen and water usage*

906 While the primary purpose of this study was to examine the role of soil N  
907 availability on nitrogen-water use tradeoffs, our experimental design manipulated  
908 both soil N and pH, providing an opportunity to isolate the roles of these variables.  
909 Previous correlational studies along environmental gradients identified soil pH as  
910 a particularly important factor that can modify tradeoffs between nutrient and  
911 water use (Smith et al. 2019; Paillassa et al. 2020; Westerband et al. 2023)  
912 and the proportion of leaf nitrogen allocated to photosynthesis (Luo et al. 2021).  
913 Such studies implied that these patterns may be driven by reductions in the cost of  
914 acquiring nutrients relative to water with increasing pH, which may be exacerbated  
915 in acidic soils.

916 Consistent with theory (Wright et al. 2003; Prentice et al. 2014), our  
917 results indicate that increasing soil pH was negatively associated with PNUE.

918 However, there was no effect of soil pH on leaf N content,  $\chi$ , or leaf N content per  
919 unit  $\chi$ , most likely because the experimental N additions increased soil N sup-  
920 ply while both increasing (sodium nitrate) and decreasing (ammonium sulfate)  
921 soil pH. These results suggest that soil pH did not play a major role in modify-  
922 ing expected photosynthetic least-cost theory patterns, contrasting findings from  
923 Paillassa et al. (2020) and other gradient studies that note positive effects of in-  
924 creasing soil pH on leaf N content, Rubisco carboxylation, and  $\chi$  (Viet et al. 2013;  
925 Cornwell et al. 2018; Luo et al. 2021). Instead, null responses to soil pH show  
926 that leaf photosynthetic parameters depend more on soil N availability than pH  
927 per se, and that inferences from gradient studies might be confounding covariation  
928 between N availability and soil acidity.

929 3.4.3 *Species identity explains a large amount of variation in leaf and whole*  
930 *plant traits*

931 Species generally explained a larger amount of variation in measured leaf  
932 traits than soil N availability or soil pH. Interspecies variation is an important  
933 factor to consider when deducing mechanisms that drive photosynthetic least-  
934 cost theory, particularly for species that form distinct mycorrhizal associations or  
935 have different photosynthetic pathways, growth forms, or leaf habit (Espelta et al.  
936 2005; Adams et al. 2016; Bialic-Murphy et al. 2021; Scott and Smith 2022). The  
937 need to consider species may also be important when comparing nutrient-water  
938 use tradeoffs in early and late successional species, or in species with different  
939 resource economic strategies (Abrams and Mostoller 1995; Ellsworth and Reich  
940 1996; Wright et al. 2004; Reich 2014; Onoda et al. 2017; Ziegler et al. 2020).

941        A strength of the study design and sampling effort is that it controls for  
942        many species differences that should modify nitrogen-water use tradeoffs expected  
943        from theory. All tree species measured in this study shared the leaf habit of decid-  
944        uous broadleaves, were growing in forests of similar successional stage, but differed  
945        in mycorrhizal association and consequent resource economic strategies. As stands  
946        tended to be dominated by trees that associate with arbuscular mycorrhizae (*Frax-*  
947        *inus* and both *Acer* species made up 70% of total aboveground biomass across  
948        stands), ecosystem biogeochemical cycle dynamics may be more closely aligned  
949        to the inorganic nutrient economy proposed in Phillips et al. (2013), which may  
950        promote stronger nitrogen-water use tradeoffs in tree species that associate with  
951        arbuscular mycorrhizae. This result was not observed here, as photosynthetic  
952        properties varied as much within as across the two mycorrhizal associations rep-  
953        resented. Given the high variability in measured photosynthetic traits within  
954        and across species, effects of mycorrhizal association likely require more intensive  
955        sampling efforts to detect than were possible here.

956 3.4.4 *Implications for photosynthetic least-cost theory model development*

957        In the field, soil nutrient availability is heterogeneous across time and space  
958 (Table S4). Unaccounted within-plot heterogeneity may have contributed to the  
959 low amount of variation explained by soil N availability in our statistical mod-  
960 els, as resin bags are a coarse surrogate for soil N availability. Despite this, we  
961 still observed evidence for nutrient-water use tradeoffs, suggesting that observed  
962 responses reported here may be an underestimate toward the net effect of soil  
963 N availability on these tradeoffs. While we urge caution in the interpretation of

**964** these results, they do provide a promising baseline for future studies investigating  
**965** patterns expected from photosynthetic least-cost theory at finer spatiotemporal  
**966** resolutions.

**967** The general stronger relationship between leaf N content and photosynthetic parameters versus between leaf N content and soil N availability suggests  
**969** that leaf N content is more directly tied to photosynthesis than soil N availability.  
**970** While this could be due to the high spatiotemporal heterogeneity of soil N availability,  
**971** principles from photosynthetic least-cost theory suggest that leaf N content is the downstream product of leaf nutrient demand to build and maintain  
**973** photosynthetic machinery, which is set by aboveground environmental conditions  
**974** such as light availability, CO<sub>2</sub>, temperature, or vapor pressure deficit (Smith  
**975** et al. 2019; Paillassa et al. 2020; Peng et al. 2021; Westerband et al. 2023). The  
**976** stronger relationship between leaf N and photosynthetic parameters paired with  
**977** the strong negative relationship between leaf N and  $\chi$  could indicate a relatively  
**978** stronger effect of climate on leaf N-photosynthesis relationships than soil resource  
**979** availability. However, the short distance between plots and across sites limited  
**980** our ability to test this mechanism.

**981** Variation in soil pH affected least cost responses less than variations in  
**982** soil N availability, in part because experimental treatments directly increased soil  
**983** N and affected soil pH in opposite directions. While soil pH has been shown  
**984** to drive nitrogen-water tradeoffs in global gradient analyses (Viet et al. 2013;  
**985** Paillassa et al. 2020), these responses may be due to covariations between soil pH  
**986** and nutrient cycling rather than a role of pH per se. The direct manipulations  
**987** of soil pH and soil N availability in this study allowed us to partly disentangle

**988** these factors and show that variation in N availability matters more for least-cost  
**989** tradeoffs than pH alone.

**990** 3.4.5 *Conclusions*

**991** Increasing soil N availability generally increased leaf N content (both area-  
**992** and mass-based), but did not significantly influence  $\chi$ . This shift in leaf N led  
**993** to a reduction in PNUE, and an increase in leaf N per unit  $\chi$  with increasing  
**994** soil N availability. Despite null effects of soil N availability on  $\chi$ , we observed a  
**995** strong negative relationship between leaf N content and  $\chi$ . These results provide  
**996** empirical support for the nutrient-water use tradeoffs expected from photosyn-  
**997** thetic least-cost theory in response to soil nutrient availability, but suggest that  
**998** all tenets of the theory may not hold in every environment. These results exper-  
**999** imentially test previous work suggesting that leaf water-nitrogen economies vary  
**1000** across gradients of soil nutrient availability and pH, and show that variations in  
**1001** nutrient availability matter more for determining variation in leaf photosynthetic  
**1002** traits than soil pH.

1003

## Chapter 4

1004 The relative cost of resource use for photosynthesis drives variance in  
1005 leaf nitrogen content across climate and soil resource availability  
1006 gradients

1007 4.1 Introduction

1008 Terrestrial biosphere models, which comprise the land surface component of  
1009 Earth system models, are sensitive to the formulation of photosynthetic processes  
1010 (Knorr 2000; Ziehn et al. 2011; Booth et al. 2012). This is because photosynthe-  
1011 sis is the largest carbon flux between the atmosphere and terrestrial biosphere,  
1012 and is constrained by ecosystem carbon and nutrient cycles (Hungate et al. 2003;  
1013 LeBauer and Treseder 2008; IPCC 2021; Fay et al. 2015). Many terrestrial bio-  
1014 sphere models formulate photosynthesis by parameterizing photosynthetic capac-  
1015 ity within plant functional groups through empirical linear relationships between  
1016 area-based leaf nitrogen content ( $N_{\text{area}}$ ) and the maximum carboxylation rate  
1017 of Ribulose-1,5-bisphosphate carboxylase/oxygenase (Kattge et al. 2009; Rogers  
1018 2014; Rogers et al. 2017). Models are also beginning to include connected carbon-  
1019 nitrogen cycles (Wieder et al. 2015; Shi et al. 2016; Davies-Barnard et al. 2020;  
1020 Braghieri et al. 2022), which allows leaf photosynthesis to be predicted directly  
1021 through changes in  $N_{\text{area}}$  and indirectly through changes in soil nitrogen avail-  
1022 ability (e.g., LPJ-GUESS, Smith et al., 2014; CLM5.0, Lawrence et al., 2019).  
1023 Despite recent model developments, open questions remain regarding the gen-  
1024 erality of ecological relationships between soil nitrogen availability, leaf nitrogen  
1025 content, and leaf photosynthesis across edaphic and climatic gradients.  
1026 Empirical support for positive relationships between soil nitrogen avail-

ability and  $N_{\text{area}}$  is abundant (Firn et al. 2019; Liang et al. 2020), and is a result often attributed to the high nitrogen cost of building and maintaining Rubisco (Evans 1989; Evans and Seemann 1989; Onoda et al. 2004; Onoda et al. 2017; Dong et al. 2020). Such patterns imply that positive relationships between soil nitrogen availability and  $N_{\text{area}}$  should cause an increase in leaf photosynthesis and photosynthetic capacity by increasing the maximum rate of Rubisco carboxylation through increased investments to Rubisco construction and maintenance. This integrated  $N_{\text{area}}$ -photosynthesis response to soil nitrogen availability has been observed both in manipulative experiments and across environmental gradients (Field and Mooney 1986; Evans 1989; Walker et al. 2014; Li et al. 2020), and is thought to be driven by ecosystem nitrogen limitation, which limits its primary productivity globally (LeBauer and Treseder 2008; Fay et al. 2015). However, this response is not consistently observed, as recent studies note variable  $N_{\text{area}}$ -photosynthesis relationships across soil nitrogen availability gradients (Liang et al. 2020; Luo et al. 2021) and that aboveground growing conditions (e.g., light availability, temperature, vapor pressure deficit) or species identity traits (e.g., photosynthetic pathway, nitrogen acquisition strategy) may be more important for explaining variance in  $N_{\text{area}}$  and photosynthetic capacity across time and space (Adams et al. 2016; Dong et al. 2017; Dong et al. 2020; Dong et al. 2022; Smith et al. 2019; Peng et al. 2021; Westerband et al. 2023).

**1047** 4.2 Methods

**1048** 4.2.1 textit{Site descriptions and sampling methodology}

**1049** We collected leaf and soil samples from 24 open grassland sites across cen-  
**1050** tral and eastern Texas in summer 2020 and summer 2021 (Fig. 4.1). Twelve  
**1051** sites were visited between June and July 2020 and 14 sites (11 unique from 2020)  
**1052** were visited between May and June 2021 (Table 1). We explicitly chose sites  
**1053** that maximized variability in precipitation and edaphic variability between sites  
**1054** while minimizing temperature variability across the environmental gradient (Ta-  
**1055** ble 1). No site with personally communicated or anecdotal evidence of grazing  
**1056** or disturbance (e.g., mowing, feral hog activity, etc.) were used. We collected  
**1057** leaf material from three individuals each of the five most abundant species at ran-  
**1058** dom locations at each site, only selecting species that were broadly classified as  
**1059** graminoid, forb/herb, shrub, or subshrub growth habits per the USDA PLANTS  
**1060** database (USDA NRCS 2022). All collected leaves were fully expanded with no  
**1061** visible herbivory or other external damage and also free from shading by nearby  
**1062** shrubs or trees. Five soil samples were collected from 0-15cm below the soil sur-  
**1063** face at each site near the leaf collection sample locations. Soil samples were later  
**1064** mixed together by hand to create one composite soil sample per site.

**1065** 4.2.2 *Leaf trait measurements*

**1066** Images of each leaf were taken immediately following each site visit using  
**1067** a flat-bed scanner. Fresh leaf area was determined from each image using the  
**1068** 'LeafArea' R package (Katabuchi 2015), which automates leaf area calculations  
**1069** using ImageJ software (Schneider et al. 2012). Each leaf was dried at 65°C for at

**1070** least 48 hours to a constant mass, weighed, and manually ground in a mortar and  
**1071** pestle until homogenized. Leaf mass per area ( $M_{\text{area}}$ ; g m<sup>-2</sup>) was calculated as the  
**1072** ratio of dry leaf biomass to fresh leaf area. Subsamples of dried and homogenized  
**1073** leaf tissue were used to measure leaf nitrogen content ( $N_{\text{mass}}$ ; gN g<sup>-1</sup>) through el-  
**1074** emental combustion analysis (Costech-4010, Costech Instruments, Valencia, CA).  
**1075** Leaf nitrogen content per unit leaf area ( $N_{\text{area}}$ ; gN m<sup>-2</sup>) was then calculated as  
**1076** the product of  $N_{\text{mass}}$  and  $M_{\text{area}}$ .

**1077** Subsamples of dried and homogenized leaf tissue were sent to the University  
**1078** of California-Davis Stable Isotope Facility to determine leaf  $\delta^{13}\text{C}$ . Leaf  $\delta^{13}\text{C}$  values  
**1079** were determined using an elemental analyzer (PDZ Europa ANCA-GSL; Sercon  
**1080** Ltd., Chestshire, UK) interfaced to an isotope ratio mass spectrometer (PDZ  
**1081** Europa 20-20 Isotope Ratio Mass Spectrometer, Sercon Ltd., Chestshire, UK).  
**1082** We used leaf  $\delta^{13}\text{C}$  values (‰; relative to Vienna Pee Dee Belemnite international  
**1083** reference standard) to estimate the ratio of intercellular ( $C_i$ ) to extracellular ( $C_a$ )  
**1084** CO<sub>2</sub> ratio (leaf  $C_i:C_a$ ,  $\chi$ ; unitless) following the approach of Farquhar et al. (1989)  
**1085** described in Cernusak et al. (2013). We derived  $\chi$  as:

$$\chi = \frac{C_i}{C_a} = \frac{\Delta^{13}\text{C} - a}{b - a} \quad (4.1)$$

**1086** where  $\Delta^{13}\text{C}$  represents the relative difference between leaf  $\delta^{13}\text{C}$  (‰) and air  $\delta^{13}\text{C}$   
**1087** (‰), and is calculated as:

$$\Delta^{13}\text{C} = \frac{\delta^{13}\text{C}_{\text{air}} - \delta^{13}\text{C}_{\text{leaf}}}{1 + \delta^{13}\text{C}_{\text{leaf}}} \quad (4.2)$$

**1088**  $\delta^{13}\text{C}_{\text{air}}$ , traditionally assumed to be -8‰ (Keeling et al. 1979; Farquhar et al.

**1089** 1989), was calculated as a function of calendar year  $t$  using an empirical equation  
**1090** derived in Feng (1999):

$$\delta^{13}C_{air} = -6.429 - 0.006e^{0.0217(t-1740)} \quad (4.3)$$

**1091** This calculation resulted in  $\delta^{13}C_{air}$  values for 2020 and 2021 as -9.04 and -9.09,  
**1092** respectively.  $a$  represents the fractionation between  $^{12}C$  and  $^{13}C$  due to diffusion  
**1093** in air, assumed to be 4.4‰, and  $b$  represents the fractionation caused by Rubisco  
**1094** carboxylation, assumed to be 27‰ (Farquhar et al. 1989). For  $C_4$  species,  $b$  in  
**1095** Eqn. 4.1 was set to 6.3‰, and was derived from:

$$b = c + (d \cdot \phi) \quad (4.4)$$

**1096** Where  $c$  was set to -5.7‰ and  $d$  was set to 30‰ (Farquhar et al. 1989).  $\phi$ , which  
**1097** is the bundle sheath leakiness term, was set to 0.4. All  $\chi$  values less than 0.2 and  
**1098** greater than 1.0 were assumed to be incorrect and removed.

**1099** We derived the unit cost of resource use ( $\beta$ ) using leaf  $\chi$  and site climate  
**1100** data with equations first described in Prentice et al. (2014) and simplified in  
**1101** Lavergne et al. (2020):

$$\beta = 1.6\eta^*D \frac{\chi - (\frac{\Gamma^*}{C_a})^2}{(1 - \chi)^2(K_m + \Gamma^*)} \quad (4.5)$$

**1102** where  $\eta^*$  is the viscosity of water relative to 25°C, calculated using elevation and  
**1103** mean air temperature of the seven days leading up to each site visit following  
**1104** equations in Huber et al. (2009).  $D$  represents vapor pressure deficit (Pa), set

**1105** to the mean vapor pressure deficit of the seven days leading up to each site visit,  
**1106**  $C_a$  represents atmospheric CO<sub>2</sub> concentration, arbitrarily set to 420  $\mu\text{mol mol}^{-1}$   
**1107** CO<sup>2</sup>.  $K_m$  (Pa) is the Michaelis-Menten coefficient for Rubisco affinity to CO<sub>2</sub> and  
**1108** O<sub>2</sub>, calculated as:

$$K_m = K_c \cdot \left(1 + \frac{O_i}{K_o}\right) \quad (4.6)$$

**1109** where  $K_c$  (Pa) and  $K_o$  (Pa) are the Michaelis-Menten coefficients for Rubisco  
**1110** affinity to CO<sub>2</sub> and O<sub>2</sub>, respectively, and  $O_i$  is the intercellular O<sub>2</sub> concentration.  
**1111**  $\Gamma^*$  (Pa) is the CO<sub>2</sub> compensation point in the absence of dark respiration.  $K_c$ ,  $K_o$ ,  
**1112** and  $\Gamma^*$  were determined using equations described in Medlyn et al. (2002) and  
**1113** derived in Bernacchi et al. (2001), invoking an elevation correction for atmospheric  
**1114** pressure as explained in Stocker et al. (2020).

**1115**

placeholder for Table 1

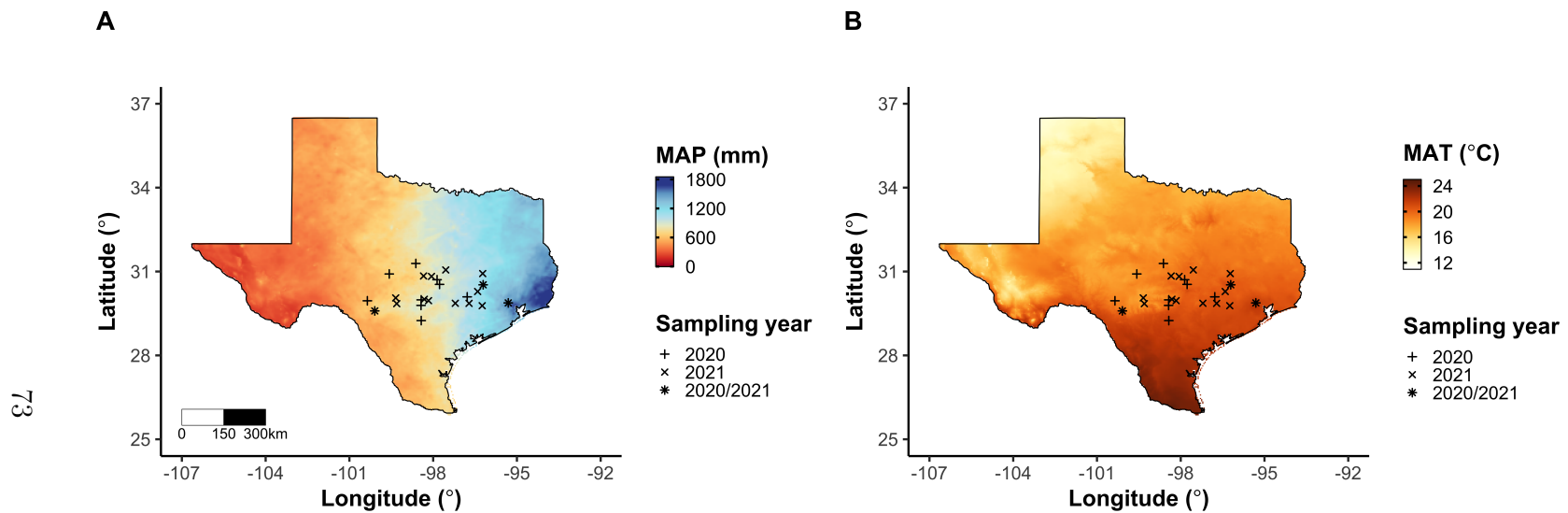


**Figure 4.1.** Maps that detail site locations along 2006-2020 mean annual precipitation (panel A) and mean annual temperature (panel B) gradients in Texas, USA. Precipitation and temperature data were plotted at a 4-km grid resolution and are masked to include only grid cells that occur in the Texas state boundary in the United States. In both panels, open circles refer to sites visited in 2020, open triangles to sites visited in 2021, and closed circles to sites visited in 2020 and 2021. The scale bar in panel A also applies to panel B.

**1116** 4.2.3 *Site climate data*

**1117** We used the Parameter-elevation Regressions on Independent Slopes Model  
**1118** (PRISM) (Daly et al. 2008) climate product to access gridded daily temperature  
**1119** and precipitation data for the coterminous United States at a 4-km grid resolution  
**1120** between January 1, 2006 and July 31, 2021 (PRISM Climate Group, Oregon State  
**1121** University, <https://prism.oregonstate.edu>, data created 4 Feb 2014, accessed 24  
**1122** Mar 2022). Daily mean air temperature, mean VPD, and total precipitation  
**1123** data were extracted from the grid cell that contained the latitude and longitude  
**1124** of each property using the ‘extract’ function in the ‘terra’ R package (Hijmans  
**1125** 2022). PRISM data were used in lieu of local weather station data because several  
**1126** rural sites did not have a local weather station present within a 20-km radius of  
**1127** the site. Daily site climate data were used to estimate mean annual precipitation  
**1128** and mean annual temperature for each site between 2006 and 2020 (Table 1). We  
**1129** then calculated total precipitation and mean daily VPD for the prior 1, 2, 3, 4, 5,  
**1130** 6, 7, 8, 9, 10, 15, 20, 25, 30, 60, and 90 days leading up to each site visit.

**1131** 4.2.4 *Site edaphic characteristics*

**1132** Subsamples of composited soil samples were sent to the Texas A & M  
**1133** Soil, Water and Forage Laboratory to quantify soil nitrate concentration (NO<sub>3</sub>-N;  
**1134** ppm). Soil NO<sub>3</sub>-N was determined by extracting composite soil samples in 1 M  
**1135** KCl, measuring absorbance values of extracts at 520 nm using the end product of  
**1136** a NO<sub>3</sub>-N to NO<sub>2</sub>-N cadmium reduction reaction (Kachurina et al. 2000). Soil tex-  
**1137** ture data from 0-15cm below the soil surface were accessed using the SoilGrids2.0  
**1138** data product (Poggio et al. 2021) through the ‘fetchSoilGrids’ function in the

**1139** ‘soilDB’ R package (Beaudette et al. 2022). We used SoilGrids2.0 to access soil  
**1140** texture data in lieu of analyses using the collected composite soil sample due to  
**1141** a lack of soil material from some sites after sending samples for soil NO<sub>3</sub>-N.

**1142** Soil moisture was not measured in the field, but was estimated using  
**1143** the ‘Simple Process-Led Algorithms for Simulating Habitats’ model (‘SPLASH’)  
**1144** (Davis et al. 2017). This model, derived from the STASH model (Cramer and  
**1145** Prentice 1988), spins up a bucket model using Priestley-Taylor equations (Priest-  
**1146** ley and Taylor 1972) to calculate daily soil moisture ( $W_n$ ; mm) as a function  
**1147** of the previous day’s soil moisture ( $W_{n-1}$ ; mm), daily precipitation ( $P_n$ ; mm),  
**1148** condensation ( $C_n$ ; mm), actual evapotranspiration ( $E_n^a$ ; mm), and runoff (RO;  
**1149** mm):

$$W_n = W_{n-1} + P_n + C_n - E_n^a - RO \quad (4.7)$$

**1150** Models were spun up by equilibrating the previous day’s soil moisture using  
**1151** successive model iterations with daily mean air temperature, daily precipitation  
**1152** total, the number of daily sunlight hours, and latitude as model inputs (Davis et al.  
**1153** 2017). Daily sunlight hours were estimated for each day at each site using the  
**1154** ‘getSunlightTimes’ function in the ‘suncalc’ R package, which estimated sunrise  
**1155** and sunset times of each property using date and site coordinates (Thieurmel and  
**1156** Elmarhraoui 2019). Water holding capacity (mm), or bucket size, was estimated  
**1157** as a function of soil texture using pedotransfer equations explained in Saxton and  
**1158** Rawls (2006), as done in Stocker et al. (2020) and Bloomfield et al. (2022). A  
**1159** summary of these equations is included in the Supplemental Information.

1160 Daily soil moisture outputs from the SPLASH model for each site were  
1161 used to calculate mean daily soil moisture for the prior 1, 2, 3, 4, 5, 6, 7, 8, 9,  
1162 10, 15, 20, 25, 30, 60, and 90 days leading up to each site visit. Mean daily  
1163 soil moisture values were then expressed as a fraction of water holding capacity  
1164 to normalize across sites with different bucket depths, as done in Stocker et al.  
1165 (2018).

1166 4.2.5 *Plant functional group assignments*

1167 Plant functional group was assigned to each species and used as the pri-  
1168 mary descriptor of species identity. Specifically, we assigned plant functional  
1169 groups based on photosynthetic pathway ( $C_3$ ,  $C_4$ ) and ability to form associations  
1170 with symbiotic nitrogen-fixing bacteria. The ability to form associations with  
1171 symbiotic nitrogen-fixing bacteria was assigned based on whether species were in  
1172 the *Fabaceae* family, and photosynthetic pathway of each species was determined  
1173 from past literature and confirmed through leaf  $\delta^{13}\text{C}$  values. We chose these plant  
1174 functional groups based on *a priori* hypotheses regarding the functional role of  
1175 nitrogen fixation and photosynthetic pathway on the sensitivity of plant nitrogen  
1176 uptake and leaf nitrogen allocation to soil nutrient availability and aboveground  
1177 growing conditions. These plant functional group classifications resulted in three  
1178 distinct plant functional groups within our dataset:  $C_3$  legumes ( $n = 53$ ),  $C_3$   
1179 non-legumes ( $n = 350$ ), and  $C_4$  non-legumes ( $n = 117$ ).

**1180** 4.2.6 *Data analysis*

**1181** All analyses and plotting were conducted in R version 4.1.1 (R Core Team  
**1182** 2021). We constructed a series of separate linear mixed-effects models to inves-  
**1183** tigate environmental drivers of  $\beta$ ,  $\chi$ ,  $N_{\text{area}}$ ,  $N_{\text{mass}}$ , and  $M_{\text{area}}$ , followed by a path  
**1184** analysis using a piecewise structural equation model to investigate direct and  
**1185** indirect effects of climate and soil resource availability on  $N_{\text{area}}$ .

**1186** To explore environmental drivers of  $\beta$ , we built a linear mixed-effects model  
**1187** that included soil moisture, soil nitrogen availability, and plant functional group  
**1188** as fixed effect coefficients. Species were designated as a random intercept term.  
**1189** Interaction coefficients between all possible combinations of the three fixed effect  
**1190** coefficients were also included.  $\beta$  was natural log transformed to linearize data.  
**1191** We used an information-theoretic model selection approach to determine whether  
**1192** 90-, 60-, 30-, 20-, 15-, 10-, 9-, 8-, 7-, 6-, 5-, 4-, 3-, 2-, or 1-day mean daily  
**1193** soil moisture conferred the best model fit for  $\beta$ . To do this, we constructed 16  
**1194** separate linear mixed-effects models where log-transformed  $\beta$  was included as the  
**1195** response variable and each soil moisture timestep was separately included as a  
**1196** single continuous fixed effect. Species were included as a random intercept term  
**1197** for all models. We used corrected Akaike Information Criterion (AICc) to select  
**1198** the soil moisture timescale that conferred the best model fit, indicated by the  
**1199** model with the lowest AICc score (Table S2; Fig. S2).

**1200** To explore environmental drivers of  $\chi$ , we constructed a second linear mixed  
**1201** effects model that included VPD, soil moisture, soil nitrogen availability, and plant  
**1202** functional group as fixed effect coefficients. Two-way interactions between plant  
**1203** functional group and VPD, soil nitrogen availability, or soil moisture were also

1204 included as fixed effect coefficients, in addition to a three-way interaction between  
1205 soil moisture, soil nitrogen availability, and plant functional group. Species were  
1206 included as a random intercept term. We used an information-theoretic model  
1207 selection approach to determine whether 90-, 60-, 30-, 20-, 15-, 10-, 9-, 8-, 7-, 6-,  
1208 5-, 4-, 3-, 2-, or 1-day mean daily VPD conferred the best model fit for  $\chi$  using  
1209 the same approach explained above for the soil moisture effect on  $\beta$ . The soil  
1210 moisture timescale was set to the same timescale that conferred the best fit for  $\beta$ .

1211 To explore environmental drivers of  $N_{\text{area}}$ ,  $N_{\text{mass}}$ , and  $M_{\text{area}}$ , we constructed  
1212 three separate linear mixed effects model that each included  $\chi$ , soil nitrogen avail-  
1213 ability, soil moisture, and plant functional group as fixed effect coefficients. Two-  
1214 way interactions between plant functional group and  $\beta$ ,  $\chi$ , soil nitrogen availability,  
1215 or soil moisture were included as additional fixed effect coefficients, in addition to  
1216 a three-way interaction between soil nitrogen availability, soil moisture, and plant  
1217 functional group. Species were included as a random intercept term, with the soil  
1218 moisture timescale set to the same timescale that conferred the best fit for  $\beta$ .

1219 In all linear mixed-effects models explained above, including those to select  
1220 relevant timescales, we used the 'lmer' function in the 'lme4' R package (Bates  
1221 et al. 2015) to fit each model and the 'Anova' function in the 'car' R package (Fox  
1222 and Weisberg 2019) to calculate Type II Wald's  $\chi^2$  and determine the significance  
1223 level ( $\alpha = 0.05$ ) of each fixed effect coefficient. We also used the 'emmeans'  
1224 R package (Lenth 2019) to conduct post-hoc comparisons using Tukey's tests,  
1225 where degrees of freedom were approximated using the Kenward-Roger approach  
1226 (Kenward and Roger 1997). Trendlines and error ribbons for all plots were drawn  
1227 using a series of 'emmeans' outputs across the range in plotted x-axis values.

Finally, we conducted a path analysis using a piecewise structural equation model to examine direct and indirect pathways that determined variance in  $N_{\text{area}}$ . Seven separate linear mixed effects models were loaded into the piecewise structural equation model. Models were constructed per our *a priori* hypotheses following patterns expected from photosynthetic least-cost theory. The first model regressed  $N_{\text{area}}$  against  $\chi$ ,  $N_{\text{mass}}$ , and  $M_{\text{area}}$ . The second model regressed  $M_{\text{area}}$  against  $\chi$ . The third model regressed  $N_{\text{mass}}$  against  $\chi$  and  $M_{\text{area}}$  (Dong et al. 2017; Dong et al. 2020). The fourth model regressed  $\chi$  against  $\beta$  and VPD. The fifth model regressed  $\beta$  against soil nitrogen availability, soil moisture, ability to associate with symbiotic nitrogen-fixing bacteria, and photosynthetic pathway. The sixth model regressed soil nitrogen availability against soil moisture, while the seventh model regressed VPD against soil moisture (Novick et al. 2016; Sulman et al. 2016). All models included the relevant timescale selected in the individual linear mixed effect models explained above (2-day soil moisture, 4-day vapor pressure deficit). Models also included species as a random intercept term, were built using the ‘lme’ function in the ‘nlme’ R package (Pinheiro and Bates 2022), and subsequently loaded into the piecewise structural equation model using the ‘psem’ function in the ‘piecewiseSEM’ R package (Lefcheck 2016).

## 1246 4.3 Results

### 1247 4.3.1 Cost to acquire nitrogen relative to water ( $\beta$ )

Model selection indicated that 2-day soil moisture was the timescale that conferred the best model fit for  $\beta$  ( $AIC_c = 1227.83$ ; Table S2; Fig. S1). Increasing soil nitrogen availability generally decreased  $\beta$  ( $p < 0.001$ ; Table 2), a

**1251** pattern driven by a negative effect of increasing soil nitrogen availability on  $\beta$  in  
**1252** C<sub>3</sub> nonlegumes (Tukey:  $p < 0.001$ ) and C<sub>3</sub> legumes (Tukey:  $p = 0.004$ ; Fig. 2a).  
**1253** C<sub>4</sub> nonlegumes also demonstrated a negative trend in the effect of increasing soil  
**1254** nitrogen availability on  $\beta$ , but this pattern was not significantly different from  
**1255** zero (Tukey:  $p = 0.307$ ; Fig. 2a). There was no apparent effect of soil moisture  
**1256** on  $\beta$  ( $p = 0.264$ ; Table 1; Fig. 2b). A functional group effect ( $p < 0.001$ ; Ta-  
**1257** ble 1) indicated that C<sub>4</sub> nonlegumes generally had lower  $\beta$  values than both C<sub>3</sub>  
**1258** legumes and C<sub>3</sub> non-legumes when averaged across soil moisture and soil nitrogen  
**1259** availability values (Tukey:  $p < 0.001$  in both cases), while average  $\beta$  values in C<sub>3</sub>  
**1260** legumes did not differ from C<sub>3</sub> nonlegumes (Tukey:  $p = 0.691$ ).

**1261**

placeholder Table 2

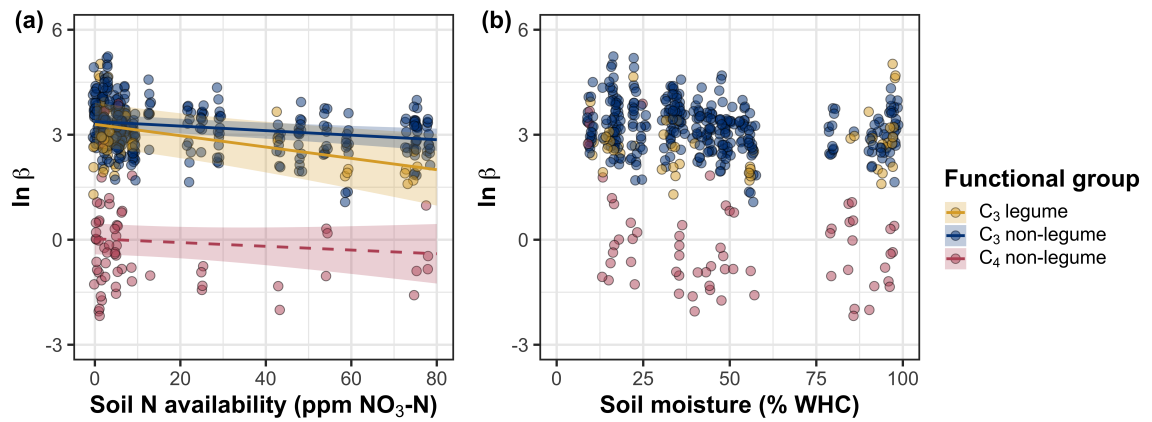


**Figure 4.2.** Effects of soil nitrogen availability (a) and soil moisture (b) on the unit cost ratio  $\beta$ . In (b), soil moisture is represented as a percent of site water holding capacity. Yellow shading and trendlines indicate C<sub>3</sub> legumes, blue shading and trendlines indicate C<sub>3</sub> non-legumes, and red shading and trendlines indicate C<sub>4</sub> non-legumes. Points are jittered for visibility. Variably colored trendlines are only included if there is an interaction between the x-axis and plant functional group, where solid trendlines indicate slopes that are different from zero ( $p < 0.05$ ) and dashed trendlines indicate slopes that are not different from zero ( $p > 0.05$ ). Error ribbons represent the upper and lower 95% confidence intervals of each fitted trendline.

**1262** 4.3.2 Leaf  $C_i:C_a$  ( $\chi$ )

**1263** Model selection indicated that 4-day daily VPD was the timescale that  
**1264** conferred the best model fit for  $\chi$  (AICc = -883.97; Table S1; Fig. S2).

**1265** Variance in  $\chi$  was driven by a series of two-way interactions between func-  
**1266** tional group and VPD ( $p = 0.006$ ; Table 3), soil moisture ( $p = 0.033$ , Table 3),  
**1267** and soil nitrogen availability ( $p = 0.022$ ; Table 3). The interaction between 4-day  
**1268** VPD and functional group revealed that the general negative effect of increasing  
**1269** VPD ( $p < 0.001$ ; Table 3) was driven by a negative effect of increasing VPD  
**1270** on  $\chi$  in C<sub>3</sub> nonlegumes (Tukey:  $p < 0.001$ ) and marginal negative effect in C<sub>3</sub>  
**1271** legumes (Tukey:  $p = 0.074$ ) paired with a positive trending, but insignificant  
**1272** effect of increasing VPD in C<sub>4</sub> nonlegumes (Tukey:  $p = 0.130$ ; Fig. 3a). The  
**1273** interaction between 2-day soil moisture and functional group indicated that the  
**1274** general negative effect of increasing soil moisture on  $\chi$  was driven by a positive  
**1275** effect of increasing soil moisture on  $\chi$  in C<sub>4</sub> nonlegumes (Tukey:  $p = 0.009$ ) de-  
**1276** spite a positive trending but insignificant effect of increasing soil moisture on  $\chi$   
**1277** in C<sub>3</sub> legumes (Tukey:  $p = 0.116$ ) and a null effect of soil moisture on  $\chi$  in C<sub>3</sub>  
**1278** nonlegumes (Tukey:  $p = 0.693$ ; Fig. 3c). The interaction between soil nitrogen  
**1279** availability and plant functional group revealed a weak negative effect of increas-  
**1280** ing soil nitrogen availability on  $\chi$  in C<sub>3</sub> legumes (Tukey:  $p = 0.045$ ), with no  
**1281** apparent effect in C<sub>3</sub> nonlegumes (Tukey:  $p = 0.706$ ) or C<sub>4</sub> nonlegumes (Tukey:  
**1282**  $p = 0.757$ ). Finally, an individual effect of functional group ( $p < 0.001$ ; Table 3)  
**1283** revealed that C<sub>4</sub> nonlegumes generally had lower  $\chi$  than C<sub>3</sub> legumes and C<sub>3</sub> non-  
**1284** legumes (Tukey:  $p < 0.001$  in both cases), with no apparent difference between  
**1285** C<sub>3</sub> legumes and C<sub>3</sub> nonlegumes (Tukey:  $p = 0.831$ ).

**1286**

placeholder Table 3



**1287** 4.3.3 *Leaf nitrogen content*

**1288** An interaction between  $\chi$  and plant functional group ( $p < 0.001$ ; Table  
**1289** 4) revealed that the general negative effect of increasing  $\chi$  on  $N_{\text{area}}$  ( $p < 0.001$ ;  
**1290** Table 4) was driven by a negative effect of increasing  $\chi$  on  $N_{\text{area}}$  in C<sub>3</sub> nonlegumes  
**1291** (Tukey:  $p < 0.001$ ) and C<sub>3</sub> legumes (Tukey:  $p = 0.002$ ) despite a null effect of  $\chi$   
**1292** on  $N_{\text{area}}$  in C<sub>4</sub> nonlegumes (Tukey:  $p = 0.795$ ; Fig. 4a). An interaction between  
**1293** soil nitrogen availability and soil moisture ( $p = 0.028$ ; Table 4) indicated that the  
**1294** marginal positive effect of increasing soil nitrogen availability on  $N_{\text{area}}$  ( $p = 0.091$ ;  
**1295** Table 4) decreased with increasing soil moisture, despite no apparent individual  
**1296** effect of soil moisture on  $N_{\text{area}}$  ( $p = 0.692$ ; Table 4). Finally, a plant functional  
**1297** group effect ( $p < 0.001$ ; Table 4) indicated that C<sub>4</sub> nonlegumes had lower  $N_{\text{area}}$   
**1298** values on average compared to C<sub>3</sub> legumes (Tukey:  $p < 0.001$ ) and C<sub>3</sub> nonlegumes  
**1299** (Tukey:  $p = 0.001$ ), while C<sub>3</sub> legumes had lower average  $N_{\text{area}}$  values compared  
**1300** to C<sub>3</sub> nonlegumes (Tukey:  $p = 0.012$ ).

**1301** A marginal interaction between  $\chi$  and plant functional group ( $p = 0.088$ ;  
**1302** Table 4) revealed that, despite no apparent general effect of  $\chi$  on  $N_{\text{mass}}$  ( $p = 0.273$ ;  
**1303** Table 4), increasing  $\chi$  decreased  $N_{\text{mass}}$  in C<sub>3</sub> nonlegumes (Tukey:  $p = 0.021$ ), but  
**1304** this effect was not apparent in C<sub>4</sub> nonlegumes (Tukey:  $p = 0.693$ ) or C<sub>3</sub> legumes  
**1305** (Tukey:  $p = 0.477$ ). An interaction between soil nitrogen availability and soil  
**1306** moisture ( $p < 0.001$ ; Table 4) indicated that the general positive effect of increas-  
**1307** ing soil nitrogen availability on  $N_{\text{mass}}$  ( $p < 0.001$ ; Table 4) generally decreased  
**1308** with increasing soil moisture, despite an apparent general positive effect of in-  
**1309** creasing soil moisture on  $N_{\text{mass}}$  ( $p < 0.001$ ; Table 4). This interaction indicated  
**1310** that the positive effect of increasing soil nitrogen availability on  $N_{\text{mass}}$  was only

1311 apparent when soil moisture was less than 70% the maximum water holding ca-  
1312 pacity (Tukey:  $p < 0.05$  in all cases) despite a positive effect of increasing soil  
1313 moisture on  $N_{\text{mass}}$  ( $p < 0.001$ ; Table 4). Finally, a plant functional group effect  
1314 ( $p < 0.001$ ; Table 4) indicated that C<sub>4</sub> nonlegumes had lower  $N_{\text{mass}}$  values on  
1315 average compared to C<sub>3</sub> legumes (Tukey:  $p = 0.002$ ) and C<sub>3</sub> nonlegumes (Tukey:  
1316  $p = 0.019$ ), while  $N_{\text{mass}}$  did not differ between C<sub>3</sub> legumes and C<sub>3</sub> nonlegumes  
1317 (Tukey:  $p = 0.149$ ).

1318 An interaction between  $\chi$  and functional group ( $p = 0.005$ ; Table 4) indi-  
1319 cated that the general negative effect of increasing  $\chi$  on  $M_{\text{area}}$  ( $p < 0.001$ ; Table  
1320 4; Fig. 4c) was driven by a negative effect of increasing  $\chi$  on  $M_{\text{area}}$  in C<sub>3</sub> legumes  
1321 and C<sub>3</sub> nonlegumes (Tukey:  $p < 0.001$  in both cases) despite a nonsignificant  
1322 effect of increasing  $\chi$  on  $M_{\text{area}}$  in C<sub>4</sub> nonlegumes (Tukey:  $p = 0.724$ ). An in-  
1323 teraction between soil nitrogen and soil moisture ( $p < 0.001$ ; Table 4) indicated  
1324 that the general negative effect of increasing soil nitrogen availability on  $M_{\text{area}}$  ( $p$   
1325  $< 0.001$ ; Table 4) decreased with increasing soil moisture, despite an apparent  
1326 general negative effect of increasing soil moisture on  $M_{\text{area}}$  ( $p = 0.002$ ; Table 4).  
1327 Specifically, the negative effect of increasing soil nitrogen availability on  $M_{\text{area}}$  was  
1328 only apparent when soil moisture was less than 65% the maximum water holding  
1329 capacity (Tukey:  $p < 0.05$  in all cases). An additional interaction between soil  
1330 nitrogen availability and functional group ( $p = 0.034$ ; Table 4) indicated that the  
1331 general negative effect of increasing soil nitrogen availability on  $M_{\text{area}}$  was driven  
1332 by decreases in C<sub>3</sub> nonlegumes (Tukey:  $p < 0.001$ ) and C<sub>4</sub> nonlegumes (Tukey:  
1333  $p = 0.003$ ), with no apparent effect of soil nitrogen availability on  $M_{\text{area}}$  in C<sub>3</sub>  
1334 legumes (Tukey:  $p = 0.997$ ).

**1335**

placeholder Table 4

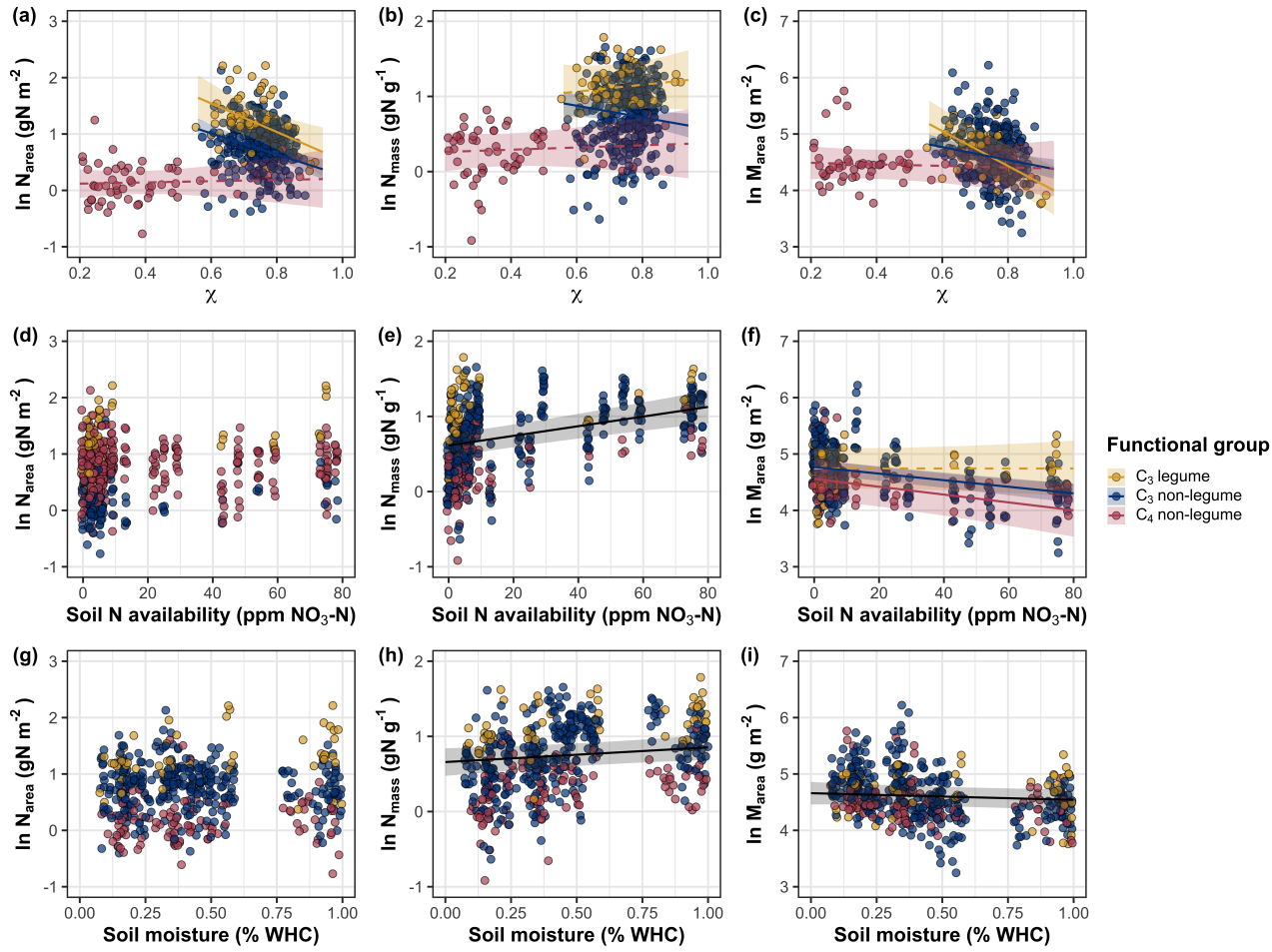


**Figure 4.4.** Effects of  $\chi$  (a-c), soil nitrogen availability (d-f), and soil moisture (g-i) on leaf nitrogen content per unit leaf area (a, d, g), leaf nitrogen content per unit leaf biomass (b, e, h), and leaf mass per area (c, f, i). Shading and trendlines are as explained in Figure 4.2. Where there is no interaction between the x-axis and plant functional group, a solid black trendline indicates the bivariate relationship between the fixed effect the x-axis and response variable on the y-axis and is only included when the slope of the bivariate relationship is different from zero ( $p < 0.05$ ). Error ribbons represent the upper and lower 95% confidence intervals of each fitted trendline.

**1336** 4.3.4 *Structural equation model*

**1337** The piecewise structural equation model explained 90%, 54%, 80%, 92%,  
**1338** and 41% of variance in  $N_{\text{area}}$ ,  $N_{\text{mass}}$ ,  $M_{\text{area}}$ ,  $\chi$ , and  $\beta$ , respectively (Table 5; Fig.  
**1339** 5). Variance in  $N_{\text{area}}$  was driven by a negative effect of increasing  $\chi$  ( $p < 0.001$ ;  
**1340** Table 5) paired with positive effects of increasing  $N_{\text{mass}}$  and  $M_{\text{area}}$  ( $p < 0.001$  in  
**1341** both cases; Table 5; Fig. 5). Model results indicated that the negative effect  
**1342** of  $\chi$  on  $N_{\text{area}}$  was driven by a strong reduction in  $M_{\text{area}}$  with increasing  $\chi$  ( $p <$   
**1343** 0.001; Table 5) paired with no change in  $\chi$  due to Nmass ( $p = 0.150$ ; Table 5).  
**1344** However, there was a strong negative effect of increasing  $M_{\text{area}}$  on  $N_{\text{mass}}$  ( $p <$   
**1345** 0.001; Table 5; Fig. 5).  $\chi$  generally increased with increasing  $\beta$  ( $p < 0.001$ ; Table  
**1346** 5) and decreased with increasing VPD ( $p < 0.001$ ; Table 5; Fig. 5). Variance in  $\beta$   
**1347** was driven by a negative effect of increasing soil nitrogen availability ( $p < 0.001$ ;  
**1348** Table 5) and was generally higher in C<sub>3</sub> species ( $p < 0.001$ ; Table 5; Fig. 5).  
**1349** However,  $\beta$  did not change with soil moisture ( $p = 0.332$ ; Table 5) or with ability  
**1350** to acquire nitrogen via symbiotic nitrogen fixation ( $p = 0.546$ ; Table 5). Finally,  
**1351** soil nitrogen availability was positively associated with increasing soil moisture ( $p$   
**1352**  $< 0.001$ ; Table 5; Fig. 5), while VPD was negatively associated with increasing  
**1353** soil moisture ( $p < 0.001$ ; Table 5; Fig. 5).

**1354**

placeholder Table 5

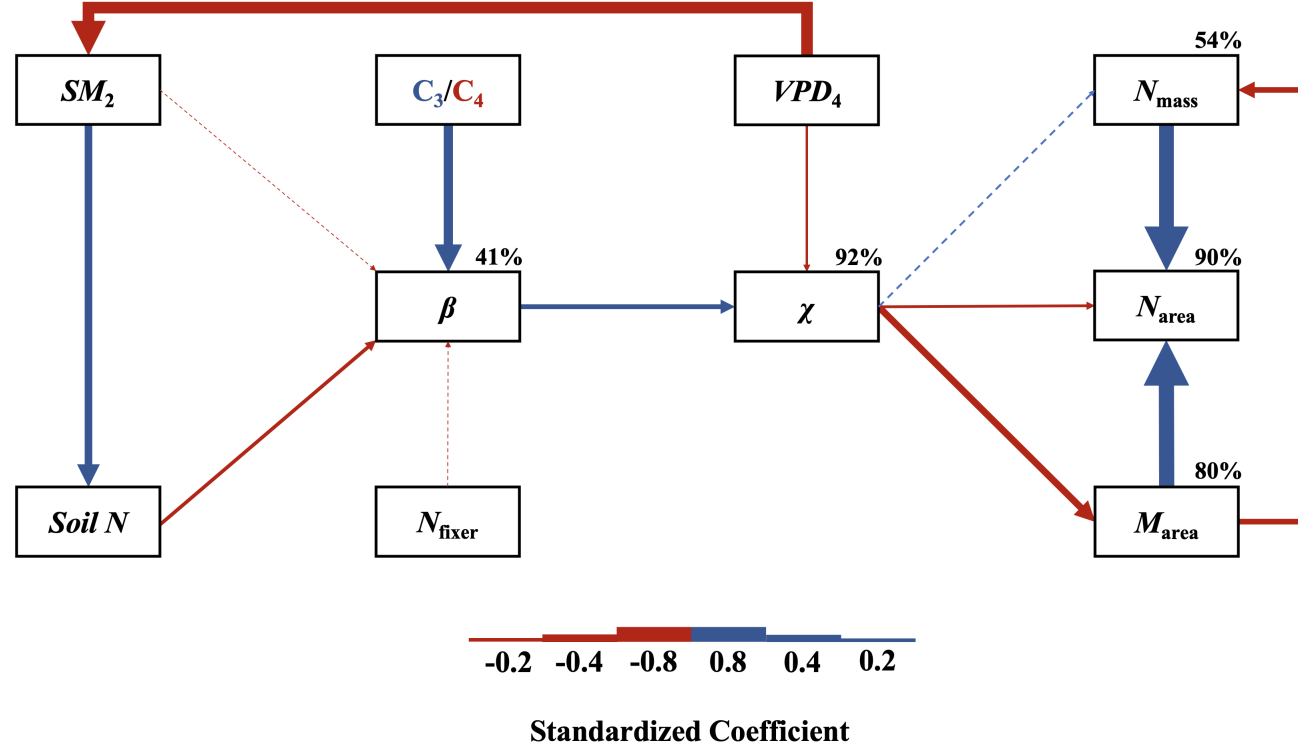


**Figure 4.5.** Structural equation model results exploring direct and indirect drivers of  $N_{area}$ . Boxes indicate measured edaphic factors, climatic factors, and leaf traits. Percentages above boxes indicate conditional  $R^2$  values of each respective leaf trait. Solid arrows indicate bivariate relationships where  $p < 0.05$ , while dashed arrows indicate bivariate relationships where  $p > 0.05$ . Positive model coefficients are indicated through blue arrows, while negative model coefficients are indicated through red arrows. Arrow thickness scales with the standardized model coefficient of each bivariate relationship. A positive coefficient for photosynthetic pathway indicates generally larger values in  $C_3$  species, while a positive coefficient for  $N_{fixer}$  indicates generally larger values in N-fixing species. Standardized model coefficients and associated  $p$ -values are reported in Table 5.

**1355** 4.4 Discussion

1356

## Chapter 5

1357  
1358

Optimal resource investment to photosynthetic capacity maximizes  
nutrient allocation to whole plant growth under elevated CO<sub>2</sub>

1359 5.1 Introduction

1360 Terrestrial ecosystems are regulated by complex carbon and nitrogen cy-  
1361 cles. As a result, terrestrial biosphere models, which are beginning to include  
1362 coupled carbon and nitrogen cycles (Shi et al. 2016; Davies-Barnard et al. 2020;  
1363 Braghieri et al. 2022), must accurately represent these cycles under different  
1364 environmental scenarios to reliably simulate carbon and nitrogen atmosphere-  
1365 biosphere fluxes (Hungate et al. 2003; Prentice et al. 2015). While the inclusion  
1366 of coupled carbon and nitrogen cycles tends to reduce model uncertainty (Arora  
1367 et al. 2020), large uncertainty in role of soil nitrogen availability and nitrogen ac-  
1368 quisition strategy on leaf and whole plant acclimation responses to CO<sub>2</sub> remains  
1369 (Smith and Dukes 2013; Terrer et al. 2018; Smith and Keenan 2020). This source  
1370 of uncertainty likely contributes to the widespread divergence in future carbon  
1371 and nitrogen flux simulations across terrestrial biosphere models (Friedlingstein  
1372 et al. 2014; Zaehle et al. 2014; Meyerholt et al. 2020).

1373 Plants grown under elevated CO<sub>2</sub> generally have less leaf nitrogen content  
1374 than those grown under ambient CO<sub>2</sub>, a response that often corresponds with  
1375 reductions in photosynthetic capacity and stomatal conductance at the leaf-level  
1376 and biomass stimulation over time at the whole plant level (Curtis 1996; Drake  
1377 et al. 1997; Ainsworth et al. 2002; Makino 2003; Morgan et al. 2004; Ainsworth  
1378 and Long 2005; Ainsworth and Rogers 2007; Smith and Dukes 2013; Poorter et al.  
1379 2022). As net primary productivity is generally limited by nitrogen availability

1380 (Vitousek and Howarth 1991; LeBauer and Treseder 2008; Fay et al. 2015), and  
1381 soil nitrogen availability is often positively correlated with leaf nitrogen content  
1382 and photosynthetic capacity (Field and Mooney 1986; Evans and Seemann 1989;  
1383 Evans 1989; Walker et al. 2014; Firn et al. 2019; Liang et al. 2020), some  
1384 have hypothesized that leaf and whole plant acclimation responses to CO<sub>2</sub> are  
1385 constrained by soil nitrogen availability. The progressive nitrogen limitation hy-  
1386 pothesis predicts that elevated CO<sub>2</sub> will increase plant nitrogen demand, which  
1387 will increase plant nitrogen uptake and progressively deplete soil nitrogen if soil  
1388 nitrogen supply does not exceed plant nitrogen demand (Luo et al. 2004). The  
1389 hypothesis predicts that this response should result in strong acute stimulations in  
1390 whole plant growth and primary productivity that diminish over time as nitrogen  
1391 becomes more limiting. Assuming a positive relationship between soil nitrogen  
1392 availability, leaf nitrogen content, and photosynthetic capacity, this hypothesis  
1393 also implies that progressive reductions in soil nitrogen availability should be the  
1394 mechanism that drives the downregulation in leaf nitrogen content and photosyn-  
1395 thetic capacity under elevated CO<sub>2</sub>. This hypothesis has received some support  
1396 from free air CO<sub>2</sub> enrichment experiments (Reich et al. 2006; Norby et al. 2010),  
1397 although is not consistently observed across experiments (Finzi et al. 2006; Moore  
1398 et al. 2006; Liang et al. 2016).

1399 While possible that progressive nitrogen limitation may determine leaf and  
1400 whole plant acclimation responses to CO<sub>2</sub>, growing evidence indicates that leaf ni-  
1401 trogen and photosynthetic capacity are more strongly determined through above-  
1402 ground growing conditions than by soil resource availability (Dong et al. 2017;  
1403 Dong et al. 2020; Dong et al. 2022; Smith et al. 2019; Smith and Keenan 2020;

1404 Paillassa et al. 2020; Peng et al. 2021; Querejeta et al. 2022; Westerband et al.  
1405 2023), and satellite-derived chlorophyll fluorescence data indicate that increasing  
1406 atmospheric CO<sub>2</sub> may decrease leaf and canopy demand for nitrogen (Dong et al.  
1407 2022). Together, results from these studies suggest that the downregulation in  
1408 leaf nitrogen content and photosynthetic capacity due to increasing CO<sub>2</sub> may not  
1409 be as tightly linked to progressive nitrogen limitation as previously hypothesized.

1410 A unification of optimal coordination and photosynthetic least-cost the-  
1411 ories predicts that leaves acclimate to elevated CO<sub>2</sub> by downregulating nitrogen  
1412 allocation to Ribulose-1,5-bisphosphate (RuBP) carboxylase/oxygenase (Rubisco)  
1413 to optimize resource use efficiencies at the leaf level, which allows for greater re-  
1414 source allocation to whole plant growth (Drake et al. 1997; Wright et al. 2003;  
1415 Prentice et al. 2014; Smith et al. 2019). The theory predicts that the downregu-  
1416 lation in nitrogen allocation to Rubisco results in a stronger downregulation in the  
1417 maximum rate of Rubisco carboxylation ( $V_{cmax}$ ) than the maximum rate of RuBP  
1418 regeneration ( $J_{max}$ ), which maximizes photosynthetic efficiency by allowing net  
1419 photosynthesis rates to be equally co-limited by Rubisco carboxylation and RuBP  
1420 regeneration (Chen et al. 1993; Maire et al. 2012). This acclimation response  
1421 allows plants to make more efficient use of available light while avoiding overin-  
1422 vestment in Rubisco, which has high nitrogen and energetic costs of building and  
1423 maintaining (Evans 1989; Evans and Clarke 2019). Instead, additional acquired  
1424 resources not needed to optimize leaf photosynthesis are allocated to the mainte-  
1425 nance of structures that support whole plant growth (e.g., total leaf area, whole  
1426 plant biomass, etc.) or to allocation processes not related to leaf photosynthesis  
1427 or growth, such as plant defense mechanisms or leaf structural tissue. Regardless,

**1428** optimized resource allocation at the leaf level should allow for greater resource  
**1429** allocation to whole plant growth. The theory indicates that leaf acclimation re-  
**1430** sponses to CO<sub>2</sub> should be independent of changes in soil nitrogen availability.  
**1431** While this leaf acclimation response maximizes nitrogen allocation to structures  
**1432** that support whole plant growth, the theory suggests that the positive effect of  
**1433** elevated CO<sub>2</sub> on whole plant growth may be further stimulated by soil nitrogen  
**1434** availability through a reduction in the cost of acquiring nitrogen (Bae et al. 2015;  
**1435** Perkowski et al. 2021; Lu et al. 2022).

**1436** Plants acquire nitrogen by allocating photosynthetically derived carbon be-  
**1437** lowground in exchange for nitrogen through different nitrogen acquisition strate-  
**1438** gies. These nitrogen acquisition strategies can include direct uptake pathways  
**1439** such as mass flow or diffusion (Barber 1962), symbioses with mycorrhizal fungi or  
**1440** symbiotic nitrogen-fixing bacteria (Vance and Heichel 1991; Marschner and Dell  
**1441** 1994; Smith and Read 2008; Udvardi and Poole 2013), or through the release  
**1442** of root exudates that prime free-living soil microbial communities (Phillips et al.  
**1443** 2011; Wen et al. 2022). Plants cannot acquire nitrogen without first allocating  
**1444** carbon belowground, which implies an inherent carbon cost to the plant for acquir-  
**1445** ing nitrogen regardless of nitrogen acquisition strategy. Carbon costs to acquire  
**1446** nitrogen often vary in species with different nitrogen acquisition strategies and  
**1447** are dependent on external environmental factors such as atmospheric CO<sub>2</sub>, light  
**1448** availability, and soil nitrogen availability (Brzostek et al. 2014; Terrer et al. 2016;  
**1449** Terrer et al. 2018; Allen et al. 2020; Perkowski et al. 2021; Lu et al. 2022), which  
**1450** suggests that acquisition strategy may be an important factor in determining ef-  
**1451** fects of soil nitrogen availability on leaf and whole plant acclimation responses to

1452 elevated CO<sub>2</sub>.

1453 A recent meta-analysis using data across 20 grassland and forest CO<sub>2</sub> en-  
1454 richment experiments suggested that species which acquire nitrogen from sym-  
1455 biotic nitrogen-fixing bacteria had reduced costs of nitrogen acquisition under  
1456 elevated CO<sub>2</sub> (Terrer et al. 2018). Findings from this meta-analysis indicated  
1457 that reductions in costs of nitrogen acquisition in species that form associations  
1458 with symbiotic nitrogen-fixing bacteria under elevated CO<sub>2</sub> may drive stronger  
1459 stimulations in whole plant growth and downregulations in  $V_{cmax}$  than species that  
1460 associate with arbuscular mycorrhizal fungi (Smith and Keenan 2020), which gen-  
1461 erally have higher costs of nitrogen acquisition under elevated CO<sub>2</sub> (Terrer et al.  
1462 2018). However, plant investments in symbiotic nitrogen fixation generally de-  
1463 cline with increasing nitrogen availability (Dovrat et al. 2018; Perkowski et al.  
1464 2021), a response that has been previously inferred to be the result of a shift in  
1465 the dominant mode of nitrogen acquisition to direct uptake pathways as costs of  
1466 direct uptake decrease with increasing soil nitrogen availability (Rastetter et al.  
1467 2001; Perkowski et al. 2021). Thus, effects of symbiotic nitrogen fixation on plant  
1468 acclimation responses to CO<sub>2</sub> should decline with increasing soil nitrogen avail-  
1469 ability, although manipulative experiments that directly test these patterns are  
1470 rare.

1471 Here, we conducted a 7-week growth chamber experiment using *Glycine*  
1472 *max* L. (Merr.) to examine the effects of soil nitrogen fertilization and inocula-  
1473 tion with symbiotic nitrogen-fixing bacteria on leaf and whole plant acclimation  
1474 responses to elevated CO<sub>2</sub>. Following patterns expected from theory, we hypoth-  
1475 esized that individual leaves should acclimate to elevated CO<sub>2</sub> by more strongly

**1476** downregulating  $V_{cmax}$  relative to  $J_{max}$ , allowing leaf photosynthesis to approach  
**1477** optimal coordination. We expected this response to correspond with a stronger  
**1478** downregulation in leaf nitrogen content than  $V_{cmax}$  and  $J_{max}$ , which would in-  
**1479** crease the fraction of leaf nitrogen content allocated to photosynthesis and photo-  
**1480** synthetic nitrogen use efficiency. At the whole-plant level, we hypothesized that  
**1481** plants would acclimate to elevated CO<sub>2</sub> by stimulating whole plant growth and  
**1482** productivity, a response that would be driven by a strong positive response of  
**1483** total leaf area and aboveground biomass to elevated CO<sub>2</sub>. We predicted that  
**1484** leaf acclimation responses to elevated CO<sub>2</sub> would be independent of soil nitro-  
**1485** gen fertilization and inoculation with symbiotic nitrogen-fixing bacteria; however,  
**1486** we expected that increasing soil nitrogen fertilization would increase the posi-  
**1487** tive effect of elevated CO<sub>2</sub> on measures of whole plant growth due to a stronger  
**1488** reduction in the cost of acquiring nitrogen under elevated CO<sub>2</sub> with increasing  
**1489** fertilization. We also expected stronger stimulations in whole plant growth due  
**1490** to inoculation, but that this effect would only be apparent under low fertilization  
**1491** due to a reduction in root nodulation with increasing fertilization.

**1492** 5.2 Methods

**1493** 5.2.1 *Seed treatments and experimental design*

**1494** *Glycine max* L. (Merr) seeds were planted in 144 6-liter surface sterilized  
**1495** pots (NS-600, Nursery Supplies, Orange, CA, USA) containing a steam-sterilized  
**1496** 70:30 v:v mix of Sphagnum peat moss (Premier Horticulture, Quakertown, PA,  
**1497** USA) to sand (Pavestone, subsidiary of Quikrete Companies, Atlanta, GA, USA).  
**1498** Before planting, all *G. max* seeds were surface sterilized in 2% sodium hypochlorite

**1499** for 3 minutes, followed by three separate 3-minute washes with ultrapure water  
**1500** (MilliQ 7000; MilliporeSigma, Burlington, MA USA). A subset of surface steril-  
**1501** ized seeds were inoculated with *Bradyrhizobium japonicum* (Verdesian N-Dure™  
**1502** Soybean, Cary, NC, USA) in a slurry following manufacturer recommendations  
**1503** (3.12 g inoculant and 241 g deionized water per 1 kg seed).

**1504** Seventy-two pots were randomly planted with surface-sterilized seeds inoc-  
**1505** ulated with *B. japonicum*, while the remaining 72 pots were planted with surface-  
**1506** sterilized uninoculated seeds. Thirty-six pots within each inoculation treatment  
**1507** were randomly placed in one of two atmospheric CO<sub>2</sub> treatments (ambient and  
**1508** 1000 μmol mol<sup>-1</sup> CO<sub>2</sub>). Pots within each unique inoculation-by-CO<sub>2</sub> treatment  
**1509** combination randomly received one of nine soil nitrogen fertilization treatments  
**1510** equivalent to 0, 35, 70, 105, 140, 210, 280, 350, or 630 ppm N. Nitrogen fertil-  
**1511** ization treatments were created using a modified Hoagland solution (Hoagland  
**1512** and Arnon 1950) designed to keep concentrations of other macronutrients and  
**1513** micronutrients equivalent across treatments (Table S1). Pots received the same  
**1514** fertilization treatment throughout the entire duration experiment, which were ap-  
**1515** plied twice per week in 150 mL doses as topical agents to the soil surface through-  
**1516** out the duration of the experiment. This experimental design yielded a fully  
**1517** factorial experiment with four replicates per unique fertilization-by-inoculation-  
**1518** by-CO<sub>2</sub> combination.

**1519** 5.2.2 *Growth chamber conditions*

**1520** Upon experiment initiation, pots were randomly placed in one of six Per-  
**1521** cival LED-41L2 growth chambers (Percival Scientific Inc., Perry, IA, USA) over

1522 two experimental iterations due to chamber space limitation. two iterations were  
1523 conducted such that one iteration included all elevated CO<sub>2</sub> pots and the second  
1524 iteration included all ambient CO<sub>2</sub> pots. Average ( $\pm$  SD) CO<sub>2</sub> concentrations  
1525 across chambers throughout the experiment were  $439 \pm 5 \mu\text{mol mol}^{-1}$  for the  
1526 ambient CO<sub>2</sub> treatment and  $989 \pm 4 \mu\text{mol mol}^{-1}$  for the elevated CO<sub>2</sub> treatment.

1527 Daytime growing conditions were simulated using a 16-hour photoperiod,  
1528 with incoming light radiation set to chamber maximum (mean  $\pm$  SD:  $1240 \pm 32$   
1529  $\mu\text{mol m}^{-2} \text{s}^{-1}$  across chambers), air temperature set to 25°C, and relative humid-  
1530 ity set to 50%. The remaining 8 hours simulated nighttime growing conditions,  
1531 with incoming light radiation set to 0  $\mu\text{mol m}^{-2} \text{s}^{-1}$ , chamber temperature set  
1532 to 17°C, and relative humidity set to 50%. Transitions between daytime and  
1533 nighttime growing conditions were simulated by ramping incoming light radiation  
1534 in 45-minute increments and temperature in 90-minute increments over a 3-hour  
1535 period (Table S2).

1536 Including the two, 3-hour ramping periods, pots grew under average ( $\pm$   
1537 SD) daytime light intensity of  $1049 \pm 27 \mu\text{mol m}^{-2} \text{s}^{-1}$ . In the elevated CO<sub>2</sub>  
1538 iteration, pots grew under  $24.0 \pm 0.2^\circ\text{C}$  during the day,  $16.4 \pm 0.8^\circ\text{C}$  during the  
1539 night, and  $51.6 \pm 0.4\%$  relative humidity. In the ambient CO<sub>2</sub> iteration, pots grew  
1540 under  $23.9 \pm 0.2^\circ\text{C}$  during the day,  $16.0 \pm 1.4^\circ\text{C}$  during the night, and  $50.3 \pm 0.2\%$   
1541 relative humidity. We accounted for climatic differences across the six chambers  
1542 by shuffling the same group of pots daily throughout the growth chambers. This  
1543 process was done by iteratively moving the group of pots on the top rack of a  
1544 chamber to the bottom rack of the same chamber, while simultaneously moving  
1545 the group of pots on the bottom rack of a chamber to the top rack of the adjacent

1546 chamber. We moved pots within and across chambers every day throughout the  
1547 course of each experiment iteration.

1548 5.2.3 *Leaf gas exchange measurements*

1549 Gas exchange measurements were collected for all individuals on the sev-  
1550 enth week of development. All gas exchange measurements were collected on  
1551 the center leaf of the most recent fully expanded trifoliate leaf set. Specifi-  
1552 cally, we measured net photosynthesis ( $A_{\text{net}}$ ;  $\mu\text{mol m}^{-2} \text{s}^{-1}$ ), stomatal conduc-  
1553 tance ( $g_{\text{sw}}$ ;  $\text{mol m}^{-2} \text{s}^{-1}$ ), and intercellular  $\text{CO}_2$  ( $C_i$ ;  $\mu\text{mol mol}^{-1}$ ) concentrations  
1554 across a range of atmospheric  $\text{CO}_2$  concentrations (i.e., an  $A_{\text{net}}/C_i$  curve) using the  
1555 Dynamic Assimilation Technique™. The Dynamic Assimilation Technique™ has  
1556 been shown to correspond well with traditional steady-state  $\text{CO}_2$  response curves  
1557 in *G. max* (Saathoff and Welles 2021).  $A_{\text{net}}/C_i$  curves were generated along a  
1558 reference  $\text{CO}_2$  ramp down from  $420 \mu\text{mol mol}^{-1} \text{CO}_2$  to  $20 \mu\text{mol mol}^{-1} \text{CO}_2$ , fol-  
1559 lowed by a ramp up from  $420 \mu\text{mol mol}^{-1} \text{CO}_2$  to  $1620 \mu\text{mol mol}^{-1} \text{CO}_2$  after  
1560 a 90-second wait period at  $420 \mu\text{mol mol}^{-1} \text{CO}_2$ . The ramp rate for each curve  
1561 was set to  $200 \mu\text{mol mol}^{-1} \text{min}^{-1}$ , logging every five seconds, which generated 96  
1562 data points per response curve. All  $A_{\text{net}}/C_i$  curves were generated after  $A_{\text{net}}$  and  
1563  $g_{\text{sw}}$  stabilized in a LI-6800 cuvette set to a  $500 \text{ mol s}^{-1}$ , 10,000 rpm mixing fan  
1564 speed, 1.5 kPa vapor pressure deficit,  $25^\circ\text{C}$  leaf temperature,  $2000 \mu\text{mol m}^{-2} \text{s}^{-1}$   
1565 incoming light radiation, and initial reference  $\text{CO}_2$  set to  $420 \mu\text{mol mol}^{-1}$ .

1566 With the same focal leaf used to generate  $A_{\text{net}}/C_i$  curves, we measured  
1567 dark respiration ( $R_{\text{d25}}$ ;  $\mu\text{mol m}^{-2} \text{s}^{-1}$ ) following at least a 30-minute period of  
1568 darkness. Measurements were collected on a 5-second log interval for 60 seconds

1569 after stabilizing in a LI-6800 cuvette set to a  $500 \text{ mol s}^{-1}$ , 10,000 rpm mixing fan  
1570 speed, 1.5 kPa vapor pressure deficit, 25°C leaf temperature, and  $420 \mu\text{mol mol}^{-1}$   
1571 reference CO<sub>2</sub> concentration (for both CO<sub>2</sub> concentrations), with incoming light  
1572 radiation set to  $0 \mu\text{mol m}^{-2} \text{ s}^{-1}$ . A single dark respiration value was determined  
1573 for each focal leaf by calculating the mean dark respiration value (i.e. the absolute  
1574 value of  $A_{\text{net}}$  during the logging period) across the logging interval.

1575 5.2.4 *Leaf trait measurements*

1576 The focal leaf used to generate  $A_{\text{net}}/C_i$  curves and dark respiration was  
1577 harvested immediately following gas exchange measurements. Images of each focal  
1578 leaf were curated using a flat-bed scanner to determine wet leaf area using the  
1579 'LeafArea' R package (Katabuchi 2015), which automates leaf area calculations  
1580 using ImageJ software (Schneider et al. 2012). Each leaf was dried at 65°C for  
1581 at least 48 hours, and subsequently weighed and ground until homogenized. Leaf  
1582 mass per area ( $M_{\text{area}}$ ; g m<sup>-2</sup>) was calculated as the ratio of dry leaf biomass  
1583 to fresh leaf area. Using subsamples of ground and homogenized leaf tissue, we  
1584 measured leaf nitrogen content ( $N_{\text{mass}}$ ; gN g<sup>-1</sup>) through elemental combustion  
1585 analysis (Costech-4010, Costech, Inc., Valencia, CA, USA). Leaf nitrogen content  
1586 per unit leaf area ( $N_{\text{area}}$ ; gN m<sup>-2</sup>) was calculated by multiplying  $N_{\text{mass}}$  and  $M_{\text{area}}$ .

1587 We extracted chlorophyll content from a second leaf in the same trifoliolate  
1588 leaf set as the focal leaf used to generate  $A_{\text{net}}/C_i$  curves. Prior to chlorophyll  
1589 extraction, we used a cork borer to punch between 3 and 5 0.6 cm<sup>2</sup> disks from  
1590 the leaf. Separate images of each punched leaf and set of leaf disks were curated  
1591 using a flat-bed scanner to determine wet leaf area, again quantified using the

1592 'LeafArea' R package (Katabuchi 2015). The punched leaf was dried and weighed  
1593 after at least 65°C in the drying oven to determine Marea of the chlorophyll leaf.

1594 Leaf disks were shuttled into a test tube containing 10mL dimethyl sul-  
1595 foxide, vortexed, and incubated at 65degreeC for 120 minutes (Barnes et al.  
1596 1992). Incubated test tubes were vortexed again before loaded in 150  $\mu$ L trip-  
1597 licate aliquots to a 96-well plate. Dimethyl sulfoxide was also loaded in a 150  
1598  $\mu$ L triplicate aliquot as a blank. Absorbance measurements at 649.1 nm ( $A_{649.1}$ )  
1599 and 665.1 nm ( $A_{665.1}$ ) were read in each well using a plate reader (Biotek Synergy  
1600 H1; Biotek Instruments, Winooski, VT USA) (Wellburn 1994), with triplicates  
1601 subsequently averaged and corrected by the mean of the blank absorbance value.  
1602 Blank-corrected absorbance values were used to estimate  $Chl_a$  ( $\mu$ g mL $^{-1}$ ) and  
1603  $Chl_b$  ( $\mu$ g mL $^{-1}$ ) following equations from Wellburn (1994):

$$Chl_a = 12.47A_{665.1} - 3.62A_{649.1} \quad (5.1)$$

1604 and

$$Chl_b = 25.06A_{665.1} - 6.50A_{649.1} \quad (5.2)$$

1605  $Chl_a$  and  $Chl_b$  were converted to mmol mL $^{-1}$  using the molar mass of chlorophyll a  
1606 (893.51 g mol $^{-1}$ ) and the molar mass of chlorophyll b (907.47 g mol $^{-1}$ ), then added  
1607 together to calculate total chlorophyll content in the dimethyl sulfoxide extractant  
1608 (mmol mL $^{-1}$ ). Total chlorophyll content was multiplied by the volume of the  
1609 dimethyl sulfoxide extractant (10 mL) and converted to area-based chlorophyll  
1610 content by dividing by the total area of the leaf disks ( $Chl_{area}$ ; mmol m $^{-2}$ ). Mass-  
1611 based chlorophyll content ( $Chl_{mass}$ ; mmol g $^{-1}$ ) was calculated by dividing  $Chl_{area}$

**1612** by the leaf mass per area of the punched leaf.

**1613** 5.2.5 *A/C<sub>i</sub> curve fitting and parameter estimation*

**1614** We fit  $A_{\text{net}}/C_i$  curves of each individual using the ‘fitaci’ function in the  
**1615** ‘plantecophys’ R package (Duursma 2015). This function estimates the maximum  
**1616** rate of Rubisco carboxylation  $V_{\text{cmax}}$ ;  $\mu\text{mol m}^{-2} \text{s}^{-1}$ ) and maximum rate of electron  
**1617** transport for RuBP regeneration ( $J_{\text{max}}$ ;  $\mu\text{mol m}^{-2} \text{s}^{-1}$ ) based on the Farquhar bio-  
**1618** chemical model of C<sub>3</sub> photosynthesis (Farquhar et al. 1980). Triose phosphate  
**1619** utilization (TPU) limitation was included in all curve fits, and all curve fits in-  
**1620** cluded measured dark respiration values. As  $A_{\text{net}}/C_i$  curves were generated using  
**1621** a common leaf temperature, curves were fit using Michaelis-Menton coefficients  
**1622** for Rubisco affinity to CO<sub>2</sub> ( $K_c$ ;  $\mu\text{mol mol}^{-1}$ ) and O<sub>2</sub> ( $K_o$ ;  $\mu\text{mol mol}^{-1}$ ), and the  
**1623** CO<sub>2</sub> compensation point ( $\Gamma^*$ ;  $\mu\text{mol mol}^{-1}$ ) reported in Bernacchi et al. (2001).  
**1624** Specifically,  $K_c$  was set to 404.9  $\mu\text{mol mol}^{-1}$ ,  $K_o$  was set to 278.4  $\mu\text{mol mol}^{-1}$ , and  
**1625**  $\Gamma^*$  was set to 42.75  $\mu\text{mol mol}^{-1}$ . The use of a common leaf temperature across  
**1626** curves and dark respiration measurements also eliminated the need to manually  
**1627** temperature standardize rate estimates. For clarity, we reference  $V_{\text{cmax}}$ ,  $J_{\text{max}}$ , and  
**1628**  $R_d$  estimates throughout the rest of the paper as  $V_{\text{cmax}25}$ ,  $J_{\text{max}25}$ , and  $R_{d25}$ .

**1629** 5.2.6 Stomatal limitation

**1630** We quantified the extent by which stomatal conductance limited photo-  
**1631** synthesis (l; unitless) following equations originally described in Farquhar and  
**1632** Sharkey (1982). Stomatal limitation was calculated as:

$$l = 1 - \frac{A_{net}}{A_{mod}} \quad (5.3)$$

**1633** where  $A_{mod}$  represents the photosynthetic rate where  $C_i = C_a$ .  $A_{mod}$  was calcu-

**1634** lated as:

$$A_{mod} = V_{cmax25} - \frac{420 - \Gamma^*}{420 + K_m} - R_{d25} \quad (5.4)$$

**1635**  $K_m$  is the Michaelis-Menten coefficient for Rubisco-limited photosynthesis, calcu-

**1636** lated as:

$$K_m = K_c \cdot \left(1 + \frac{O_i}{K_o}\right) \quad (5.5)$$

**1637** where  $O_i$  refers to leaf intercellular  $O_2$  concentrations, set to  $210 \mu\text{mol mol}^{-1}$ .

**1638** 5.2.7 *Proportion of leaf nitrogen allocated to photosynthesis and structure*

**1639** We used equations from Niinemets and Tenhunen (1997) to estimate the

**1640** proportion of leaf N content allocated to Rubisco bioenergetics, and light harvest-

**1641** ing proteins. The proportion of leaf N allocated to Rubisco ( $\rho_{rub}$ ;  $\text{gN gN}^{-1}$ ) was

**1642** calculated as a function of  $V_{cmax25}$  and  $N_{area}$ :

$$\rho_{rubisco} = \frac{V_{cmax25} N_r}{V_{cr} N_{area}} \quad (5.6)$$

**1643** where  $N_r$  is the amount of nitrogen in Rubisco, set to  $0.16 \text{ gN (gN in Rubisco)}^{-1}$

**1644** and  $V_{cr}$  is the maximum rate of RuBP carboxylation per unit Rubisco protein,

**1645** set to  $20.5 \mu\text{mol CO}_2 (\text{g Rubisco})^{-1}$ . The proportion of leaf nitrogen allocated to

**1646** bioenergetics ( $\rho_{bioe}$ ;  $\text{gN gN}^{-1}$ ) was similarly calculated as a function of  $J_{max25}$  and

**1647**  $N_{\text{area}}$ :

$$\rho_{\text{bioe}} = \frac{J_{\text{max}25} N_b}{J_{\text{mc}} N_{\text{area}}} \quad (5.7)$$

**1648** where  $N_b$  is the amount of nitrogen in cytochrome f, set to 0.12407 gN ( $\mu\text{mol}$  cytochrome f) $^{-1}$  assuming a constant 1: 1: 1.2 cytochrome f: ferredoxin NADP reductase: coupling factor molar ratio (Evans and Seemann 1989; Niinemets and Tenhunen 1997), and  $J_{\text{mc}}$  is the capacity of electron transport per cytochrome f, set to 156  $\mu\text{mol}$  electron ( $\mu\text{mol}$  cytochrome f) $^{-1}\text{s}^{-1}$ .

**1653** The proportion of leaf nitrogen allocated to light harvesting proteins was calculated as a function of  $Chl_{\text{mass}}$  and  $N_{\text{mass}}$ :

$$\rho_{\text{light}} = \frac{Chl_{\text{mass}}}{N_{\text{mass}} c_b} \quad (5.8)$$

**1655** where  $c_b$  is the stoichiometry of the light-harvesting chlorophyll complexes of photosystem II, set to 2.75 mmol chlorophyll (gN in chlorophyll) $^{-1}$ . We used the  $N_{\text{mass}}$  value of the focal leaf used to generate  $A_{\text{net}}/C_i$  curves instead of the leaf used to extract chlorophyll content, as the two leaves are from the same trifoliolate leaf set and are highly correlated with each other (Figure SX).

**1660** The proportion of leaf nitrogen content allocated to photosynthetic tissue ( $\rho_{\text{photo}}$ ; gN gN $^{-1}$ ) was estimated as the sum of  $\rho_{\text{rubisco}}$ ,  $\rho_{\text{bioe}}$ , and  $\rho_{\text{light}}$ .

**1662** Finally, the proportion of leaf N content allocated to structural tissue ( $\rho_{\text{str}}$ ; gN gN $^{-1}$ ) was estimated as:

$$\rho_{\text{structure}} = \frac{N_{\text{cw}}}{N_{\text{area}}} \quad (5.9)$$

1664 where  $N_{cw}$  is the leaf N content allocated to cell walls ( $\text{gN m}^{-2}$ ), calculated as a  
1665 function of  $M_{area}$  using an empirical equation from Onoda et al. (2017):

$$N_{cw} = 0.000355 * M_{area}^{1.39} \quad (5.10)$$

1666 5.2.8 *Whole plant traits*

1667 Seven weeks after experiment initiation and immediately following gas ex-  
1668 change measurements, we harvested all experimental individuals and separated  
1669 biomass of each experimental individual into major organ types (leaves, stems,  
1670 roots, and nodules when present). Fresh leaf area of all harvested leaves was mea-  
1671 sured using an LI-3100C (Li-COR Biosciences, Lincoln, Nebraska, USA). Total  
1672 fresh leaf area ( $\text{cm}^2$ ) was calculated as the sum of all leaf areas, including the focal  
1673 leaf used to collect gas exchange data and the focal leaf used to extract chlorophyll  
1674 content. All harvested material was dried in an oven set to 65°C for at least 48  
1675 hours, weighed, and ground to homogeneity. Leaves and nodules were manually  
1676 ground either with a mortar and pestle, while stems and roots were ground using  
1677 a Wiley mill (E3300 Mini Mill; Eberbach Corp., MI, USA). Total dry biomass (g)  
1678 was calculated as the sum of dry leaf (including focal leaf for both the  $A_{net}/C_i$   
1679 curve and leaf used to extract chlorophyll content), stem, root, and root nodule  
1680 biomass. We also quantified carbon and nitrogen content of each respective organ  
1681 type through elemental combustion (Costech-4010, Costech, Inc., Valencia, CA,  
1682 USA) using subsamples of ground and homogenized organ tissue.

1683 Following the approach explained in Perkowski et al. (2021), we calcu-  
1684 lated structural carbon costs to acquire nitrogen as the ratio of total belowground

1685 carbon biomass to whole plant nitrogen biomass ( $N_{\text{cost}}$ ; gC gN<sup>-1</sup>). Belowground  
1686 carbon biomass ( $C_{\text{bg}}$ ; gC) was calculated as the sum of root carbon biomass  
1687 and root nodule carbon biomass. Root carbon biomass and root nodule carbon  
1688 biomass was calculated as the product of the organ biomass and the respective  
1689 organ carbon content. Whole plant nitrogen biomass ( $N_{\text{wp}}$ ; gN) was similarly  
1690 calculated as the sum of total leaf, stem, root, and root nodule nitrogen biomass,  
1691 including the focal leaf used for  $A_{\text{net}}/C_i$  curve and chlorophyll extractions. Leaf,  
1692 stem, root, and root nodule nitrogen biomass was calculated as the product of  
1693 the organ biomass and the respective organ nitrogen content. This calculation  
1694 only quantifies plant structural carbon costs to acquire nitrogen and does not  
1695 include any additional costs of nitrogen acquisition associated with respiration,  
1696 root exudation, or root turnover. An explicit explanation of the limitations for  
1697 interpreting this calculation can be found in Perkowski et al. (2021) and Terrer  
1698 et al. (2018).

1699 Finally, plant investments in nitrogen fixation were calculated as the ratio  
1700 of root nodule biomass to root biomass, where increasing values indicate an in-  
1701 crease in plant investments to nitrogen fixation (Dovrat et al. 2018; Dovrat et al.  
1702 2020; Perkowski et al. 2021).

1703 5.2.9 *Statistical analyses*

1704 Any uninoculated pots that had substantial root nodule formation (nodule  
1705 biomass: root biomass values greater than 0.05 g g<sup>-1</sup>) were removed from our  
1706 analyses. This was because they were assumed to have been colonized by symbiotic  
1707 nitrogen-fixing bacteria from outside sources. This decision resulted in the removal

1708 of sixteen pots from our analysis: two pots in the elevated CO<sub>2</sub> treatment that  
1709 received 35 ppm N, three pots in the elevated CO<sub>2</sub> treatment that received 70  
1710 ppm N, one pot in the elevated CO<sub>2</sub> treatment that received 210 ppm N, two pots  
1711 in the elevated CO<sub>2</sub> treatment that received 280 ppm N, two pots in the ambient  
1712 CO<sub>2</sub> treatment that received 0 ppm N, three pots in the ambient CO<sub>2</sub> treatment  
1713 that received 70 ppm N, two pots in the ambient CO<sub>2</sub> treatment that received  
1714 105 ppm N, and one pot in the ambient CO<sub>2</sub> treatment that received 280 ppm N.

1715 We built a series of linear mixed effects models to investigate the impacts of  
1716 CO<sub>2</sub> concentration, soil nitrogen fertilization, and inoculation with *B. japonicum*  
1717 on *G. max* gas exchange, tradeoffs between nitrogen and water use, whole plant  
1718 growth, and investment in nitrogen fixation. All models included CO<sub>2</sub> treatment  
1719 as a categorical fixed effect, inoculation treatment as a categorical fixed effect,  
1720 soil nitrogen fertilization as a continuous fixed effect, with interaction terms be-  
1721 tween all three fixed effects. All models also accounted for climatic difference  
1722 between chambers across experiment iterations by including a random intercept  
1723 term that nested starting chamber rack by CO<sub>2</sub> treatment. Models with this  
1724 independent variable structure were created for each of the following dependent  
1725 variables:  $N_{\text{area}}$ ,  $M_{\text{area}}$ ,  $N_{\text{mass}}$ ,  $Chl_{\text{area}}$ ,  $V_{\text{cmax25}}$ ,  $J_{\text{max25}}$ ,  $J_{\text{max25}}:V_{\text{cmax25}}$ ,  $R_{\text{d25}}$ ,  $g_{\text{sw}}$ ,  
1726 stomatal limitation,  $\rho_{\text{rubisco}}$ ,  $\rho_{\text{bioe}}$ ,  $\rho_{\text{light}}$ ,  $\rho_{\text{photo}}$ ,  $\rho_{\text{structure}}$ ,  $N_{\text{cost}}$ ,  $C_{\text{bg}}$ ,  $N_{\text{wp}}$ , total  
1727 biomass, total leaf area, nodule biomass, and the ratio of nodule biomass to root  
1728 biomass.

1729 We used Shapiro-Wilk tests of normality to determine whether linear mixed  
1730 effects models satisfied residual normality assumptions. If residual normality as-  
1731 sumptions were not met (Shapiro-Wilk:  $p < 0.05$ ), then models were fit using

**1732** dependent variables that were natural log transformed. All residual normality  
**1733** assumptions that did not originally satisfy residual normality assumptions were  
**1734** met with either a natural log or square root data transformation (Shapiro-Wilk:  
**1735**  $p > 0.05$  in all cases). Specifically, models for  $N_{\text{area}}$ ,  $N_{\text{mass}}$ ,  $Chl_{\text{area}}$ ,  $V_{\text{cmax25}}$ ,  
**1736**  $J_{\text{max25}}$ ,  $J_{\text{max25}}:V_{\text{cmax25}}$ ,  $g_{\text{sw}}$ , stomatal limitation,  $\rho_{\text{rubisco}}$ ,  $\rho_{\text{bioe}}$ ,  $\rho_{\text{light}}$ ,  $\rho_{\text{photo}}$ , and to-  
**1737** tal leaf area satisfied residual normality assumptions without data transformation.  
**1738** Models for  $M_{\text{area}}$ ,  $\rho_{\text{structure}}$ ,  $N_{\text{cost}}$ ,  $C_{\text{bg}}$ ,  $N_{\text{wp}}$ , and total biomass satisfied residual  
**1739** normality assumptions with a natural log data transformation, while models for  
**1740** nodule biomass and nodule biomass: root biomass satisfied residual normality  
**1741** assumptions with a square root data transformation.

**1742** In all statistical models, we used the 'lmer' function in the 'lme4' R package  
**1743** (Bates et al. 2015) to fit each model and the 'Anova' function in the 'car' R  
**1744** package (Fox and Weisberg 2019) to calculate Type II Wald's  $\chi^2$  and determine the  
**1745** significance ( $\alpha = 0.05$ ) of each fixed effect coefficient. We then used the 'emmeans'  
**1746** R package (Lenth 2019) to conduct post-hoc comparisons using Tukey's tests,  
**1747** where degrees of freedom were approximated using the Kenward-Roger approach  
**1748** (Kenward and Roger 1997). All analyses and plots were conducted in R version  
**1749** 4.2.0 (R Core Team 2021).

**1750** 5.3 Results

**1751** 5.4 Discussion

**1752**

**Chapter 6**

**1753**

**Conclusions**

1754

References

- 1755 Abrams, M. D. and S. A. Mostoller (1995). Gas exchange, leaf structure and  
1756 nitrogen in contrasting successional tree species growing in open and under-  
1757 story sites during a drought. *Tree Physiology* 15(6), 361–370.
- 1758 Adams, M. A., T. L. Turnbull, J. I. Sprent, and N. Buchmann (2016). Legumes  
1759 are different: Leaf nitrogen, photosynthesis, and water use efficiency. *Pro-  
1760 ceedings of the National Academy of Sciences of the United States of Amer-  
1761 ica* 113(15), 4098–4103.
- 1762 Ainsworth, E. A., P. A. Davey, C. J. Bernacchi, O. C. Dermody, E. A. Heaton,  
1763 D. J. Moore, P. B. Morgan, S. L. Naidu, H. S. Y. Ra, X. G. Zhu, P. S. Curtis,  
1764 and S. P. Long (2002). A meta-analysis of elevated [CO<sub>2</sub>] effects on soybean  
1765 (*Glycine max*) physiology, growth and yield. *Global Change Biology* 8(8),  
1766 695–709.
- 1767 Ainsworth, E. A. and S. P. Long (2005). What have we learned from 15 years of  
1768 free-air CO<sub>2</sub> enrichment (FACE)? A meta-analytic review of the responses  
1769 of photosynthesis, canopy properties and plant production to rising CO<sub>2</sub>.  
1770 *New Phytologist* 165(2), 351–372.
- 1771 Ainsworth, E. A. and A. Rogers (2007). The response of photosynthesis and  
1772 stomatal conductance to rising [CO<sub>2</sub>]: mechanisms and environmental in-  
1773 teractions. *Plant, Cell and Environment* 30(3), 258–270.
- 1774 Allen, K., J. B. Fisher, R. P. Phillips, J. S. Powers, and E. R. Brzostek (2020).  
1775 Modeling the carbon cost of plant nitrogen and phosphorus uptake across  
1776 temperate and tropical forests. *Frontiers in Forests and Global Change* 3,

- 1777** 1–12.
- 1778** Allison, S. D., C. I. Czimczik, and K. K. Treseder (2008). Microbial activity
- 1779** and soil respiration under nitrogen addition in Alaskan boreal forest. *Global*
- 1780** *Change Biology* 14(5), 1156–1168.
- 1781** Andersen, M. K., H. Hauggaard-Nielsen, P. Ambus, and E. S. Jensen (2005).
- 1782** Biomass production, symbiotic nitrogen fixation and inorganic N use in dual
- 1783** and tri-component annual intercrops. *Plant and Soil* 266(1-2), 273–287.
- 1784** Arndal, M. F., A. Tolver, K. S. Larsen, C. Beier, and I. K. Schmidt (2018). Fine
- 1785** root growth and vertical distribution in response to elevated CO<sub>2</sub>, warming
- 1786** and drought in a mixed heathland–grassland. *Ecosystems* 21(1), 15–30.
- 1787** Arnone, J. A. (1997). Indices of plant N availability in an alpine grassland under
- 1788** elevated atmospheric CO<sub>2</sub>. *Plant and Soil* 190(1), 61–66.
- 1789** Arora, V. K., A. Katavouta, R. G. Williams, C. D. Jones, V. Brovkin,
- 1790** P. Friedlingstein, J. Schwinger, L. Bopp, O. Boucher, P. Cadule, M. A.
- 1791** Chamberlain, J. R. Christian, C. Delire, R. A. Fisher, T. Hajima, T. Ilyina,
- 1792** E. Joetzjer, M. Kawamiya, C. D. Koven, J. P. Krasting, R. M. Law, D. M.
- 1793** Lawrence, A. Lenton, K. Lindsay, J. Pongratz, T. Raddatz, R. Séférian,
- 1794** K. Tachiiri, J. F. Tjiputra, A. Wiltshire, T. Wu, and T. Ziehn (2020).
- 1795** Carbon-concentration and carbon-climate feedbacks in CMIP6 models and
- 1796** their comparison to CMIP5 models. *Biogeosciences* 17(16), 4173–4222.
- 1797** Bae, K., T. J. Fahey, R. D. Yanai, and M. Fisk (2015). Soil nitrogen availabil-
- 1798** ity affects belowground carbon allocation and soil respiration in northern
- 1799** hardwood forests of New Hampshire. *Ecosystems* 18(7), 1179–1191.

- 1800 Barber, S. A. (1962). A diffusion and mass-flow concept of soil nutrient avail-  
1801 ability. *Soil Science* 93(1), 39–49.
- 1802 Barnes, J. D., L. Balaguer, E. Manrique, S. Elvira, and A. W. Davison (1992).  
1803 A reappraisal of the use of DMSO for the extraction and determination  
1804 of chlorophylls a and b in lichens and higher plants. *Environmental and*  
1805 *Experimental Botany* 32(2), 85–100.
- 1806 Bates, D., M. Mächler, B. Bolker, and S. Walker (2015). Fitting linear mixed-  
1807 effects models using lme4. *Journal of Statistical Software* 67(1), 1–48.
- 1808 Beaudette, D., J. Skovlin, S. Roeker, and A. Brown (2022). soilDB: Soil  
1809 Database Interface.
- 1810 Bengtson, P., J. Barker, and S. J. Grayston (2012). Evidence of a strong cou-  
1811 pling between root exudation, C and N availability, and stimulated SOM  
1812 decomposition caused by rhizosphere priming effects. *Ecology and Evolu-*  
1813 *tion* 93(8), 1843–1852.
- 1814 Bernacchi, C. J., E. L. Singsaas, C. Pimentel, A. R. Portis, and S. P. Long  
1815 (2001). Improved temperature response functions for models of Rubisco-  
1816 limited photosynthesis. *Plant, Cell and Environment* 24(2), 253–259.
- 1817 Bialic-Murphy, L., N. G. Smith, P. Voothuluru, R. M. McElderry, M. D.  
1818 Roche, S. T. Cassidy, S. N. Kivlin, and S. Kalisz (2021). Invasion-induced  
1819 root-fungal disruptions alter plant water and nitrogen economies. *Ecology*  
1820 *Letters* 24(6), 1145–1156.
- 1821 Bloom, A. J., F. S. Chapin, and H. A. Mooney (1985). Resource limitation  
1822 in plants - an economic analogy. *Annual Review of Ecology and Systemat-*

- 1823       *ics* 16(1), 363–392.
- 1824       Bloomfield, K. J., B. D. Stocker, T. F. Keenan, and I. C. Prentice (2022).
- 1825       Environmental controls on the light use efficiency of terrestrial gross primary
- 1826       production. *Global Change Biology*, 0–2.
- 1827       Bonan, G. B., M. D. Hartman, W. J. Parton, and W. R. Wieder (2013). Evaluat-
- 1828       ing litter decomposition in earth system models with long-term litterbag ex-
- 1829       periments: an example using the Community Land Model version 4 (CLM4).
- 1830       *Global Change Biology* 19(3), 957–974.
- 1831       Bonan, G. B., P. J. Lawrence, K. W. Oleson, S. Levis, M. Jung, M. Reich-
- 1832       stein, D. M. Lawrence, and S. C. Swenson (2011). Improving canopy pro-
- 1833       cesses in the Community Land Model version 4 (CLM4) using global flux
- 1834       fields empirically inferred from FLUXNET data. *Journal of Geophysical Re-*
- 1835       *search* 116(G2), G02014.
- 1836       Booth, B. B. B., C. D. Jones, M. Collins, I. J. Totterdell, P. M. Cox, S. Sitch,
- 1837       C. Huntingford, R. A. Betts, G. R. Harris, and J. Lloyd (2012). High sen-
- 1838       sitivity of future global warming to land carbon cycle processes. *Environ-*
- 1839       *mental Research Letters* 7(2), 024002.
- 1840       Borer, E. T., W. S. Harpole, P. B. Adler, E. M. Lind, J. L. Orrock, E. W.
- 1841       Seabloom, and M. D. Smith (2014). Finding generality in ecology: A model
- 1842       for globally distributed experiments. *Methods in Ecology and Evolution* 5(1),
- 1843       65–73.
- 1844       Braghiere, R. K., J. B. Fisher, K. Allen, E. Brzostek, M. Shi, X. Yang, D. M.
- 1845       Ricciuto, R. A. Fisher, Q. Zhu, and R. P. Phillips (2022). Modeling global
- 1846       carbon costs of plant nitrogen and phosphorus acquisition. *Journal of Ad-*

- 1847 *vances in Modeling Earth Systems* 14(8), 1–23.
- 1848 Brix, H. (1971). Effects of nitrogen fertilization on photosynthesis and respiration in Douglas-fir. *Forest Science* 17(4), 407–414.
- 1850 Brzostek, E. R., J. B. Fisher, and R. P. Phillips (2014). Modeling the carbon cost of plant nitrogen acquisition: Mycorrhizal trade-offs and multipath resistance uptake improve predictions of retranslocation. *Journal of Geophysical Research: Biogeosciences* 119, 1684–1697.
- 1854 Bubier, J. L., R. Smith, S. Juutinen, T. R. Moore, R. Minocha, S. Long, and S. Minocha (2011). Effects of nutrient addition on leaf chemistry, morphology, and photosynthetic capacity of three bog shrubs. *Oecologia* 167(2), 355–368.
- 1858 Cernusak, L. A., N. Ubierna, K. Winter, J. A. M. Holtum, J. D. Marshall, and G. D. Farquhar (2013). Environmental and physiological determinants of carbon isotope discrimination in terrestrial plants. *New Phytologist* 200(4), 950–965.
- 1862 Chen, J.-L., J. F. Reynolds, P. C. Harley, and J. D. Tenhunen (1993). Coordination theory of leaf nitrogen distribution in a canopy. *Oecologia* 93(1), 63–69.
- 1865 Clark, D. B., L. M. Mercado, S. Sitch, C. D. Jones, N. Gedney, M. J. Best, M. Pryor, G. G. Rooney, R. L. H. Essery, E. Blyth, O. Boucher, R. J. Harding, C. Huntingford, and P. M. Cox (2011). The Joint UK Land Environment Simulator (JULES), model description. Part 2: Carbon fluxes and vegetation dynamics. *Geoscientific Model Development* 4(3), 701–722.

- 1870** Cornwell, W. K., J. H. C. Cornelissen, K. Amatangelo, E. Dorrepaal, V. T.  
**1871** Eviner, O. Godoy, S. E. Hobbie, B. Hoorens, H. Kurokawa, N. Pérez-  
**1872** Harguindeguy, H. M. Quested, L. S. Santiago, D. A. Wardle, I. J. Wright,  
**1873** R. Aerts, S. D. Allison, P. van Bodegom, V. Brovkin, A. Chatain, T. V.  
**1874** Callaghan, S. Díaz, E. Garnier, D. E. Gurvich, E. Kazakou, J. A. Klein,  
**1875** J. Read, P. B. Reich, N. A. Soudzilovskaia, M. V. Vaieretti, and M. Westoby  
**1876** (2008). Plant species traits are the predominant control on litter decompo-  
**1877** sition rates within biomes worldwide. *Ecology Letters* 11(10), 1065–1071.
- 1878** Cornwell, W. K., I. J. Wright, J. Turner, V. Maire, M. M. Barbour, L. A.  
**1879** Cernusak, T. E. Dawson, D. S. Ellsworth, G. D. Farquhar, H. Griffiths,  
**1880** C. Keitel, A. Knohl, P. B. Reich, D. G. Williams, R. Bhaskar, J. H. C. Cor-  
**1881** nelissen, A. Richards, S. Schmidt, F. Valladares, C. Körner, E.-D. Schulze,  
**1882** N. Buchmann, and L. S. Santiago (2018). Climate and soils together regulate  
**1883** photosynthetic carbon isotope discrimination within C<sub>3</sub> plants worldwide.  
**1884** *Global Ecology and Biogeography* 27(9), 1056–1067.
- 1885** Cramer, W. and I. C. Prentice (1988). Simulation of regional soil moisture  
**1886** deficits on a European scale. *Norsk Geografisk Tidsskrift - Norwegian Jour-  
**1887** nal of Geography* 42(2-3), 149–151.
- 1888** Curtis, P. S. (1996). A meta-analysis of leaf gas exchange and nitrogen in trees  
**1889** grown under elevated carbon dioxide. *Plant, Cell and Environment* 19(2),  
**1890** 127–137.
- 1891** Daly, C., M. Halbleib, J. I. Smith, W. P. Gibson, M. K. Doggett, G. H. Taylor,  
**1892** J. Curtis, and P. P. Pasteris (2008). Physiographically sensitive mapping  
**1893** of climatological temperature and precipitation across the conterminous

- 1894** United States. *International Journal of Climatology* 28(15), 2031–2064.
- 1895** Davies-Barnard, T., J. Meyerholt, S. Zaehle, P. Friedlingstein, V. Brovkin,
- 1896** Y. Fan, R. A. Fisher, C. D. Jones, H. Lee, D. Peano, B. Smith, D. Wårlind,
- 1897** and A. J. Wiltshire (2020). Nitrogen cycling in CMIP6 land surface models:
- 1898** progress and limitations. *Biogeosciences* 17(20), 5129–5148.
- 1899** Davis, T. W., I. C. Prentice, B. D. Stocker, R. T. Thomas, R. J. Whitley,
- 1900** H. Wang, B. J. Evans, A. V. Gallego-Sala, M. T. Sykes, and W. Cramer
- 1901** (2017). Simple process-led algorithms for simulating habitats (SPLASH
- 1902** v.1.0): robust indices of radiation, evapotranspiration and plant-available
- 1903** moisture. *Geoscientific Model Development* 10, 689–708.
- 1904** Delaire, M., E. Frak, M. Sigogne, B. Adam, F. Beaujard, and X. Le Roux
- 1905** (2005). Sudden increase in atmospheric CO<sub>2</sub> concentration reveals strong
- 1906** coupling between shoot carbon uptake and root nutrient uptake in young
- 1907** walnut trees. *Tree Physiology* 25(2), 229–235.
- 1908** Doane, T. A. and W. R. Horwáth (2003). Spectrophotometric determination of
- 1909** nitrate with a single reagent. *Analytical Letters* 36(12), 2713–2722.
- 1910** Dong, N., I. C. Prentice, B. J. Evans, S. Caddy-Retalic, A. J. Lowe, and I. J.
- 1911** Wright (2017). Leaf nitrogen from first principles: field evidence for adaptive
- 1912** variation with climate. *Biogeosciences* 14(2), 481–495.
- 1913** Dong, N., I. C. Prentice, I. J. Wright, B. J. Evans, H. F. Togashi, S. Caddy-
- 1914** Retalic, F. A. McInerney, B. Sparrow, E. Leitch, and A. J. Lowe (2020).
- 1915** Components of leaf-trait variation along environmental gradients. *New Phy-*
- 1916** *tologist* 228(1), 82–94.

- 1917** Dong, N., I. C. Prentice, I. J. Wright, H. Wang, O. K. Atkin, K. J. Bloomfield,  
**1918** T. F. Domingues, S. M. Gleason, V. Maire, Y. Onoda, H. Poorter, and N. G.  
**1919** Smith (2022). Leaf nitrogen from the perspective of optimal plant function.  
**1920** *Journal of Ecology* 110(11), 2585–2602.
- 1921** Dong, N., I. J. Wright, J. M. Chen, X. Luo, H. Wang, T. F. Keenan, N. G.  
**1922** Smith, and I. C. Prentice (2022). Rising CO<sub>2</sub> and warming reduce global  
**1923** canopy demand for nitrogen. *New Phytologist* 235(5), 1692–1700.
- 1924** Dovrat, G., H. Bakhshian, T. Masci, and E. Sheffer (2020). The nitrogen eco-  
**1925** nomic spectrum of legume stoichiometry and fixation strategy. *New Phytol-  
ogist* 227(2), 365–375.
- 1927** Dovrat, G., T. Masci, H. Bakhshian, E. Mayzlish Gati, S. Golan, and E. Shef-  
**1928** fer (2018). Drought-adapted plants dramatically downregulate dinitrogen  
**1929** fixation: Evidences from Mediterranean legume shrubs. *Journal of Ecol-  
ogy* 106(4), 1534–1544.
- 1931** Drake, B. G., M. A. González-Meler, and S. P. Long (1997). More efficient  
**1932** plants: a consequence of rising atmospheric CO<sub>2</sub>? *Annual Review of Plant  
Biology* 48, 609–639.
- 1934** Duursma, R. A. (2015). Plantecophys - An R Package for Analysing and Mod-  
**1935**elling Leaf Gas Exchange Data. *PLOS ONE* 10(11), e0143346.
- 1936** Eastman, B. A., M. B. Adams, E. R. Brzostek, M. B. Burnham, J. E. Carrara,  
**1937** C. Kelly, B. E. McNeil, C. A. Walter, and W. T. Peterjohn (2021). Altered  
**1938** plant carbon partitioning enhanced forest ecosystem carbon storage after 25  
**1939** years of nitrogen additions. *New Phytologist* 230(4), 1435–1448.

- 1940** Ellsworth, D. S. and P. B. Reich (1996). Photosynthesis and leaf nitrogen in five  
**1941** Amazonian tree species during early secondary succession. *Ecology* 77(2),  
**1942** 581–594.
- 1943** Espelta, J. M., P. Cortés, M. Mangirón, and J. Retana (2005). Differences in  
**1944** biomass partitioning, leaf nitrogen content, and water use efficiency d13C  
**1945** result in similar performance of seedlings of two Mediterranean oaks with  
**1946** contrasting leaf habit. *Ecoscience* 12(4), 447–454.
- 1947** Evans, J. R. (1989). Photosynthesis and nitrogen relationships in leaves of C<sub>3</sub>  
**1948** plants. *Oecologia* 78(1), 9–19.
- 1949** Evans, J. R. and V. C. Clarke (2019). The nitrogen cost of photosynthesis.  
**1950** *Journal of Experimental Botany* 70(1), 7–15.
- 1951** Evans, J. R. and H. Poorter (2001). Photosynthetic acclimation of plants to  
**1952** growth irradiance: the relative importance of specific leaf area and nitrogen  
**1953** partitioning in maximizing carbon gain. *Plant, Cell and Environment* 24(8),  
**1954** 755–767.
- 1955** Evans, J. R. and J. R. Seemann (1989). The allocation of protein nitrogen in  
**1956** the photosynthetic apparatus: costs, consequences, and control. *Photosyn-*  
**1957** *thesis* 8, 183–205.
- 1958** Exbrayat, J.-F., A. A. Bloom, P. Falloon, A. Ito, T. L. Smallman, and  
**1959** M. Williams (2018). Reliability ensemble averaging of 21<sup>st</sup> century projec-  
**1960** tions of terrestrial net primary productivity reduces global and regional  
**1961** uncertainties. *Earth System Dynamics* 9(1), 153–165.
- 1962** Farquhar, G. D., J. R. Ehleringer, and K. T. Hubick (1989). Carbon Isotope

- 1963** Discrimination and Photosynthesis. *Annual Review of Plant Physiology and Plant Molecular Biology* 40(1), 503–537.
- 1964** Farquhar, G. D. and T. D. Sharkey (1982). Stomatal conductance and photosynthesis. *Annual Review of Plant Physiology* 33(1), 317–345.
- 1965** Farquhar, G. D., S. von Caemmerer, and J. A. Berry (1980). A biochemical model of photosynthetic CO<sub>2</sub> assimilation in leaves of C3 species.
- 1966** *Planta* 149(1), 78–90.
- 1967** Farquhar, G. D., S. von Caemmerer, and J. A. Berry (1980). A biochemical model of photosynthetic CO<sub>2</sub> assimilation in leaves of C3 species.
- 1968** *Planta* 149(1), 78–90.
- 1969** Fay, P. A., S. M. Prober, W. S. Harpole, J. M. H. Knops, J. D. Bakker, E. T. Borer, E. M. Lind, A. S. MacDougall, E. W. Seabloom, P. D. Wragg, P. B. Adler, D. M. Blumenthal, Y. M. Buckley, C. Chu, E. E. Cleland, S. L. Collins, K. F. Davies, G. Du, X. Feng, J. Firn, D. S. Gruner, N. Hagenah, Y. Hautier, R. W. Heckman, V. L. Jin, K. P. Kirkman, J. A. Klein, L. M. Ladwig, Q. Li, R. L. McCulley, B. A. Melbourne, C. E. Mitchell, J. L. Moore, J. W. Morgan, A. C. Risch, M. Schütz, C. J. Stevens, D. A. Wedin, and L. H. Yang (2015). Grassland productivity limited by multiple nutrients.
- 1970** *Nature Plants* 1(7), 15080.
- 1971** Feng, X. (1999). Trends in intrinsic water-use efficiency of natural trees for the past 100–200 years: A response to atmospheric CO<sub>2</sub> concentration. *Geochimica et Cosmochimica Acta* 63(13–14), 1891–1903.
- 1972** Field, C. B. and H. A. Mooney (1986). The photosynthesis-nitrogen relationship in wild plants. In T. J. Givnish (Ed.), *On the Economy of Plant Form and Function*, pp. 25–55. Cambridge: Cambridge University Press.
- 1973** Finzi, A. C., D. J. P. Moore, E. H. DeLucia, J. Lichter, K. S. Hofmockel, R. B. Jackson, H. S. Kim, R. Matamala, H. R. McCarthy, R. Oren, J. S. Pippen,
- 1974** *Nature Plants* 1(7), 15080.
- 1975** Feng, X. (1999). Trends in intrinsic water-use efficiency of natural trees for the past 100–200 years: A response to atmospheric CO<sub>2</sub> concentration. *Geochimica et Cosmochimica Acta* 63(13–14), 1891–1903.
- 1976** Field, C. B. and H. A. Mooney (1986). The photosynthesis-nitrogen relationship in wild plants. In T. J. Givnish (Ed.), *On the Economy of Plant Form and Function*, pp. 25–55. Cambridge: Cambridge University Press.
- 1977** Finzi, A. C., D. J. P. Moore, E. H. DeLucia, J. Lichter, K. S. Hofmockel, R. B. Jackson, H. S. Kim, R. Matamala, H. R. McCarthy, R. Oren, J. S. Pippen,
- 1978** *Nature Plants* 1(7), 15080.
- 1979** Feng, X. (1999). Trends in intrinsic water-use efficiency of natural trees for the past 100–200 years: A response to atmospheric CO<sub>2</sub> concentration. *Geochimica et Cosmochimica Acta* 63(13–14), 1891–1903.
- 1980** Field, C. B. and H. A. Mooney (1986). The photosynthesis-nitrogen relationship in wild plants. In T. J. Givnish (Ed.), *On the Economy of Plant Form and Function*, pp. 25–55. Cambridge: Cambridge University Press.
- 1981** Finzi, A. C., D. J. P. Moore, E. H. DeLucia, J. Lichter, K. S. Hofmockel, R. B. Jackson, H. S. Kim, R. Matamala, H. R. McCarthy, R. Oren, J. S. Pippen,
- 1982** *Nature Plants* 1(7), 15080.
- 1983** Field, C. B. and H. A. Mooney (1986). The photosynthesis-nitrogen relationship in wild plants. In T. J. Givnish (Ed.), *On the Economy of Plant Form and Function*, pp. 25–55. Cambridge: Cambridge University Press.
- 1984** Finzi, A. C., D. J. P. Moore, E. H. DeLucia, J. Lichter, K. S. Hofmockel, R. B. Jackson, H. S. Kim, R. Matamala, H. R. McCarthy, R. Oren, J. S. Pippen,
- 1985** *Nature Plants* 1(7), 15080.
- 1986** Field, C. B. and H. A. Mooney (1986). The photosynthesis-nitrogen relationship in wild plants. In T. J. Givnish (Ed.), *On the Economy of Plant Form and Function*, pp. 25–55. Cambridge: Cambridge University Press.

- 1987** and W. H. Schlesinger (2006). Progressive nitrogen limitation of ecosystem processes under elevated CO<sub>2</sub> in a warm-temperate forest. *Ecology* 87(1), 15–25.
- 1990** Firn, J., J. M. McGree, E. Harvey, H. Flores Moreno, M. Schutz, Y. M. Buckley,
- 1991** E. T. Borer, E. W. Seabloom, K. J. La Pierre, A. M. MacDougall, S. M.
- 1992** Prober, C. J. Stevens, L. L. Sullivan, E. Porter, E. Ladouceur, C. Allen,
- 1993** K. H. Moromizato, J. W. Morgan, W. S. Harpole, Y. Hautier, N. Eisen-
- 1994** hauer, J. P. Wright, P. B. Adler, C. A. Arnillas, J. D. Bakker, L. Biederman,
- 1995** A. A. D. Broadbent, C. S. Brown, M. N. Bugalho, M. C. Caldeira, E. E. Cle-
- 1996** land, A. Ebeling, P. A. Fay, N. Hagenah, A. R. Kleinhesselink, R. Mitchell,
- 1997** J. L. Moore, C. Nogueira, P. L. Peri, C. Roscher, M. D. Smith, P. D. Wragg,
- 1998** and A. C. Risch (2019). Leaf nutrients, not specific leaf area, are consistent
- 1999** indicators of elevated nutrient inputs. *Nature Ecology and Evolution* 3(3),
- 2000** 400–406.
- 2001** Fisher, J. B., S. Sitch, Y. Malhi, R. A. Fisher, C. Huntingford, and S.-Y. Tan
- 2002** (2010). Carbon cost of plant nitrogen acquisition: A mechanistic, globally
- 2003** applicable model of plant nitrogen uptake, retranslocation, and fixation.
- 2004** *Global Biogeochemical Cycles* 24(1), 1–17.
- 2005** Fox, J. and S. Weisberg (2019). *An R companion to applied regression* (Third
- 2006** edit ed.). Thousand Oaks, California: Sage.
- 2007** Franklin, O., R. E. McMurtrie, C. M. Iversen, K. Y. Crous, A. C. Finzi, D. Tis-
- 2008** sue, D. S. Ellsworth, R. Oren, and R. J. Norby (2009). Forest fine-root
- 2009** production and nitrogen use under elevated CO<sub>2</sub>: contrasting responses
- 2010** in evergreen and deciduous trees explained by a common principle. *Global*

- 2011** *Change Biology* 15(1), 132–144.
- 2012** Friedlingstein, P., M. Meinshausen, V. K. Arora, C. D. Jones, A. Anav, S. K.
- 2013** Liddicoat, and R. Knutti (2014). Uncertainties in CMIP5 climate projections
- 2014** due to carbon cycle feedbacks. *Journal of Climate* 27(2), 511–526.
- 2015** Friel, C. A. and M. L. Friesen (2019). Legumes modulate allocation to rhizobial
- 2016** nitrogen fixation in response to factorial light and nitrogen manipulation.
- 2017** *Frontiers in Plant Science* 10, 1316.
- 2018** Fujikake, H., A. Yamazaki, N. Ohtake, K. Sueoshi, S. Matsuhashi, T. Ito,
- 2019** C. Mizuniwa, T. Kume, S. Hoshimoto, N.-S. Ishioka, S. Watanabe, A. Osa,
- 2020** T. Sekine, H. Uchida, A. Tsuji, and T. Ohya (2003). Quick and reversible
- 2021** inhibition of soybean root nodule growth by nitrate involves a decrease in
- 2022** sucrose supply to nodules. *Journal of Experimental Botany* 54(386), 1379–
- 2023** 1388.
- 2024** Ghimire, B., W. J. Riley, C. D. Koven, J. Kattge, A. Rogers, P. B. Reich, and
- 2025** I. J. Wright (2017). A global trait-based approach to estimate leaf nitro-
- 2026** gen functional allocation from observations:. *Ecological Applications* 27(5),
- 2027** 1421–1434.
- 2028** Giardina, C. P., M. D. Coleman, J. E. Hancock, J. S. King, E. A. Lilleskov,
- 2029** W. M. Loya, K. S. Pregitzer, M. G. Ryan, and C. C. Trettin (2005). The
- 2030** response of belowground carbon allocation in forests to global change. In
- 2031** D. Binkley and O. Manyailo (Eds.), *Tree Species Effects on Soils: Implica-*
- 2032** *tions for Global Change* (Volume 55 ed.), Chapter Chapter 7, pp. 119–154.
- 2033** Berlin/Heidelberg: Springer-Verlag.
- 2034** Gibson, A. H. and J. E. Harper (1985). Nitrate effect on nodulation of soybean

- 2035 by *Bradyrhizobium japonicum*. *Crop Science* 25(3), 497–501.
- 2036 Gill, A. L. and A. C. Finzi (2016). Belowground carbon flux links biogeochemical  
2037 cycles and resource-use efficiency at the global scale. *Ecology Letters* 19(12),  
2038 1419–1428.
- 2039 Goll, D. S., V. Brovkin, B. R. Parida, C. H. Reick, J. Kattge, P. B. Reich, P. M.  
2040 van Bodegom, and Ü. Niinemets (2012). Nutrient limitation reduces land  
2041 carbon uptake in simulations with a model of combined carbon, nitrogen  
2042 and phosphorus cycling. *Biogeosciences Discussions* 9(3), 3173–3232.
- 2043 Gregory, L. M., A. M. McClain, D. M. Kramer, J. D. Pardo, K. E. Smith, O. L.  
2044 Tessmer, B. J. Walker, L. G. Ziccardi, and T. D. Sharkey (2021, oct). The  
2045 triose phosphate utilization limitation of photosynthetic rate: Out of global  
2046 models but important for leaf models. *Plant, Cell and Environment* 44(10),  
2047 3223–3226.
- 2048 Guerrieri, R., M. Mencuccini, L. J. Sheppard, M. Saurer, M. P. Perks, P. Levy,  
2049 M. A. Sutton, M. Borghetti, and J. Grace (2011). The legacy of enhanced  
2050 N and S deposition as revealed by the combined analysis of  $\delta^{13}\text{C}$ ,  $\delta^{18}\text{O}$  and  
2051  $\delta^{15}\text{N}$  in tree rings. *Global Change Biology* 17(5), 1946–1962.
- 2052 Gulmon, S. L. and C. C. Chu (1981). The effects of light and nitrogen on pho-  
2053 tosynthesis, leaf characteristics, and dry matter allocation in the chaparral  
2054 shrub, <i>Diplacus aurantiacus</i>. *Oecologia* 49(2), 207–212.
- 2055 Gutschick, V. P. (1981). Evolved strategies in nitrogen acquisition by plants.  
2056 *The American Naturalist* 118(5), 607–637.
- 2057 Hallik, L., Ü. Niinemets, and I. J. Wright (2009). Are species shade and drought

- 2058 tolerance reflected in leaf-level structural and functional differentiation in  
2059 Northern Hemisphere temperate woody flora? *New Phytologist* 184(1), 257–  
2060 274.
- 2061 Harrison, M. T., E. J. Edwards, G. D. Farquhar, A. B. Nicotra, and J. R.  
2062 Evans (2009). Nitrogen in cell walls of sclerophyllous leaves accounts for  
2063 little of the variation in photosynthetic nitrogen-use efficiency. *Plant, Cell  
and Environment* 32(3), 259–270.
- 2064 Harrison, S. P., W. Cramer, O. Franklin, I. C. Prentice, H. Wang,  
2065 Å. Brännström, H. de Boer, U. Dieckmann, J. Joshi, T. F. Keenan,  
2066 A. Lavergne, S. Manzoni, G. Mengoli, C. Morfopoulos, J. Peñuelas,  
2067 S. Pietsch, K. T. Rebel, Y. Ryu, N. G. Smith, B. D. Stocker, and I. J.  
2068 Wright (2021). Eco-evolutionary optimality as a means to improve vegeta-  
2069 tion and land-surface models. *New Phytologist* 231(6), 2125–2141.
- 2070
- 2071 Henneron, L., P. Kardol, D. A. Wardle, C. Cros, and S. Fontaine (2020). Rhizo-  
2072 sphere control of soil nitrogen cycling: a key component of plant economic  
2073 strategies. *New Phytologist* 228(4), 1269–1282.
- 2074 Hijmans, R. J. (2022). terra: Spatial Data Analysis.
- 2075 Hikosaka, K. and A. Shigeno (2009). The role of Rubisco and cell walls in the  
2076 interspecific variation in photosynthetic capacity. *Oecologia* 160(3), 443–  
2077 451.
- 2078 Hoagland, D. R. and D. I. Arnon (1950). The water culture method for growing  
2079 plants without soil. *California Agricultural Experiment Station: 347* 347(2),  
2080 1–32.

- 2081** Hobbie, E. A. (2006). Carbon allocation to ectomycorrhizal fungi correlates  
**2082** with belowground allocation in culture studies. *Ecology* 87(3), 563–569.
- 2083** Hobbie, E. A. and J. E. Hobbie (2008). Natural abundance of  $^{15}\text{N}$  in nitrogen-  
**2084** limited forests and tundra can estimate nitrogen cycling through mycorrhizal  
**2085** fungi: a review. *Ecosystems* 11(5), 815–830.
- 2086** Hoek, T. A., K. Axelrod, T. Biancalani, E. A. Yurtsev, J. Liu, and J. Gore  
**2087** (2016). Resource availability modulates the cooperative and competitive na-  
**2088** nature of a microbial cross-feeding mutualism. *PLOS Biology* 14(8), e1002540.
- 2089** Höglberg, M. N., M. J. I. Briones, S. G. Keel, D. B. Metcalfe, C. Campbell, A. J.  
**2090** Midwood, B. Thornton, V. Hurry, S. Linder, T. Näsholm, and P. Höglberg  
**2091** (2010). Quantification of effects of season and nitrogen supply on tree below-  
**2092** ground carbon transfer to ectomycorrhizal fungi and other soil organisms in  
**2093** a boreal pine forest. *New Phytologist* 187(2), 485–493.
- 2094** Höglberg, P., M. N. Höglberg, S. G. Göttlicher, N. R. Betson, S. G. Keel, D. B.  
**2095** Metcalfe, C. Campbell, A. Schindlbacher, V. Hurry, T. Lundmark, S. Linder,  
**2096** and T. Näsholm (2008). High temporal resolution tracing of photosynthate  
**2097** carbon from the tree canopy to forest soil microorganisms. *New Phytolo-*  
**2098** *gist* 177(1), 220–228.
- 2099** Houlton, B. Z., Y.-P. Wang, P. M. Vitousek, and C. B. Field (2008). A uni-  
**2100** fying framework for dinitrogen fixation in the terrestrial biosphere. *Nature*  
**2101** 454(7202), 327–330.
- 2102** Huber, M. L., R. A. Perkins, A. Laesecke, D. G. Friend, J. V. Sengers, M. J.  
**2103** Assael, I. N. Metaxa, E. Vogel, R. Mareš, and K. Miyagawa (2009). New  
**2104** international formulation for the viscosity of H<sub>2</sub>O. *Journal of Physical and*

- 2105** *Chemical Reference Data* 38(2), 101–125.
- 2106** Hungate, B. A., J. S. Dukes, M. R. Shaw, Y. Luo, and C. B. Field (2003).
- 2107** Nitrogen and climate change. *Science* 302(5650), 1512–1513.
- 2108** IPCC (2021). *Climate Change 2021: The Physical Science Basis. Contribution of Working Group I to the Sixth Assessment Report of the Intergovernmental Panel on Climate Change*. Cambridge University Press.
- 2109**
- 2110**
- 2111** Johnson, N. C., J. H. Graham, and F. A. Smith (1997). Functioning of mycorrhizal associations along the mutualism-parasitism continuum. *New Phytologist* 135(4), 575–585.
- 2112**
- 2113**
- 2114** Kachurina, O. M., H. Zhang, W. R. Raun, and E. G. Krenzer (2000). Simultaneous determination of soil aluminum, ammonium- and nitrate- nitrogen using 1 M potassium chloride. *Communications in Soil Science and Plant Analysis* 31(7-8), 893–903.
- 2115**
- 2116**
- 2117**
- 2118** Kaiser, C., M. R. Kilburn, P. L. Clode, L. Fuchsleger, M. Koranda, J. B. Cliff,
- 2119** Z. M. Solaiman, and D. V. Murphy (2015). Exploring the transfer of recent plant photosynthates to soil microbes: mycorrhizal pathway vs direct root exudation. *New Phytologist* 205(4), 1537–1551.
- 2120**
- 2121**
- 2122** Katabuchi, M. (2015). LeafArea: An R package for rapid digital analysis of leaf area. *Ecological Research* 30(6), 1073–1077.
- 2123**
- 2124** Kattge, J. and W. Knorr (2007). Temperature acclimation in a biochemical model of photosynthesis: a reanalysis of data from 36 species. *Plant, Cell and Environment* 30(9), 1176–1190.
- 2125**
- 2126**
- 2127** Kattge, J., W. Knorr, T. Raddatz, and C. Wirth (2009). Quantifying photosyn-

- 2128       thetic capacity and its relationship to leaf nitrogen content for global-scale  
2129       terrestrial biosphere models. *Global Change Biology* 15(4), 976–991.
- 2130       Kayler, Z., A. Gessler, and N. Buchmann (2010). What is the speed of link  
2131       between aboveground and belowground processes? *New Phytologist* 187(4),  
2132       885–888.
- 2133       Kayler, Z., C. Keitel, K. Jansen, and A. Gessler (2017). Experimental evi-  
2134       dence of two mechanisms coupling leaf-level C assimilation to rhizosphere  
2135       CO<sub>2</sub> release. *Environmental and Experimental Botany* 135,  
2136       21–26.
- 2137       Keeling, C. D., W. G. Mook, and P. P. Tans (1979, jan). Recent trends in the  
2138       <sup>13</sup>C/<sup>12</sup>C ratio of atmospheric carbon dioxide.  
2139       *Nature* 277(5692), 121–123.
- 2140       Kenward, M. G. and J. H. Roger (1997). Small sample inference for fixed effects  
2141       from restricted maximum likelihood. *Biometrics* 53(3), 983.
- 2142       Knapp, A. K., M. L. Avolio, C. Beier, C. J. W. Carroll, S. L. Collins, J. S.  
2143       Dukes, L. H. Fraser, R. J. Griffin-Nolan, D. L. Hoover, A. Jentsch, M. E.  
2144       Loik, R. P. Phillips, A. K. Post, O. E. Sala, I. J. Slette, L. Yahdjian, and  
2145       M. D. Smith (2017). Pushing precipitation to the extremes in distributed  
2146       experiments: recommendations for simulating wet and dry years. *Global  
2147       Change Biology* 23(5), 1774–1782.
- 2148       Knorr, W. (2000). Annual and interannual CO<sub>2</sub> exchanges of the  
2149       terrestrial biosphere: process-based simulations and uncertainties. *Global  
2150       Ecology and Biogeography* 9(3), 225–252.

- 2151 Knorr, W. and M. Heimann (2001). Uncertainties in global terrestrial biosphere  
2152 modeling: 1. A comprehensive sensitivity analysis with a new photosynthesis  
2153 and energy balance scheme. *Global Biogeochemical Cycles* 15(1), 207–225.
- 2154 Kulmatiski, A., P. B. Adler, J. M. Stark, and A. T. Tredennick (2017). Water  
2155 and nitrogen uptake are better associated with resource availability than  
2156 root biomass. *Ecosphere* 8(3), e01738.
- 2157 Lavergne, A., D. Sandoval, V. J. Hare, H. Graven, and I. C. Prentice (2020).  
2158 Impacts of soil water stress on the acclimated stomatal limitation of pho-  
2159 tosynthesis: Insights from stable carbon isotope data. *Global Change Biol-*  
2160 *ogy* 26(12), 7158–7172.
- 2161 Lawrence, D. M., R. A. Fisher, C. D. Koven, K. W. Oleson, S. C. Swen-  
2162 son, G. B. Bonan, N. Collier, B. Ghimire, L. Kampenhout, D. Kennedy,  
2163 E. Kluzeck, P. J. Lawrence, F. Li, H. Li, D. L. Lombardozzi, W. J. Riley,  
2164 W. J. Sacks, M. Shi, M. Vertenstein, W. R. Wieder, C. Xu, A. A. Ali,  
2165 A. M. Badger, G. Bisht, M. Broeke, M. A. Brunke, S. P. Burns, J. Buzan,  
2166 M. Clark, A. Craig, K. M. Dahlin, B. Drewniak, J. B. Fisher, M. Flanner,  
2167 A. M. Fox, P. Gentine, F. M. Hoffman, G. Keppel-Aleks, R. Knox, S. Ku-  
2168 mar, J. Lenaerts, L. R. Leung, W. H. Lipscomb, Y. Lu, A. Pandey, J. D.  
2169 Pelletier, J. Perket, J. T. Randerson, D. M. Ricciuto, B. M. Sanderson,  
2170 A. Slater, Z. M. Subin, J. Tang, R. Q. Thomas, M. Val Martin, and X. Zeng  
2171 (2019). The Community Land Model Version 5: description of new features,  
2172 benchmarking, and impact of forcing uncertainty. *Journal of Advances in*  
2173 *Modeling Earth Systems* 11(12), 4245–4287.
- 2174 LeBauer, D. S. and K. K. Treseder (2008). Nitrogen limitation of net primary

- 2175 productivity. *Ecology* 89(2), 371–379.
- 2176 Lefcheck, J. S. (2016). piecewiseSEM: Piecewise structural equation modelling  
2177 in r for ecology, evolution, and systematics. *Methods in Ecology and Evolution*  
2178 7(5), 573–579.
- 2179 Lenth, R. (2019). emmeans: estimated marginal means, aka least-squares  
2180 means.
- 2181 Li, W., H. Zhang, G. Huang, R. Liu, H. Wu, C. Zhao, and N. G. McDowell  
2182 (2020). Effects of nitrogen enrichment on tree carbon allocation: A global  
2183 synthesis. *Global Ecology and Biogeography* 29(3), 573–589.
- 2184 Liang, J., X. Qi, L. Souza, and Y. Luo (2016). Processes regulating progressive  
2185 nitrogen limitation under elevated carbon dioxide: a meta-analysis. *Biogeosciences*  
2186 13(9), 2689–2699.
- 2187 Liang, X., T. Zhang, X. Lu, D. S. Ellsworth, H. BassiriRad, C. You, D. Wang,  
2188 P. He, Q. Deng, H. Liu, J. Mo, and Q. Ye (2020). Global response patterns of  
2189 plant photosynthesis to nitrogen addition: A meta-analysis. *Global Change  
2190 Biology* 26(6), 3585–3600.
- 2191 Lu, J., J. Yang, C. Keitel, L. Yin, P. Wang, W. Cheng, and F. A. Dijkstra  
2192 (2022). Belowground Carbon Efficiency for Nitrogen and Phosphorus Ac-  
2193 quisition Varies Between *Lolium perenne* and *Trifolium repens* and Depends  
2194 on Phosphorus Fertilization. *Frontiers in Plant Science* 13, 1–9.
- 2195 Luo, X., T. F. Keenan, J. M. Chen, H. Croft, I. C. Prentice, N. G. Smith,  
2196 A. P. Walker, H. Wang, R. Wang, C. Xu, and Y. Zhang (2021). Global  
2197 variation in the fraction of leaf nitrogen allocated to photosynthesis. *Nature*

- 2198** *Communications* 12(1), 4866.
- 2199** Luo, Y., W. S. Currie, J. S. Dukes, A. C. Finzi, U. A. Hartwig, B. A. Hungate,  
**2200** R. E. McMurtrie, R. Oren, W. J. Parton, D. E. Pataki, R. M. Shaw, D. R.  
**2201** Zak, and C. B. Field (2004). Progressive nitrogen limitation of ecosystem  
**2202** responses to rising atmospheric carbon dioxide. *BioScience* 54(8), 731–739.
- 2203** Maire, V., P. Martre, J. Kattge, F. Gastal, G. Esser, S. Fontaine, and J.-F.  
**2204** Soussana (2012). The coordination of leaf photosynthesis links C and N  
**2205** fluxes in C<sub>3</sub> plant species. *PLoS ONE* 7(6), e38345.
- 2206** Makino, A. (2003). Rubisco and nitrogen relationships in rice: leaf photosyn-  
**2207** thesis and plant growth. *Soil Science and Plant Nutrition* 49(3), 319–327.
- 2208** Markham, J. H. and C. Zekveld (2007). Nitrogen fixation makes biomass al-  
**2209** location to roots independent of soil nitrogen supply. *Canadian Journal of*  
**2210** *Botany* (9), 787–793.
- 2211** Marschner, H. and B. Dell (1994). Nutrient uptake in mycorrhizal symbiosis.  
**2212** *Plant and Soil* 159(1), 89–102.
- 2213** Matamala, R. and W. H. Schlesinger (2000). Effects of elevated atmospheric  
**2214** CO<sub>2</sub> on fine root production and activity in an intact tem-  
**2215** perate forest ecosystem. *Global Change Biology* 6(8), 967–979.
- 2216** Medlyn, B. E., E. Dreyer, D. S. Ellsworth, M. Forstreuter, P. C. Harley,  
**2217** M. U. F. Kirschbaum, X. Le Roux, P. Montpied, J. Strassmeyer, A. Wal-  
**2218** croft, K. Wang, and D. Loustau (2002). Temperature response of parameters  
**2219** of a biochemically based model of photosynthesis. II. A review of experimen-  
**2220** tal data. *Plant, Cell and Environment* 25(9), 1167–1179.

- 2221** Menge, D. N. L., S. A. Levin, and L. O. Hedin (2008). Evolutionary tradeoffs can  
**2222** select against nitrogen fixation and thereby maintain nitrogen limitation.  
**2223** *Proceedings of the National Academy of Sciences* 105(5), 1573–1578.
- 2224** Menne, M. J., I. Durre, R. S. Vose, B. E. Gleason, and T. G. Houston (2012).  
**2225** An overview of the global historical climatology network-daily database.  
**2226** *Journal of Atmospheric and Oceanic Technology* 29(7), 897–910.
- 2227** Meyerholt, J., K. Sickel, and S. Zaehle (2020). Ensemble projections elucidate  
**2228** effects of uncertainty in terrestrial nitrogen limitation on future carbon up-  
**2229** take. *Global Change Biology* 26(7), 3978–3996.
- 2230** Meyerholt, J., S. Zaehle, and M. J. Smith (2016). Variability of pro-  
**2231** jected terrestrial biosphere responses to elevated levels of atmospheric  
**2232** CO<sub>2</sub> due to uncertainty in biological nitrogen fixation. *Bio-*  
**2233** *geosciences* 13(5), 1491–1518.
- 2234** Minocha, R., S. Long, A. H. Magill, J. D. Aber, and W. H. McDowell (2000).  
**2235** Foliar free polyamine and inorganic ion content in relation to soil and soil  
**2236** solution chemistry in two fertilized forest stands at the Harvard Forest,  
**2237** Massachusetts. *Plant and Soil* 222(1-2), 119–137.
- 2238** Moore, D. J., S. Aref, R. M. Ho, J. S. Pippen, J. G. Hamilton, and E. H. De  
**2239** Lucia (2006). Annual basal area increment and growth duration of *Pinus*  
**2240** *taeda* in response to eight years of free-air carbon dioxide enrichment. *Global*  
**2241** *Change Biology* 12(8), 1367–1377.
- 2242** Morgan, J. A., D. E. Pataki, C. Körner, H. Clark, S. J. Del Gross, J. M.  
**2243** Grünzweig, A. K. Knapp, A. R. Mosier, P. C. D. Newton, P. A. Niklaus,  
**2244** J. B. Nippert, R. S. Nowak, W. J. Parton, H. W. Polley, and M. R. Shaw

- 2245 (2004). Water relations in grassland and desert ecosystems exposed to ele-  
2246 vated atmospheric CO<sub>2</sub>. *Oecologia* 140(1), 11–25.
- 2247 Muñoz, N., X. Qi, M. W. Li, M. Xie, Y. Gao, M. Y. Cheung, F. L. Wong, and  
2248 H.-M. Lam (2016). Improvement in nitrogen fixation capacity could be part  
2249 of the domestication process in soybean. *Heredity* 117(2), 84–93.
- 2250 Nadelhoffer, K. J. and J. W. Raich (1992). Fine root production estimates and  
2251 belowground carbon allocation in forest ecosystems. *Ecology* 73(4), 1139–  
2252 1147.
- 2253 Niinemets, Ü. and J. D. Tenhunen (1997). A model separating leaf struc-  
2254 tural and physiological effects on carbon gain along light gradients for the  
2255 shade-tolerant species *< i>Acer saccharum</i>*. *Plant, Cell and Environ-  
2256 ment* 20(7), 845–866.
- 2257 Norby, R. J., J. Ledford, C. D. Reilly, N. E. Miller, and E. G. O'Neill  
2258 (2004). Fine-root production dominates response of a deciduous forest to  
2259 atmospheric CO<sub>2</sub> enrichment. *Proceedings of the National Academy of Sci-  
2260 ences* 101(26), 9689–9693.
- 2261 Norby, R. J., J. M. Warren, C. M. Iversen, B. E. Medlyn, and R. E. Mc-  
2262 Murtrie (2010). CO<sub>2</sub> enhancement of forest productivity constrained by  
2263 limited nitrogen availability. *Proceedings of the National Academy of Sci-  
2264 ences* 107(45), 19368–19373.
- 2265 Novick, K. A., D. L. Ficklin, P. C. Stoy, C. A. Williams, G. Bohrer, A. C.  
2266 Oishi, S. A. Papuga, P. D. Blanken, A. Noormets, B. N. Sulman, R. L.  
2267 Scott, L. Wang, and R. P. Phillips (2016). The increasing importance of  
2268 atmospheric demand for ecosystem water and carbon fluxes. *Nature Climate*

- 2269** *Change* 6(11), 1023–1027.
- 2270** Noyce, G. L., M. L. Kirwan, R. L. Rich, and J. P. Megonigal (2019). Asynchronous nitrogen supply and demand produce nonlinear plant allocation
- 2271** responses to warming and elevated CO<sub>2</sub>. *Proceedings of the*
- 2272** *National Academy of Sciences* 116(43), 21623–21628.
- 2273**
- 2274** Onoda, Y., K. Hikosaka, and T. Hirose (2004). Allocation of nitrogen to
- 2275** cell walls decreases photosynthetic nitrogen-use efficiency. *Functional Ecol-*
- 2276** *ogy* 18(3), 419–425.
- 2277** Onoda, Y., I. J. Wright, J. R. Evans, K. Hikosaka, K. Kitajima, Ü. Niinemets,
- 2278** H. Poorter, T. Tosens, and M. Westoby (2017). Physiological and structural
- 2279** tradeoffs underlying the leaf economics spectrum. *New Phytologist* 214(4),
- 2280** 1447–1463.
- 2281** Oreskes, N., K. Shrader-Frechette, and K. Belitz (1994). Verification, vali-
- 2282** dation, and confirmation of numerical models in the Earth sciences. *Sci-*
- 2283** *ence* 263(5147), 641–646.
- 2284** Paillassa, J., I. J. Wright, I. C. Prentice, S. Pepin, N. G. Smith, G. Ethier,
- 2285** A. C. Westerband, L. J. Lamarque, H. Wang, W. K. Cornwell, and V. Maire
- 2286** (2020). When and where soil is important to modify the carbon and water
- 2287** economy of leaves. *New Phytologist* 228(1), 121–135.
- 2288** Parvin, S., S. Uddin, S. Tausz Posch, R. Armstrong, and M. Tausz (2020). Car-
- 2289** bon sink strength of nodules but not other organs modulates photosynthesis
- 2290** of faba bean (*i>Vicia faba</i>*) grown under elevated [CO<sub>2</sub>] and different
- 2291** water supply. *New Phytologist* 227(1), 132–145.

- 2292** Peng, Y., K. J. Bloomfield, L. A. Cernusak, T. F. Domingues, and I. C. Prentice (2021). Global climate and nutrient controls of photosynthetic capacity.
- 2293**
- 2294** *Communications Biology* 4(1), 462.
- 2295** Perkowski, E. A., E. F. Waring, and N. G. Smith (2021). Root mass carbon
- 2296** costs to acquire nitrogen are determined by nitrogen and light availability
- 2297** in two species with different nitrogen acquisition strategies. *Journal of*
- 2298** *Experimental Botany* 72(15), 5766–5776.
- 2299** Phillips, R. P., E. R. Brzostek, and M. G. Midgley (2013). The mycorrhizal-
- 2300** associated nutrient economy: a new framework for predicting carbon-
- 2301** nutrient couplings in temperate forests. *New Phytologist* 199(1), 41–51.
- 2302** Phillips, R. P., A. C. Finzi, and E. S. Bernhardt (2011). Enhanced root ex-
- 2303** udation induces microbial feedbacks to N cycling in a pine forest under
- 2304** long-term CO<sub>2</sub> fumigation. *Ecology Letters* 14(2), 187–194.
- 2305** Pinheiro, J. and D. Bates (2022). nlme: linear and nonlinear mixed effects
- 2306** models.
- 2307** Poggio, L., L. M. De Sousa, N. H. Batjes, G. B. M. Heuvelink, B. Kempen,
- 2308** E. Ribeiro, and D. Rossiter (2021). SoilGrids 2.0: Producing soil information
- 2309** for the globe with quantified spatial uncertainty. *Soil* 7(1), 217–240.
- 2310** Pons, T. L. and R. W. Pearcy (1994). Nitrogen reallocation and photosynthetic
- 2311** acclimation in response to partial shading in soybean plants. *Physiologia*
- 2312** *Plantarum* 92(4), 636–644.
- 2313** Poorter, H., J. Bühler, D. Van Dusschoten, J. Climent, and J. A. Postma (2012).
- 2314** Pot size matters: A meta-analysis of the effects of rooting volume on plant

- 2315 growth. *Functional Plant Biology* 39(11), 839–850.
- 2316 Poorter, H., O. Knopf, I. J. Wright, A. A. Temme, S. W. Hogewoning, A. Graf,  
2317 L. A. Cernusak, and T. L. Pons (2022). A meta-analysis of responses of C<sub>3</sub>  
2318 plants to atmospheric CO<sub>2</sub>: dose–response curves for 85 traits ranging from  
2319 the molecular to the whole-plant level. *New Phytologist* 233(4), 1560–1596.
- 2320 Prentice, I. C., N. Dong, S. M. Gleason, V. Maire, and I. J. Wright (2014).  
2321 Balancing the costs of carbon gain and water transport: testing a new theo-  
2322 retical framework for plant functional ecology. *Ecology Letters* 17(1), 82–91.
- 2323 Prentice, I. C., X. Liang, B. E. Medlyn, and Y.-P. Wang (2015). Reliable, ro-  
2324 bust and realistic: The three R’s of next-generation land-surface modelling.  
2325 *Atmospheric Chemistry and Physics* 15, 5987–6005.
- 2326 Priestley, C. H. B. and R. J. Taylor (1972). On the Assessment of Surface  
2327 Heat Flux and Evaporation Using Large-Scale Parameters. *Monthly Weather  
2328 Review* 100(2), 81–92.
- 2329 Querejeta, J. I., I. Prieto, C. Armas, F. Casanoves, J. S. Diémé, M. Diouf,  
2330 H. Yossi, B. Kaya, F. I. Pugnaire, and G. M. Rusch (2022). Higher leaf  
2331 nitrogen content is linked to tighter stomatal regulation of transpiration  
2332 and more efficient water use across dryland trees. *New Phytologist* 235(4),  
2333 1351–1364.
- 2334 R Core Team (2021). R: A language and environment for statistical computing.
- 2335 Raich, J. W., D. A. Clark, L. Schwendenmann, and T. E. Wood (2014). Above-  
2336 ground tree growth varies with belowground carbon allocation in a tropical  
2337 rainforest environment. *PLoS ONE* 9(6), e100275.

- 2338** Rastetter, E. B., P. M. Vitousek, C. B. Field, G. R. Shaver, D. Herbert, and  
**2339** G. I. Ågren (2001). Resource optimization and symbiotic nitrogen fixation.  
**2340** *Ecosystems* 4(4), 369–388.
- 2341** Reich, P. B. (2014). The world-wide 'fast-slow' plant economics spectrum: a  
**2342** traits manifesto. *Journal of Ecology* 102(2), 275–301.
- 2343** Reich, P. B., S. E. Hobbie, T. Lee, D. S. Ellsworth, J. B. West, D. Tilman,  
**2344** J. M. H. Knops, S. Naeem, and J. Trost (2006). Nitrogen limitation con-  
**2345** strains sustainability of ecosystem response to CO<sub>2</sub>. *Na-  
**2346** ture* 440(7086), 922–925.
- 2347** Rhine, E. D., R. L. Mulvaney, E. J. Pratt, and G. K. Sims (1998). Improving  
**2348** the Berthelot reaction for determining ammonium in soil extracts and water.  
**2349** *Soil Science Society of America Journal* 62(2), 473.
- 2350** Rogers, A. (2014). The use and misuse of  $V_{cmax}$  in Earth System Models. *Pho-*  
**2351** *tosynthesis Research* 119(1-2), 15–29.
- 2352** Rogers, A., B. E. Medlyn, J. S. Dukes, G. B. Bonan, S. Caemmerer, M. C.  
**2353** Dietze, J. Kattge, A. D. B. Leakey, L. M. Mercado, Ü. Niinemets, I. C.  
**2354** Prentice, S. P. Serbin, S. Sitch, D. A. Way, and S. Zaehle (2017). A roadmap  
**2355** for improving the representation of photosynthesis in Earth system models.  
**2356** *New Phytologist* 213(1), 22–42.
- 2357** Saathoff, A. J. and J. Welles (2021). Gas exchange measurements in the un-  
**2358** steady state. *Plant Cell and Environment* 44(11), 3509–3523.
- 2359** Saleh, A. M., M. Abdel-Mawgoud, A. R. Hassan, T. H. Habeeb, R. S. Yehia,  
**2360** and H. AbdElgawad (2020). Global metabolic changes induced by arbuscular

- 2361 mycorrhizal fungi in oregano plants grown under ambient and elevated levels  
2362 of atmospheric CO<sub>2</sub>. *Plant Physiology and Biochemistry* 151, 255–263.
- 2363 Saxton, K. E. and W. J. Rawls (2006). Soil water characteristic estimates by  
2364 texture and organic matter for hydrologic solutions. *Soil Science Society of  
2365 America Journal* 70(5), 1569–1578.
- 2366 Schaefer, K., C. R. Schwalm, C. Williams, M. A. Arain, A. Barr, J. M. Chen,  
2367 K. J. Davis, D. Dimitrov, T. W. Hilton, D. Y. Hollinger, E. Humphreys,  
2368 B. Poulter, B. M. Racza, A. D. Richardson, A. Sahoo, P. Thornton, R. Var-  
2369 gas, H. Verbeeck, R. Anderson, I. Baker, T. A. Black, P. Bolstad, J. Chen,  
2370 P. S. Curtis, A. R. Desai, M. C. Dietze, D. Dragoni, C. M. Gough, R. F.  
2371 Grant, L. Gu, A. K. Jain, C. Kucharik, B. E. Law, S. Liu, E. Lokipitiya,  
2372 H. A. Margolis, R. Matamala, J. H. McCaughey, R. Monson, J. W. Munger,  
2373 W. Oechel, C. Peng, D. T. Price, D. Ricciuto, W. J. Riley, N. Roulet,  
2374 H. Tian, C. Tonitto, M. Torn, E. Weng, and X. Zhou (2012). A model-  
2375 data comparison of gross primary productivity: Results from the North  
2376 American Carbon Program site synthesis. *Journal of Geophysical Research:  
2377 Biogeosciences* 117(G3), G03010.
- 2378 Schneider, C. A., W. S. Rasband, and K. W. Eliceiri (2012). NIH Image to  
2379 ImageJ: 25 years of image analysis. *Nature Methods* 9(7), 671–675.
- 2380 Scott, H. G. and N. G. Smith (2022). A Model of C4 Photosynthetic Acclimation  
2381 Based on Least-Cost Optimality Theory Suitable for Earth System Model  
2382 Incorporation. *Journal of Advances in Modeling Earth Systems* 14(3), 1–16.
- 2383 Shi, M., J. B. Fisher, E. R. Brzostek, and R. P. Phillips (2016). Carbon cost  
2384 of plant nitrogen acquisition: Global carbon cycle impact from an improved

- 2385 plant nitrogen cycle in the Community Land Model. *Global Change Biology*  
2386 22(3), 1299–1314.
- 2387 Shi, M., J. B. Fisher, R. P. Phillips, and E. R. Brzostek (2019). Neglecting  
2388 plant–microbe symbioses leads to underestimation of modeled climate im-  
2389 pacts. *Biogeosciences* 16(2), 457–465.
- 2390 Smith, N. G. and J. S. Dukes (2013). Plant respiration and photosynthesis in  
2391 global-scale models: incorporating acclimation to temperature and CO<sub>2</sub>.  
2392 *Global Change Biology* 19(1), 45–63.
- 2393 Smith, N. G. and T. F. Keenan (2020). Mechanisms underlying leaf photosyn-  
2394 thetic acclimation to warming and elevated CO<sub>2</sub> as inferred from least-cost  
2395 optimality theory. *Global Change Biology* 26(9), 5202–5216.
- 2396 Smith, N. G., T. F. Keenan, I. C. Prentice, H. Wang, I. J. Wright, Ü. Niinemets,  
2397 K. Y. Crous, T. F. Domingues, R. Guerrieri, F. oko Ishida, J. Kattge, E. L.  
2398 Kruger, V. Maire, A. Rogers, S. P. Serbin, L. Tarvainen, H. F. Togashi,  
2399 P. A. Townsend, M. Wang, L. K. Weerasinghe, and S.-X. Zhou (2019).  
2400 Global photosynthetic capacity is optimized to the environment. *Ecology*  
2401 *Letters* 22(3), 506–517.
- 2402 Smith, N. G., D. L. Lombardozzi, A. Tawfik, G. B. Bonan, and J. S. Dukes  
2403 (2017). Biophysical consequences of photosynthetic temperature acclimation  
2404 for climate. *Journal of Advances in Modeling Earth Systems* 9(1), 536–547.
- 2405 Smith, N. G., S. L. Malyshev, E. Shevliakova, J. Kattge, and J. S. Dukes  
2406 (2016). Foliar temperature acclimation reduces simulated carbon sensitivity  
2407 to climate. *Nature Climate Change* 6(4), 407–411.

- 2408** Smith, S. E. and D. J. Read (2008). *Mycorrhizal Symbiosis*. Academic Press.
- 2409** Soil Survey Staff (2022). Web Soil Survey.
- 2410** Soudzilovskaia, N. A., J. C. Douma, A. A. Akhmetzhanova, P. M. van Bodegom, W. K. Cornwell, E. J. Moens, K. K. Treseder, and J. H. C. Cornelissen (2015). Global patterns of plant root colonization intensity by mycorrhizal fungi explained by climate and soil chemistry. *Global Ecology and Biogeography* 24(3), 371–382.
- 2415** Stocker, B. D., H. Wang, N. G. Smith, S. P. Harrison, T. F. Keenan, D. Sandoval, T. Davis, and I. C. Prentice (2020). P-model v1.0: An optimality-based light use efficiency model for simulating ecosystem gross primary production. *Geoscientific Model Development* 13(3), 1545–1581.
- 2419** Stocker, B. D., J. Zscheischler, T. F. Keenan, I. C. Prentice, J. Peñuelas, and S. I. Seneviratne (2018). Quantifying soil moisture impacts on light use efficiency across biomes. *New Phytologist* 218(4), 1430–1449.
- 2422** Sulman, B. N., D. T. Roman, K. Yi, L. Wang, R. P. Phillips, and K. A. Novick (2016). High atmospheric demand for water can limit forest carbon uptake and transpiration as severely as dry soil. *Geophysical Research Letters* 43(18), 9686–9695.
- 2426** Sulman, B. N., E. Shevliakova, E. R. Brzostek, S. N. Kivlin, S. L. Malyshev, D. N. L. Menge, and X. Zhang (2019). Diverse mycorrhizal associations enhance terrestrial C storage in a global model. *Global Biogeochemical Cycles* 33(4), 501–523.
- 2430** Sweet, S. K., D. W. Wolfe, A. DeGaetano, and R. Benner (2017). Anatomy

- 2431 of the 2016 drought in the Northeastern United States: Implications for  
2432 agriculture and water resources in humid climates. *Agricultural and Forest*  
2433 *Meteorology* 247, 571–581.
- 2434 Taylor, B. N. and D. N. L. Menge (2018). Light regulates tropical symbiotic  
2435 nitrogen fixation more strongly than soil nitrogen. *Nature Plants* 4(9), 655–  
2436 661.
- 2437 Terrer, C., S. Vicca, B. A. Hungate, R. P. Phillips, and I. C. Prentice (2016).  
2438 Mycorrhizal association as a primary control of the CO<sub>2</sub> fertilization effect.  
2439 *Science* 353(6294), 72–74.
- 2440 Terrer, C., S. Vicca, B. D. Stocker, B. A. Hungate, R. P. Phillips, P. B. Reich,  
2441 A. C. Finzi, and I. C. Prentice (2018). Ecosystem responses to elevated CO<sub>2</sub>  
2442 governed by plant–soil interactions and the cost of nitrogen acquisition. *New*  
2443 *Phytologist* 217(2), 507–522.
- 2444 Thieurmel, B. and A. Elmarhraoui (2019). suncalc: Compute sun position,  
2445 sunlight phases, moon position, and lunar phase.
- 2446 Thomas, R. Q., E. N. J. Brookshire, and S. Gerber (2015). Nitrogen limita-  
2447 tion on land: how can it occur in Earth system models? *Global Change*  
2448 *Biology* 21(5), 1777–1793.
- 2449 Thomas, R. Q., S. Zaehle, P. H. Templer, and C. L. Goodale (2013). Global pat-  
2450 terns of nitrogen limitation: confronting two global biogeochemical models  
2451 with observations. *Global Change Biology* 19(10), 2986–2998.
- 2452 Thornton, P. E., J.-F. Lamarque, N. A. Rosenbloom, and N. M. Mahowald  
2453 (2007). Influence of carbon-nitrogen cycle coupling on land model response

- 2454 to CO<sub>2</sub> fertilization and climate variability. *Global Biogeochemical Cycles* 21(4), GB4018.
- 2455
- 2456 Tingey, D. T., D. L. Phillips, and M. G. Johnson (2000). Elevated CO<sub>2</sub> and  
2457 conifer roots: effects on growth, life span and turnover. *New Phytologist*  
2458 147(1), 87–103.
- 2459 Udvardi, M. and P. S. Poole (2013). Transport and metabolism in legume-  
2460 rhizobia symbioses. *Annual Review of Plant Biology* 64, 781–805.
- 2461 USDA NRCS (2022). The PLANTS Database.
- 2462 Uselman, S. M., R. G. Qualls, and R. B. Thomas (2000). Effects of increased  
2463 atmospheric CO<sub>2</sub>, temperature, and soil N availability on root exudation of  
2464 dissolved organic carbon by a N-fixing tree (*Robinia pseudoacacia* L.). *Plant  
2465 and Soil* 222, 191–202.
- 2466 van Diepen, L. T. A., E. A. Lilleskov, K. S. Pregitzer, and R. M. Miller (2007).  
2467 Decline of arbuscular mycorrhizal fungi in northern hardwood forests ex-  
2468 posed to chronic nitrogen additions. *New Phytologist* 176(1), 175–183.
- 2469 Vance, C. P. and G. H. Heichel (1991). Carbon in N<sub>2</sub> fixation: Limitation or  
2470 exquisite adaptation. *Annual Review of Plant Physiology and Plant Molec-  
2471 ular Biology* 42(1), 373–392.
- 2472 Viet, H. D., J.-H. Kwak, K.-S. Lee, S.-S. Lim, M. Matsushima, S. X. Chang,  
2473 K.-H. Lee, and W.-J. Choi (2013). Foliar chemistry and tree ring δ<sup>13</sup>C of  
2474 *Pinus densiflora* in relation to tree growth along a soil pH gradient. *Plant  
2475 and Soil* 363(1-2), 101–112.
- 2476 Vitousek, P. M., K. Cassman, C. C. Cleveland, T. Crews, C. B. Field, N. B.

- 2477** Grimm, R. W. Howarth, R. Marino, L. Martinelli, E. B. Rastetter, and  
**2478** J. I. Sprent (2002). Towards an ecological understanding of biological nitro-  
**2479** gen fixation. In *The Nitrogen Cycle at Regional to Global Scales*, pp. 1–45.  
**2480** Springer Netherlands.
- 2481** Vitousek, P. M. and R. W. Howarth (1991). Nitrogen limitation on land and in  
**2482** the sea: How can it occur? *Biogeochemistry* 13(2), 87–115.
- 2483** Vitousek, P. M., S. Porder, B. Z. Houlton, and O. A. Chadwick (2010).  
**2484** Terrestrial phosphorus limitation: mechanisms, implications, and nitro-  
**2485** gen–phosphorus interactions. *Ecological Applications* 20(1), 5–15.
- 2486** Walker, A. P., A. P. Beckerman, L. Gu, J. Kattge, L. A. Cernusak, T. F.  
**2487** Domingues, J. C. Scales, G. Wohlfahrt, S. D. Wullschleger, and F. I. Wood-  
**2488** ward (2014). The relationship of leaf photosynthetic traits -  $V_{cmax}$  and  $J_{max}$   
**2489** - to leaf nitrogen, leaf phosphorus, and specific leaf area: a meta-analysis  
**2490** and modeling study. *Ecology and Evolution* 4(16), 3218–3235.
- 2491** Wang, H., I. C. Prentice, T. F. Keenan, T. W. Davis, I. J. Wright, W. K.  
**2492** Cornwell, B. J. Evans, and C. Peng (2017). Towards a universal model for  
**2493** carbon dioxide uptake by plants. *Nature Plants* 3(9), 734–741.
- 2494** Wang, W., Y. Wang, G. Hoch, Z. Wang, and J. Gu (2018). Linkage of root mor-  
**2495** phology to anatomy with increasing nitrogen availability in six temperate  
**2496** tree species. *Plant and Soil* 425(1-2), 189–200.
- 2497** Weatherburn, M. W. (1967). Phenol-hypochlorite reaction for determination of  
**2498** ammonia. *Analytical Chemistry* 39(8), 971–974.
- 2499** Wellburn, A. R. (1994). The spectral determination of chlorophylls a and b, as

- 2500 well as total carotenoids, using various solvents with spectrophotometers of  
2501 different resolution. *Journal of Plant Physiology* 144(3), 307–313.
- 2502 Wen, Z., P. J. White, J. Shen, and H. Lambers (2022). Linking root exuda-  
2503 tion to belowground economic traits for resource acquisition. *New Phytolo-*  
2504 *gist* 233(4), 1620–1635.
- 2505 Westerband, A. C., I. J. Wright, V. Maire, J. Paillassa, I. C. Prentice, O. K.  
2506 Atkin, K. J. Bloomfield, L. A. Cernusak, N. Dong, S. M. Gleason, C. Guil-  
2507 herme Pereira, H. Lambers, M. R. Leishman, Y. Malhi, and R. H. Nolan  
2508 (2023). Coordination of photosynthetic traits across soil and climate gradi-  
2509 ents. *Global Change Biology* 29(3), 1–29.
- 2510 Wieder, W. R., C. C. Cleveland, W. K. Smith, and K. Todd-Brown (2015).  
2511 Future productivity and carbon storage limited by terrestrial nutrient avail-  
2512 ability. *Nature Geoscience* 8(6), 441–444.
- 2513 Wieder, W. R., D. M. Lawrence, R. A. Fisher, G. B. Bonan, S. J. Cheng, C. L.  
2514 Goodale, A. S. Grandy, C. D. Koven, D. L. Lombardozzi, K. W. Oleson,  
2515 and R. Q. Thomas (2019). Beyond static benchmarking: using experimental  
2516 manipulations to evaluate land model assumptions. *Global Biogeochemical*  
2517 *Cycles* 33(10), 1289–1309.
- 2518 Wright, I. J., P. B. Reich, and M. Westoby (2003). Least-cost input mixtures  
2519 of water and nitrogen for photosynthesis. *The American Naturalist* 161(1),  
2520 98–111.
- 2521 Wright, I. J., P. B. Reich, M. Westoby, D. D. Ackerly, Z. Baruch, F. Bongers,  
2522 J. Cavender-Bares, T. Chapin, J. H. C. Cornelissen, M. Diemer, J. Flexas,  
2523 E. Garnier, P. K. Groom, J. Gulias, K. Hikosaka, B. B. Lamont, T. Lee,

- 2524 W. Lee, C. Lusk, J. J. Midgley, M.-L. Navas, Ü. Niinemets, J. Oleksyn,  
2525 N. Osada, H. Poorter, P. Poot, L. Prior, V. I. Pyankov, C. Roumet, S. C.  
2526 Thomas, M. G. Tjoelker, E. J. Veneklaas, and R. Villar (2004). The world-  
2527 wide leaf economics spectrum. *Nature* 428(6985), 821–827.
- 2528 Xu-Ri and I. C. Prentice (2017). Modelling the demand for new nitrogen fixation  
2529 by terrestrial ecosystems. *Biogeosciences* 14(7), 2003–2017.
- 2530 Zaehle, S., B. E. Medlyn, M. G. De Kauwe, A. P. Walker, M. C. Dietze, T. Hick-  
2531 ler, Y. Luo, Y. P. Wang, B. El-Masri, P. Thornton, A. Jain, S. Wang,  
2532 D. Warlind, E. Weng, W. Parton, C. M. Iversen, A. Gallet-Budynek, H. Mc-  
2533 carthy, A. C. Finzi, P. J. Hanson, I. C. Prentice, R. Oren, and R. J. Norby  
2534 (2014). Evaluation of 11 terrestrial carbon-nitrogen cycle models against  
2535 observations from two temperate Free-Air CO<sub>2</sub> Enrichment studies. *New*  
2536 *Phytologist* 202(3), 803–822.
- 2537 Zaehle, S., S. Sitch, B. Smith, and F. Hatterman (2005). Effects of parame-  
2538 ter uncertainties on the modeling of terrestrial biosphere dynamics. *Global*  
2539 *Biogeochemical Cycles* 19(3), GB3020.
- 2540 Zhu, Q., W. J. Riley, J. Tang, N. Collier, F. M. Hoffman, X. Yang, and G. Bisht  
2541 (2019). Representing nitrogen, phosphorus, and carbon interactions in the  
2542 E3SM land model: development and global benchmarking. *Journal of Ad-*  
2543 *vances in Modeling Earth Systems* 11(7), 2238–2258.
- 2544 Ziegler, C., M. E. Dusenge, B. Nyirambangutse, E. Zibera, G. Wallin, and  
2545 J. Uddling (2020). Contrasting Dependencies of Photosynthetic Capacity  
2546 on Leaf Nitrogen in Early- and Late-Successional Tropical Montane Tree  
2547 Species. *Frontiers in Plant Science* 11, 1–12.

- 2548** Ziehn, T., J. Kattge, W. Knorr, and M. Scholze (2011). Improving the pre-  
**2549** dictability of global CO<sub>2</sub> assimilation rates under climate change. *Geophysical Research Letters* 38(10), L10404.  
**2550**